The Role of H$_2$O in Borate and Borosilicate Glasses: Implications on Structure and Relaxation Mechanisms

Von der Naturwissenschaftlichen Fakultät der

Gottfried Wilhelm Leibniz Universität Hannover

zur Erlangung des Grades

Doktorin der Naturwissenschaften (Dr. rer. nat.)

genehmigte Dissertation

von

Ute Dietrich (geb. Bauer), M. Sc.

2017

ABSTRACT

This study aims to improve the understanding of mechanisms controlling water-related fatigue and sub-critical crack growth in technical glasses. One borosilicate base composition (16 mol% Na_2O, 10 mol% B_2O_3 and 74 mol% SiO_2) and three soda-lime borate base compositions NCBx (x = 5, 15 and 25), corresponding to x Na_2O, 10 CaO, 90-x B_2O_3 (in mol%) were chosen to study the impact of water in these systems. Glasses with water contents between 0.5 and 8.0 wt.% H_2O (2-22 mol% H_2O) were produced by high-pressure synthesis (500 MPa, 1423 K) in an Internally Heated Pressure Vessel (IHPV). Hydrous glasses with water contents <0.5 wt.% were synthesized by water steam bubbling at 0.7 MPa pressure and 1753 K.

The structure of hydrous borate- and borosilicate glasses was characterized in terms of water speciation, boron speciation as well as Q^n-speciation (n= number of non-bridging oxygen associated with SiO_4 tetrahedra) using Infrared-, ^{11}B MAS NMR- (Magic Angle Spinning Nuclear Magnetic Resonance) and Raman spectroscopy. The glass transition temperature (T_g) and viscosity as well as internal friction have been analyzed by differential thermal analysis (DTA), sphere penetration viscometry and dynamic mechanical analysis (DMA) to investigate the effect of water on relaxation processes in borate- and borosilicate glasses.

Water, present as hydroxyl groups was found to be increasingly stabilized in the borate glasses compared to borosilicate glasses. While only ~1 wt.% of molecular water is present at ~7.5 wt.% H_2O in borate glasses, molecular water becomes the dominating species above 7 wt.% H_2O in the borosilicate glass.

The effect of water on decreasing T_g in borosilicate glasses was found to be more pronounced at low water contents (<2 wt.%). In borate glasses the decrease was observed to be less drastic and more continuously. Thus, higher rigidity and strong connections of the network in silicon-based systems are suggested to be more affected by depolymerization upon water addition. The model of the reduced glass transition temperature (Tomozawa et al., J. Non. Cryst. Solids. 56 (1983) 343–348) allows the estimation of the individual influence of water species and the dry glass on T_g. Whereas molecular water only plays a minor role in reducing T_g, the influence of dissociated water was found to be up to ca. 20 times stronger in the investigated glasses.

Depolymerization of the borosilicate network structure by incorporation of water is also observed in the frequency region of Si-O stretching in Raman spectra. The peak area of the modes associated with Q^2 species increases from 5.5 % in the dry borosilicate glass to 17% for glasses with 8 wt.% H_2O. Concomitantly, Q^4 species decrease to the same degree. On the other hand, the area assigned to Q^3 species remains constant upon water addition. Contributions of species with and without bonding to BO_4 tetrahedra can be separated in the Raman spectra for both Q^2 and Q^3 species. Comparison to the NMR data suggests that BO_4 tetrahedra are preferentially connected with Q^3 species, stabilizing these species against depolymerization.

Comparison of the influence of water and alkalis on the boron speciation show a strong increase of tetrahedrally coordinated boron with increasing alkali content in the case of borate glasses. In contrast, an effect of water was observed to be approximately ten times lower. In hydrous borosilicate glasses the influence of water is more pronounced. The addition of ~ 3 wt.% H_2O increases the amount of four-fold coordinated boron from 87% in the dry glass to 99% in the hydrous glass.

Keywords: Glass structure, H_2O speciation, boron speciation, relaxation

ZUSAMMENFASSUNG

Ziel dieser Arbeit ist es, das Verständnis über die Mechanismen zu verbessern, die bei wasserbedingter Materialermüdung und beim subkritischen Risswachstum in technischen Gläsern ein Rolle spielen. Eine Borosilikat Basiszusammensetzung (16 mol% Na_2O, 10 mol% B_2O_3 and 74 mol% SiO_2) und drei Kalk-Natron Borat Basiszusammensetzungen NCBx (x = 5, 15 and 25) wurden ausgewählt um den Einfluss des Wassers in diesen Systemen zu untersuchen. Gläser mit Wassergehalten zwischen 0.5 und 8.0 wt.% H_2O (2-22 mol% H_2O) wurden durch Hochdruck-Synthese (500 MPa, 1423 K) in einer intern beheizten Gasdruckanlage (IHPV) hergestellt. Wasserhaltige Gläser mit <0.5 wt.% H_2O wurden durch Wasserdampfeinleitung bei 0.7 MPa und 1753 K hergestellt.

Die Struktur der wasserhaltigen Borat- und Borosilikatgläser wurde hinsichtlich der Wasserspeziation, Borspeziation, sowie Q^n-Speziation (n=Anzahl der nicht-brückenbildenden Sauerstoffatome in einem SiO_4 Tetraeder) mittels Infrarot-, ^{11}B MAS NMR- (Magic Angle Spinning Nuclear Magnetic Resonance) und Raman Spektroskopie charakterisiert. Die Glasübergangstemperatur (T_g), Viskosität, sowie die innere Reibung wurden mit Differentieller Thermischer Analyse (DTA), Kugel-Eindruck Viskometrie und Dynamisch-Mechanischer Analyse (DMA) ermittelt, um den Effekt von Wasser auf Relaxationsprozesse in Borat- und Borosilikatgläser zu untersuchen.

Wasser in Form von OH Gruppen wird in Boratgläsern im Vergleich zu Borosilikaten zunehmend stabilisiert. Während nur ~1 wt.% des molekularen Wassers bei 7.5 wt.% H_2O in Boratgläsern vorhanden ist, ist das molekularen Wassers die dominierende Spezies bei Wassergehalten über 7 wt.% in Borosililkatgläsern. Der Effekt von Wasser auf die Abnahme von T_g in Borosilikatgläsern ist bei niedrigen Wassergehalten (<2 wt.%) stärker ausgeprägt. In Boratgläsern hingegen ist die Abnahme von T_g weniger drastisch und kontinuierlicher. Dies deutet darauf hin, dass die Depolymerisierung im Zuge der Wasserzugabe einen stärkeren Einfluss auf die in silikatischen Systemen ausgeprägtere Starrheit und Bindungsstärke des Netzwerkes hat. Das Model der Reduzierten Glasübergangstemperatur (Tomozawa et al., J. Non. Cryst. Solids. 56 (1983)) erlaubt die Abschätzung des individuellen Einflusses der Wasserspezies und des trockenen Glasses auf T_g. Während molekulares Wasser nur eine untergeordnete Rolle bei der Absenkung von T_g spielt, ist der Einfluss der dissoziierten Wasserspezies in den untersuchten Gläsern bis zu 20 mal stärker.

Depolymerisierung der Borosilikatnetzwerkstruktur durch den Einbau von Wasser wird auch in dem Frequenzbereich der Si-O Streckschwingung in Raman-Spektren beobachtet. Die Peakfläche die mit Schwingungen der Q^2 Spezies assoziiert wird nimmt von 5.5% im trockenen Borosilikatglas auf 17% im Glas mit 8 wt.% H_2O zu. Gleichzeitig nimmt im selben Maße die Q^4 Spezies ab. Hingegen bleibt die Fläche die den Q^3 Spezies zugeordnet ist konstant. Beiträge von Spezies mit und ohne Bindungen zu BO_4 Tetraedern können in den Raman-Spektren für Q^3 und Q^2 separiert werden. Ein Vergleich mit den NMR Daten deutet auf eine bevorzugte Bindung von BO_4 Tetraedern mit Q^3 Spezies hin, wodurch diese Spezies gegenüber der Depolymerisierung stabilisiert ist.

Der Vergleich des Einflusses von Wasser und Alkalien auf die Borkoordination zeigt einen starken Anstieg des tetraedrisch koordinierten Bors mit zunehmendem Alkaligehalt in Falle der Boratgläser. Im Gegensatz dazu wurde ein ungefähr 10 mal kleinerer Effekt des Wassers beobachtet. In den wasserhaltigen Borosilikatgläsern ist der Einfluss des Wasser stärker ausgeprägt. Die Zugabe von ~3 wt.% H_2O führt zu einer Zunahme des vier-fach koordinierten Bors von 87% im trockenen Glas auf 99% im wasserhaltigen Glas.

Schlagworte: Glas Struktur, H_2O Speziation, Bor Speziation, Relaxation

DANKSAGUNG

TABLE OF CONTENTS

Preface

Boron-bearing oxide glasses were intensively investigated in the past because of their various technical applications. For instance, borosilicate glasses are applied as optical glasses or as container material of nuclear waste. Properties of such glasses are e.g. high chemical durability and thermal-shock resistivity.

One special feature of such glasses is the so called boron anomaly, which describes the property of boron to change its coordination number (CN) from 3 to 4 and back to 3 surrounding oxygens in response to the addition of network modifiers as alkalis or alkaline-earth oxides. This trend reflects the preservation of a completely interconnected framework at low contents of network modifiers, and the formation of non-bridging oxygens (NBO) at high contents of network modifiers [1,2].

Temperature and pressure were also found to be crucial parameters affecting the boron coordination number [3–6]. The decrease in boron coordination number with higher fictive temperatures (T_f) due to faster cooling is stronger pronounced for glasses containing significant contents of NBOs, i.e. at high alkali content [4,7–9].

Isostatic pressurization above the glass transition temperature only weakly increases the fraction of tetrahedral coordinated boron in soda-lime borate glasses, i.e. by ~ 2.5% from 0.1 to 600 MPa [10]. Consistent with these findings in pure B_2O_3 glass the increase of BO_4 upon pressurization to 6 GPa is 27 % [6]. It has been found that relaxation of boron speciation below the ambient glass transition temperature (0.9 T_g) in compressed soda-lime borate glasses is decoupled from changes in macroscopic glass properties such as hardness, refractive index and density [13].

In contrast to effects of temperature, pressure and network modifier almost nothing is known about the role of structural bonded water on the boron speciation. A crucial question is,

whether the influence of H_2O on borate and borosilicate glass structure is similar to other network modifiers, in particular alkali oxides. For silicate and aluminosilicate glasses it was found that the effect of water and alkali oxides on melt properties such as viscosity is rather similar [11,12].

Infrared spectroscopy gives evidence that two main water species are present in glasses: as molecular water (H_2O_{mol}) and as water dissolved in form of OH groups [14,15,16,17]. In silicate and aluminosilicate glasses the strongest decrease of T_g occurs in the range of low water contents ($\leq$ 2 wt.% H_2O), where OH groups are the predominant water species. At water contents above ~3 wt.% the content of hydroxyl groups apparently level off and the amount of molecular water rises strongly. This trend is a consequence of the decrease in fictive temperature of the glass with increasing water content, i.e. water speciation is frozen in at different temperatures.

Glasses of technical relevance typically contain much less than one weight percent H_2O (e.g. < 0.1 wt.% H_2O in silicate and borosilicate < 1 wt.% H_2O in borate and phosphate glasses). High water contents of several weight percent are common in natural systems such as volcanic glasses, but are usually of minor importance for industrial glass production. However, such high water contents may become of interest for water-related fatigue of glasses since water easily can be absorbed and accumulated for instance at crack tips or near the glass surface and lead to corrosion.

Sub-T_g relaxation processes play a major role for crack propagation, but are poorly investigated in glasses with high contents of structural bonded water [13].

In contrast, network relaxation in the range of T_g is well investigated for a wide range of hydrous and anhydrous silicate and aluminosilicate glasses [11,12,14]. Considerable less information is available about relaxation processes in the range of glass transition for hydrous boron-bearing glasses.

2

Free and forced oscillation methods can be used (mostly torsion and bending of glass beams) to get insights into relaxation of the glass network and fast sub-T_g relaxation modes. These modes are often denoted as α-, β-, and γ- relaxation in the order of decreasing temperature [18,19]. Whereas the interpretation of α- and γ- relaxation modes is quite clear, the mechanisms responsible for $β$-relaxation is still under debate.

$α$-relaxation is characterized by a broad internal friction peak, dominating the mechanical loss spectra, and large activation energies ($E_α ≈ 419$-502 kJmol^{-1}) [20] which are in agreement with those of viscosity at T_g. The interpretation of $β$-relaxation phenomena is still controversial and has been assigned to several different mechanisms including movements of non-bridging oxygens (NBOs) in alkali silicate glasses [19,20], a cooperative movement of equal or dissimilar mobile species such as alkali or alkaline-earth ions [21–26] or movements within a cluster of alkaline-earth cations [19]. In water-poor (≤ 0.3 wt.% H_2O) phosphate, borate and silicate glasses $β$-relaxation was correlated with cooperative motions of alkali ions and neighboring protons [27–32]. $β$-relaxation phenomena in glasses with higher water contents, where significant amounts of molecular water is present are rarely investigated. In the study of Reinsch et al. [13] two distinct $β$-relaxation peaks in mechanical loss spectra were attributed to dynamics of OH groups and molecular water in hydrated silicate glasses (≤ 1.9 wt% H_2O). The relaxation mode of H_2O_{mol} was found to be faster compared to OH groups and is probably caused by jumps of H_2O molecules between adjacent cavities in the network. It is worth noting that rotation of H_2O molecules around their bisector axis, another low temperature process in hydrous glasses identified by NMR spectroscopy and quasielastic neutron scattering, is too fast to contribute to the $β$-relaxation peak [33,34].

The γ- relaxation mode at temperatures $<$ 373 K ($T_γ/T_α ≈ 0.38$) [35] is attributed to the motion of alkalis, since the range of activation energies (E$_γ ≈ 63$-105 kJmol^{-1}) [36] resemble activation energies of alkali diffusion (63- 84 kJmol^{-1}) [20].

The thesis is subdivided into four chapters. In the first chapter the structure of three soda-lime borate glasses in terms of water speciation and boron speciation is characterized. The second chapter focuses on α-relaxation processes of the hydrous borate glasses. The structure and relaxation mechanisms of hydrous borosilicate glasses is investigated in the third and fourth chapter respectively.

Chapter 1A[1]

Water- and Boron Speciation in Hydrous Soda-Lime Borate Glasses

Abstract

The structural investigation of hydrated borate glasses provides new insights on the influence of water on boron speciation using spectroscopic methods. In the present study three soda-lime borate glasses (NCBx with x = 5, 15 and 25 corresponding to x Na_2O, 10 CaO, 90-x B_2O_3 in mol%) were prepared with water contents up to 8 wt.%. The water speciation in the glasses was derived by near-infrared (NIR) spectroscopy while boron speciation was investigated by ^{11}B MAS-NMR (Magic Angle Spinning - Nuclear Magnetic Resonance). For the three glasses effective molar absorption coefficients were determined experimentally for the bands at 5200 cm^{-1} and 4600 cm^{-1}, corresponding to combination modes of H_2O molecules and OH groups, respectively. In contrast to silicate glasses, in which at most ~2 wt.% H_2O are dissociated to OH groups, the amount of dissociated H_2O may even exceed 5 wt.% in borate glasses. The fraction of tetrahedral to total boron ($N_4 = BO_4/ BO_4 + BO_3$) is predominantly controlled by the ratio of $Na_2O + CaO/B_2O_3$, but only weakly affected by the water content of the glasses. When increasing the H_2O content from 0 to 8 wt.%, N_4 increases from 25% to 26% for NCB5 and from 42% to 47% for NCB25 glasses.

_____

1. Introduction

Boron-bearing oxide glasses were intensively investigated in the past because of their various technical applications. One special feature of such glasses is the so called boron anomaly, which describes the property of boron to change its coordination number (CN) from 3 to 4 and back to 3 surrounding oxygens in response to the addition of network modifiers as alkalis or alkaline-earth oxides. This trend reflects the preservation of a completely interconnected framework at low contents of network modifiers, and the formation of non-bridging oxygens (NBO) which can be expressed by the equilibrium reaction (1) at high contents of network modifiers [1,2].

$$BO_4 = BO_3 + NBO \tag{1}$$

In binary borate glasses ($x\ M_2O \cdot 1\text{-}x\ (B_2O_3)$) it was observed that the increase of the fraction of tetrahedral coordinated boron occurs up to $x = 0.33\text{-}0.43$ [37–39], depending on the type of cation [38,39]. It was found that lithium is more efficient in charge compensating the BO_4-units than other alkalis, due to its small size [38,39].

Temperature and pressure were also found to be crucial parameters affecting the boron coordination number [3–6]. With increasing temperature the reaction in Eq.1 shifts to the right. The decrease in boron coordination number with higher fictive temperatures (T_f) due to faster cooling is stronger pronounced for glasses containing significant contents of NBOs, i.e. at high alkali content [4,7–9].

Isostatic pressurization above the glass transition temperature only weakly increases the fraction of tetrahedral coordinated boron in soda-lime borate glasses, i.e. by ~ 2.5% from 0.1 to 600 MPa [10]. Consistent with these findings in pure B_2O_3 glass the increase of (BO_4) upon pressurization to 6 GPa is 27 % [6]. It has been found that relaxation of boron speciation below the ambient glass transition temperature (0.9 T_g) in compressed soda-lime borate

glasses is decoupled from changes in macroscopic glass properties such as hardness, refractive index and density [13].

In contrast to effects of temperature, pressure and network modifier almost nothing is known about the role of structural bonded water on the boron speciation. A crucial question is, whether the influence of H_2O on the borate glass structure is similar to other network modifiers, in particular alkali oxides. For silicate and aluminosilicate glasses it was found that the effect of water and alkali oxides on melt properties such as viscosity is rather similar [11,12].

Infrared spectroscopy gives evidence that two main water species are present in glasses: molecular water and OH groups [14–16,40]. OH groups are formed in the melt by the interaction of water molecules with the network and anhydrous bridging oxygen (BO), as represented in Eq. 2.

$$H_2O_{(melt)} + O_{(melt)} \leftrightarrow 2\, OH_{(melt)} \tag{2}$$
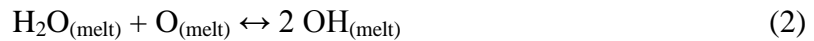
Accompanied with this reaction is a depolymerization of the network. Assuming ideal mixing of $H_2O_{(melt)}$, $O_{(melt)}$, and $OH_{(melt)}$, the equilibrium constant K for Eq. 2 is

$$K = \frac{[OH]^2}{[H_2O] \cdot [O]} \tag{3}$$

where square brackets signify mole fractions on a single oxygen basis, e.g. [14,15,17,40]. A basic assumption for the interpretation of the data is that the measured speciation in glasses at room temperature correspond to the equilibrium water speciation in the melt, which was frozen in at T_g [41,42].

Quantification of hydrous species can be obtained with the Lambert-Beer law after measuring the peak heights of the combination of stretching and bending vibration bands of OH groups and molecular water, respectively. Since the linear molar absorption coefficients of the bands are strongly dependent on the glass composition [43–45] and no such data for soda-lime borate glasses is available, a calibration of near-infrared spectroscopy was performed for the different borate glasses under investigation.

Information on water speciation in water-rich glasses of technical interest are rare [46–48]. To incorporate several wt.% of water into glasses pressures in the order of several 100 MPa are required. Such high volatile contents facilitate the investigation of water-related processes such as diffusion and relaxation mechanisms or the study of glass properties as density, elastic moduli, refractive index, crack initiation probability, hardness etc.

2. Experimental and Analytical Methods

2.1 Starting Materials

The three soda-lime borate glasses with nominal compositions NCBx (x = 5, 15 and 25), corresponding to x Na_2O, 10 CaO, 90-x B_2O_3 (in mol%), were prepared from Na_2CO_3, $CaCO_3$ and H_3BO_3 powders. The mixtures were melted at 1373 K for only 10 min in a covered Pt-crucible in order to avoid a loss of alkalis or boron during the high temperature dwell. Improved glass homogeneity was achieved by crushing the glass and subsequent repeated melting. By quenching the melts in air on a brass plate clear glass products were produced.

The compositions of the glasses were analyzed by the inductively coupled plasma optic emission spectroscopy (ICP-OES, 715-ES VARIAN). From each starting material ~ 100 mg was dissolved by microwave digestion using 3 ml 65% HNO_3 and 2 ml H_2O. The ICP-OES

analyses of the sodium and calcium contents were verified using electron micro probe analyses (EMPA). On each glass sample 60-100 analyses were performed using a Cameca SX-100 microprobe. Only the Na_2O and CaO contents could be measured with the microprobe, because boron is too light for this method. In the case of EMPA measurements, the B_2O_3 content of the glasses was estimated by difference of the total of measured oxides to 100 wt.%. Measurement conditions included a beam current of 15 nA, acceleration voltage of 15 kV, defocused beam of 5 µm spot size, and counting times of 10 to 20 s. The programmed matrix correction "PAP" according to Pouchou and Pichoir [49], was used to correct the measured oxide content. The concentrations of sodium, calcium and boron oxides are given in Tab.1. A good agreement between the analysis obtained by ICP-OES and EMPA was obtained (Tab. 1).

Tab.1 Chemical composition of starting material of soda-lime borate glasses oxide in mol% normalized to 100

	Na_2O	CaO	B_2O_3	
NCB5	5.42	10.24	84.34	OES
	5.57 (0.35)	10.06 (0.24)	84.37[*]	EMPA
NCB15	15.26	10.04	74.71	OES
	15.18 (0.54)	10.33 (0.28)	74.49[*]	EMPA
NCB25	24.90	9.95	65.15	OES
	25.96 (0.61)	10.37 (0.25)	63.66[*]	EMPA

Notes. EMPA analyses are based on 100 measurements (NCB5 and NCB25) and 60 measurements (NCB15). 1 standard deviation is given in parentheses. [*] Boron oxide content is calculated by difference based on Na_2O and CaO contents. OES data are based on single measurements.

2.2 Hydrous and Compressed Glasses

For syntheses of hydrous glasses containing up to 8 wt.%, glass powder and distilled water were filled stepwise in turn in a platinum capsule (diameter: 6 mm, length: 25-30 mm) to facilitate homogeneous distribution of water in the glass. To produce anhydrous compressed glasses only the starting glass powders were loaded into platinum capsules. By subsequent compaction of the material in the capsule using a steal piston a cylindrical shape of glass bodies was achieved. After sealing the capsules with a PUK welding device (PUK[3] professional plus, Co. Lampert), possible weight loss due to a leakage were checked by placing the capsules in a drying furnace at 373 K.

All syntheses were performed in an internally heated pressure vessel (IHPV) at 500 MPa and 1423 K for 14-20 hours using argon as pressure medium. A detailed description of the apparatus is given in Berndt et al. [50]. For all syntheses similar pressure was chosen to eliminate pressure induced differences in the glass structure and properties. For each run two capsules were placed in the hot spot of the sample holder between the two furnace-controlling K-type thermocouples (Ni-CrNi). The temperature of the samples was controlled by a third thermocouple located in the middle of the hot spot zone. The maximum variation in temperature was $\pm$ 10°C and pressure accuracy is within $\pm$ 50 bars. In order to preserve pressure-induced structural changes and to avoid water loss of the glasses, samples were isobarically quenched (by switching of the furnace) using an automatic pressure controller. This leads to a cooling rate of ~ 200 Kmin^{-1} through the glass transition range.

All glass cylinders after high pressure synthesis were clear and no crystals or bubbles could be observed. For IR and KFT measurements glass pieces were cut from each end of the glass body to test the homogeneous distribution of water (Tab. 2). Exposure to water was avoided and oil was used for sawing and polishing of the samples, e.g. for preparation of thin-sections. All samples were stored in a desiccator with P_2O_5 as desiccant.

2.3 IR Spectroscopy

Infrared absorption spectra were recorded in the mid-infrared to investigate network vibrations and fundamental OH-stretching vibrations, and in the near-infrared to study combination modes of hydrous species.

Mid-infrared (MIR) spectra were collected in the range of 370 to 5000 cm^{-1} using a Fourier Transform Infrared (FTIR) spectrometer (Bruker Vertex 80v) with a globar light source, a KBr beamsplitter and a pyroelectric deuterated, L-alanine doped triglycerine sulfate (DLaTGS) detector. The powdered sample was embedded into a KBr matrix (2.5 mg sample in 200 mg KBr) and measured relatively to a KBr pellet without sample to probe the contribution of contamination of KBr to the spectrum in the range of OH stretching vibrations. The spectral resolution was 2 cm^{-1} and 32 scans for each spectrum were accumulated.

Near-infrared (NIR) spectra in the range of 2000 - 8000 cm^{-1} were collected using a FTIR spectrometer (Bruker IFS88) coupled with an IR microscope (Bruker IR scope II) equipped with a tungsten lamp as light source, a CaF_2 beam splitter and a mercury-cadmium-tellurium (MCT) detector. The spectral resolution was 4 cm^{-1}, 100 scans for each spectrum were accumulated. A slit aperture between the objective and the detector was used to limit the analyzed sample volume. In the focus plane, the area selected by the slit was typically 100 x 100 μm^2. At least three NIR-spectra for each sample were collected to check the reproducibly of the collected spectra and the homogeneity of water distribution in the glass. The thickness of the double polished glass sections was measured using a digital micrometer (Mitutoyo) with a precision of ± 2 µm. The average thickness of each sample is listed in Tab. 2.

2.4. Karl-Fischer Titration

The total water content of the glasses was determined using Karl-Fischer Titration (KFT). The sample material, usually a 10-20 mg glass piece, is rapidly heated up (within 4 min) to ~1300°C and the thermal released water is measured [43,47,51–53]:

$$H_2O + SO_2 + I_2 = 2HI + SO_3 \tag{3}$$
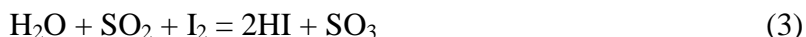
HI and SO_3 are bonded by reagents in the titration solution (methanol, pyridine derivates), so that the reaction proceeds quantitatively to the right hand side. The amount of I_2 required for the reaction is generated electrochemically at the anode in the titration cell.

$$I^- = \frac{1}{2}I_2 + e^- \tag{4}$$

The reacting quantity of H_2O is directly correlated to the quantity of electrons consumed by reaction (4). Because 1 mg H_2O correspond to 10.71 coulombs no standards are needed to calibrate the method. Detailed description of KFT analysis is given in [43,47,51–53].

It should be noted that some borate glasses tend to release the H_2O explosively upon heating. This was especially the case for samples containing high amounts of water. In that case some glass fragments may eject from the heated part of the sample holder, which would result in an incomplete dehydration. To depress ejection of glass fragments, samples were placed in platinum capsules which were tightly bended on top. Additionally, the apparatus was carefully checked after each analysis for ejected particles.

2.5 DTA Measurements

The glass transition temperature, T_g, was measured by differential thermal analysis (DTA) in air using glass pieces or powdered glass of 15 - 20 mg placed in Pt-crucibles (thermobalance TAG 24, Setaram, Caluire, France). For each sample four heating and cooling cycles with 10 Kmin^{-1} were performed. The maximum temperature did not exceed T_g by more than 50 K. The first cycle represents the fictive temperature T_f of the glasses, since the cooling history of the samples reflects the status of quenching after IHPV synthesis. The following three cycles were used for the determination of T_g. According to Mazurin [54,55] the onset of the endothermic step in the DTA curve was used to determine T_f and T_g. The average T_g values for all investigated glasses are shown in Tab. 2. T_f values were found to be a few degrees higher than the determined T_g values. The deviation originates from differences in cooling rate and fictive pressure between sample synthesis and DTA measurements.

In order to register a possible loss of water of high water-bearing glasses, the thermal gravimetric (TG) signal was simultaneously recorded during DTA measurement. Additionally, a mass spectrometer (Balzers Quadstar 421) was used for analysis of evolved gases, coupled to the DTA by a heated (453 K) quartz glass capillary. Neither a significant mass loss nor a distinct signal for water by mass spectroscopy could be detected. The good reproducibility of T_g determination further supports a negligible water loss during the DTA procedure. The maximum error of temperature for this method is 5 K.

2.6 ^{11}B MAS NMR Experiments

All NMR spectra were recorded on a Bruker ASX 400 NMR spectrometer at room temperature. ^{11}B MAS NMR measurements were carried out at 128.38 MHz using a standard Bruker 4 mm MAS probe with sample spinning at 12.5 kHz. Solid $NaBH_4$ was used as secondary reference standard (δ_{iso} = -42.0 ppm). For the ^{11}B MAS NMR experiments, a short single pulse duration of 0.6 μs was applied to ensure homogenous excitation of the central and all satellite transitions. A recycle delay of 1 s was used, and 3200 scans were accumulated. The ^{11}B MAS NMR spectra were fitted with quadrupolar lineshapes including convolution using the DmFit 2010 program [56]. Tolerances were estimated by varying the parameters in the fit function, observing χ^2 until a distinct change of χ^2 took place.

3. Results

3.1 Glass transition

The glass transition temperatures T_g of the starting glasses synthesized at 1 atm pressure (NCB5: 718 K; NCB15: 775 K; NCB25: 761 K) are in fairly good agreement with data from Smedskjaer et al. [57] (NCB5: 708 K; NCB15: 775 K; NCB25: 764 K). The nominal composition of the glasses is identical in both studies, but different synthesis charges were used and the deviation by 10 K for NCB5 may originate from slight difference in actual composition. However, this supposition cannot be approved since no chemical data are given in [57]. The T_g values are slightly lower for nominal dry glasses synthesized at 500 MPa than for the air-melted glasses, i.e. by 13 K for NCB5, by 4 K for NCB15 and by 21 K for NCB25 (Tab. 2). The reason is a small amount of water in the high pressure glasses (~ 0.25 wt.% H_2O, see Tab. 2) which originates from water adsorbed on the powder used in the synthesis.

The glass transition temperature T_g decreases strongly upon hydration, i.e. T_g decreases for NCB5 to 526 K (4.82 wt.% H_2O), for NCB15 to 510 K (7.53 wt.% H_2O, and for NCB25 to 542 K (6.14 wt.% H_2O).

3.2 Band assignment

MIR spectra of NCB5, NCB15 and NCB25 containing 1 wt.% H_2O are shown in Fig. 1a,b. Three main groups of bands are visible in Fig. 1a. The assignment of bands below 2000 cm^{-1} follows Yiannopoulus et al. [2] and Kamitsos and Chryssikos [58]. Consistent with these papers we attribute the absorption features between 1200 and 1600 cm^{-1} to BO_3 units and bands between 750 and 1200 cm^{-1} to BO_4-tetrahedra (Fig. 1a). This interpretation is supported by the relative increase of the BO_4-related bands and a corresponding decrease of the BO_3-related bands when increasing the sodium content (Fig. 1a).

In the high frequency region of the MIR spectra we observe the main absorption band at 3440 cm^{-1} with shoulders at around 3500 cm^{-1} and around 3230 cm^{-1} (Fig. 1b). These features are attributed to OH stretching vibrations of weakly to moderately H-bonded hydrous species [17,40]. It is noteworthy that the bands in the range of OH stretching vibrations do not allow distinguishing between molecular H_2O and OH groups.
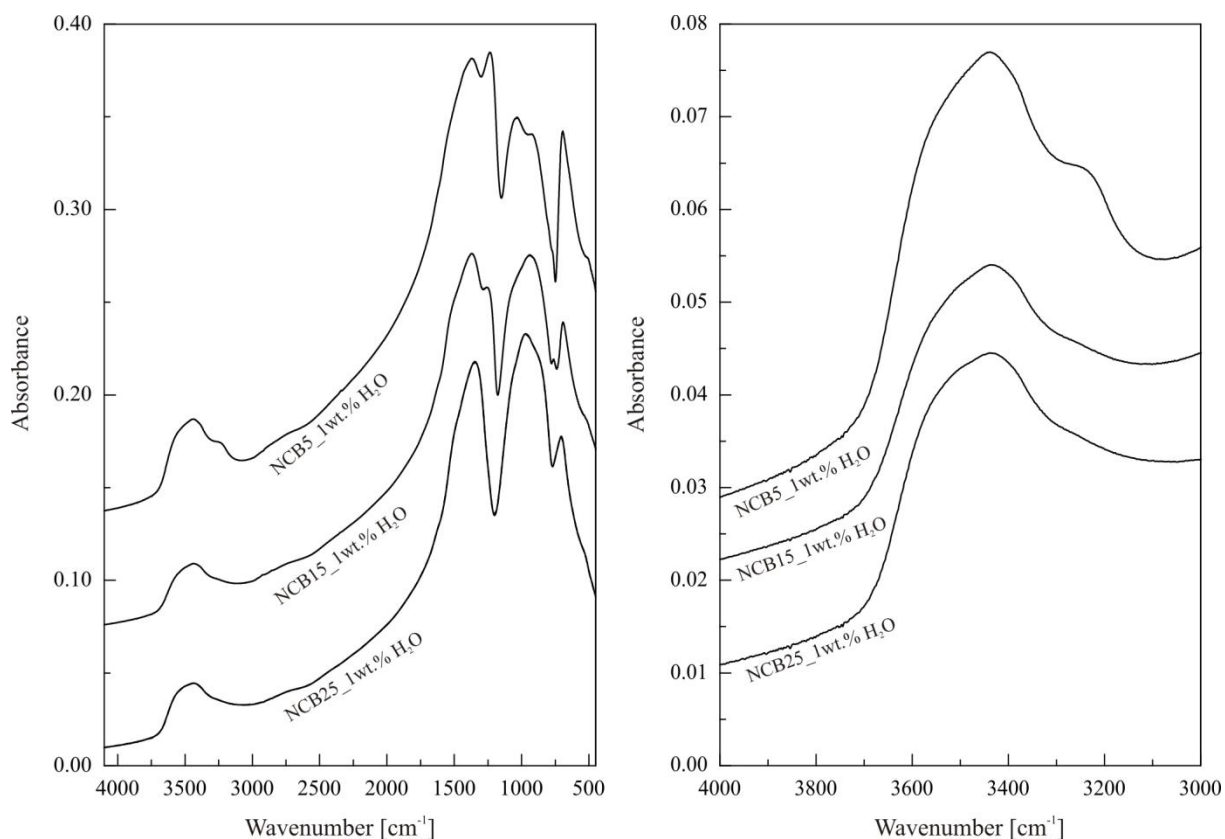
Fig. 1 a) MIR spectra of soda-lime borate glasses containing 1 wt.% H_2O. b) Frequency range of OH stretching vibrations. Spectra were shifted in intensity for clarity. The sample names include the nominal water content of the glasses.

The NIR spectra of hydrous soda-lime borate glasses containing up to 8 wt.% H_2O are shown in Fig. 2. In accordance with literature on water-bearing silicate glasses [20], the band at ~7000 cm^{-1} is assigned to the first overtone of the fundamental stretching vibrations of OH groups and H_2O molecules at ~3500 cm^{-1}.

In the frequency range between 3600-6000 cm^{-1} four main absorption features are visible. Analogue to silicate glasses [40], the band at 4100 cm^{-1} is attributed to the combination of OH stretching vibrations with a low frequent lattice vibration. Absorption bands near 4600 cm^{-1} and at 5200 cm^{-1} are assigned to the combination of stretching and bending vibration modes of terminal OH groups and of molecular water, respectively [14,16,17,40,59,60].

In general, peak intensities of the molecular water species (5200 cm^{-1}) and OH groups (4600 cm^{-1}) increases with rising total H_2O content (Fig. 2). In all three compositions molecular

water is first measurable at ~ 2 wt.% H_2O. Compared to silicate and aluminosilicate glasses, the main combination band of OH groups is shifted to higher wavenumber. Two additional adsorption features are visible in the NIR spectra of the borate glasses. A shoulder of the main OH combination band is located at ~ 4750 cm^{-1} and is most prominent in the spectrum of NCB25. With decreasing alkali content the intensity of the shoulder decreases, and this feature is invisible in NCB5 glass. In NCB5 glass a small peak is visible at 4900 cm^{-1}. With increasing Na_2O content this band becomes weaker and it almost diminishes for NCB25.

Peak positions do not noticeably vary with water content, but the sodium content causes some shift of the maxima. The position for the 4100 cm^{-1} band moves to lower wavenumber from 4123 cm^{-1} (NCB5) over 4112 cm^{-1} (NCB15) to 4105 cm^{-1} (NCB25), see Tab. 2. Additionally, with increasing sodium content a shift for the 5200 cm^{-1} peak to lower wavenumbers (NCB5: 5204 cm^{-1}; NCB25: 5170 cm^{-1}) and a shift for the 4600 cm^{-1} peak to higher wavenumbers (NCB5: 4580 cm^{-1}; NCB25: 4600 cm^{-1}) is observed.

Fig. 2. NIR spectra of hydrous soda-lime borate glasses a) NCB5, b) NCB15, c) NCB25. The spectra are normalized to the respective sample thickness of ~ 0.3 mm and are shifted in intensity for clarity. The sample names include the nominal water content of the glasses.

Tab. 2. Sample characterization and spectroscopic data of NIR measurements

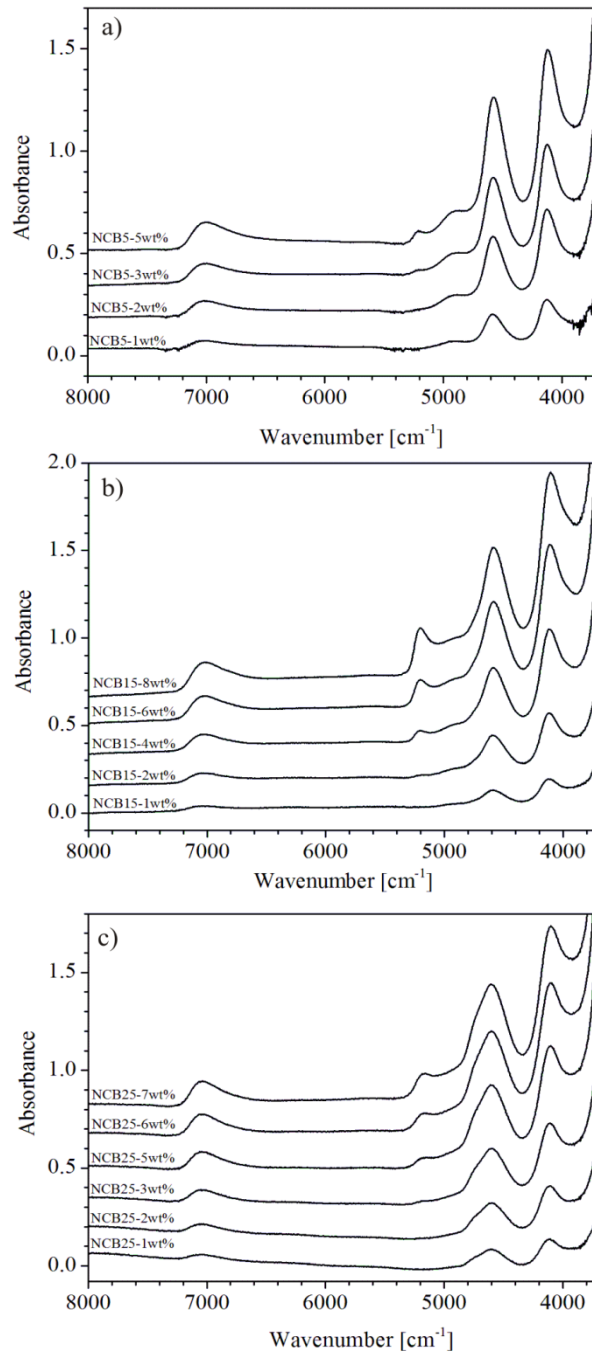|	cH$_2$O$_t$ KFT [wt.%]	T_f [K]	T_g [K]	density [g/l]	d [mm]	Peak position [cm^{-1}]	[cm^{-1}]	[cm^{-1}]	A 5200 [mm^{-1}]	A 4600 [mm^{-1}]	A 4100 [mm^{-1}]	cOH [wt.%]	cH$_2$O [wt.%]	cH$_2$O$_t$ IR [wt.%]
NCB5_dry (1atm)	-	728	718 ± 6	2133 ± 2		-	-	-	-	-	-	-	-	-
NCB5_dry (500 MPa)	-	710	697 ± 2	2241 ± 3		-	-	-	-	-	-	-	-	-
NCB5_1wt.%-I	0.96 ± 0.03	648	654 ± 2	2201 ± 4	0.2840	-	4583	4125	-	0.171	0.242	0.93 ± 0.03	-	0.93 ± 0.01
NCB5_1wt.%-II	1.03 ± 0.06				0.2880				-	0.169	0.237	0.88 ± 0.01	-	0.88 ± 0.01
NCB5_2wt.%-I	2.17 ± 0.07	-	-	2225 ± 5	0.2920	5200	4579	4125	0.005	0.363	0.497	2.02 ± 0.04	0.26 ± 0.01	2.28 ± 0.04
NCB5_2wt.%-II	1.94 ± 0.08				0.2880				0.003	0.327	0.452	2.06 ± 0.04	0.22 ± 0.01	2.28 ± 0.04
NCB5_3wt.%-I	2.93 ± 0.08	601	595 ± 6	2232 ± 4	0.3050	5205	4580	4122	0.026	0.481	0.644	2.70 ± 0.07	0.37 ± 0.01	3.07 ± 0.07
NCB5_3wt.%-II	2.84 ± 0.08				0.2970				0.014	0.435	0.584	2.57 ± 0.06	0.34 ± 0.01	2.91 ± 0.06
NCB5_5wt.%-I	4.93 ± 0.10	531	526 ± 3	2240 ± 4	0.3020	5208	4577	4120	0.055	0.715	0.950	4.31 ± 0.13	1.07 ± 0.04	5.38 ± 0.14
NCB5_5wt.%-II	4.71 ± 0.11				0.3150				0.048	0.675	0.896	3.97 ± 0.12	0.90 ± 0.03	4.87 ± 0.12
NCB15_dry (1atm)	-	775	775 ± 1	2301 ± 3		-	-	-	-	-	-	-	-	-
NCB15_dry (500 MPa)	-	770	771 ± 1	2364 ± 5	0.2900	-	4601	-	-	0.008	-	0.24 ± 0.01	-	0.24 ± 0.01
NCB15_1wt.%-I	0.77 ± 0.05	-	-	2366 ± 5	0.2930	-	4588	4114	-	0.098	0.156	0.71 ± 0.01	-	0.71 ± 0.01
NCB15_1wt.%-II	0.73 ± 0.07				0.2880				-	0.094	0.161	0.77 ± 0.01	-	0.77 ± 0.01
NCB15_2wt.%-I	2.06 ± 0.07	675	671 ± 3	2351 ± 3	0.2950	5204	4588	4118	0.019	0.241	0.366	1.88 ± 0.03	0.09 ± 0.01	1.97 ± 0.03
NCB15_2wt.%-II	2.04 ± 0.08				0.2950				0.017	0.239	0.364	1.87 ± 0.03	0.09 ± 0.01	1.96 ± 0.03
NCB15_4wt.%-I	3.82 ± 0.11	608	607 ± 1	2323 ± 3	0.2950	5202	4586	4114	0.072	0.426	0.642	3.33 ± 0.08	0.33 ± 0.01	3.66 ± 0.08
NCB15_4wt.%-II	3.84 ± 0.08				0.2910				0.072	0.439	0.667	3.42 ± 0.08	0.36 ± 0.01	3.78 ± 0.08
NCB15_6wt.%-I	5.53 ± 0.12	560	552 ± 2	2290 ± 4	0.2880	5201	4583	4110	0.167	0.612	0.939	4.81 ± 0.14	0.82 ± 0.07	5.63 ± 0.16
NCB15_6wt.%-II	5.70 ± 0.11				0.2920				0.164	0.608	0.932	4.87 ± 0.15	0.81 ± 0.07	5.69 ± 0.16
NCB15_8wt.%-I	7.53 ± 0.10	509	510 ± 1	2256 ± 3	0.2900	5204	4585	4104	0.283	0.744	1.174	5.84 ± 0.25	1.40 ± 0.06	7.24 ± 0.26
NCB15_8wt.%-II	8.99 ± 0.14				0.2950				0.268	0.736	1.151	5.94 ± 0.26	1.34 ± 0.06	7.28 ± 0.26

	$c\mathrm{H_2O_t}$ KFT [wt.%]	T_f [K]	T_g [K]	density [g/l]	d [mm]	Peak position [cm^{-1}]	[cm^{-1}]	[cm^{-1}]	A 5200 [mm^{-1}]	A 4600 [mm^{-1}]	A 4100 [mm^{-1}]	cOH [wt.%]	$c\mathrm{H_2O}$ [wt.%]	$c\mathrm{H_2O_t}$ IR [wt.%]
NCB25_dry (1atm)	-	762	761 ± 1	2426 ± 2		-	-	-	-	-	-	-	-	-
NCB25_dry (500 MPa)	-	758	748 ± 1	2471 ± 3	0.3160	-		-	-	0.012	-	0.17 ± 0.01	-	0.17 ± 0.01
NCB25_1wt.%-I	1.18 ± 0.05	696	696 ± 1	2466 ± 5	0.2980	-	4604	4112	-	0.097	0.145	0.91 ± 0.01	-	0.91 ± 0.01
NCB25_1wt.%-II	1.07 ± 0.05				0.3190				-	0.102	0.152	0.89 ± 0.01	-	0.89 ± 0.01
NCB25_2wt.%-I	1.85 ± 0.07	669	666 ± 2	2464 ± 5	0.3100	-	4600	4110	-	0.182	0.273	1.53 ± 0.02	-	1.53 ± 0.03
NCB25_2wt.%-II	1.78 ± 0.08				0.2950				-	0.176	0.262	1.53 ± 0.02	-	1.53 ± 0.02
NCB25_3wt.%-I	2.68 ± 0.08	637	634 ± 2	2449 ± 3	0.2910	5179	4599	4106	0.011	0.275	0.401	2.40 ± 0.05	0.26 ± 0.01	2.66 ± 0.04
NCB25_3wt.%-II	2.75 ± 0.09				0.2950				0.015	0.283	0.414	2.37 ± 0.05	0.26 ± 0.01	2.63 ± 0.04
NCB25_5wt.%-I	4.17 ± 0.13	592	588 ± 3	2423 ± 3	0.2920	5171	4599	4103	0.052	0.424	0.625	3.55 ± 0.11	0.68 ± 0.02	4.23 ± 0.11
NCB25_5wt.%-II	4.27 ± 0.09				0.2880				0.056	0.434	0.630	3.60 ± 0.11	0.69 ± 0.02	4.29 ± 0.11
NCB25_6wt.%-I	5.30 ± 0.12	567	564 ± 3	2406 ± 3	0.2950	5170	4598	4099	0.090	0.511	0.758	4.17 ± 0.16	1.13 ± 0.04	5.30 ± 0.16
NCB25_6wt.%-II	5.11 ± 0.13				0.2900				0.090	0.515	0.765	4.24 ± 0.16	1.10 ± 0.04	5.34 ± 0.16
NCB25_7wt.%-I	6.22 ± 0.11	544	542 ± 2	2387 ± 4	0.3050	5163	4601	4101	0.129	0.579	0.871	4.56 ± 0.17	1.51 ± 0.05	6.08 ± 0.18
NCB25_7wt.%-II	6.06 ± 0.16				0.3020				0.138	0.592	0.892	4.64 ± 0.17	1.53 ± 0.05	6.17 ± 0.18

I or II at the end of the sample name refer to analysis of pieces cut from both ends of a glass cylinder. $c\mathrm{H_2O_t}$ = total water concentration determined using KFT. The fictive temperature T_f of the synthesized glasses and the glass transition temperature T_g were determined with DTA. T_g values based on the average of three heating cycles (see text for details). Standard deviation of T_g is listed. Densities were determined via the buoyancy method by measuring the sample weight in air and in ethanol. Error are ± 2 µm of thickness and ± 0.003 mm^{-1} for absorbances normalized to the sample thickness.
Peak positions are average values for each set of hydrated NCB glass sample. Estimated errors for the peak position: ± 5 cm^{-1}.

3.3 ^{11}B MAS NMR

In the NMR spectra BO$_3$ groups cause a broad quadrupolar pattern due to second-order quadrupolar interaction. The sharp Lorentzian resonance located around 0 ppm represents tetrahedral BO$_4$, with nearly no quadrupolar interaction (Fig. 3).

The spectra shown in Fig. 3 are normalized to the intensity of the BO$_4$ resonance at around 0 ppm to show differences in the shape of the spectra related to increasing H$_2$O content in the glasses. It can be observed that the intensity of the BO$_3$ resonance decreases slightly with increasing water content. This effect is most pronounced in the NCB25 glass.
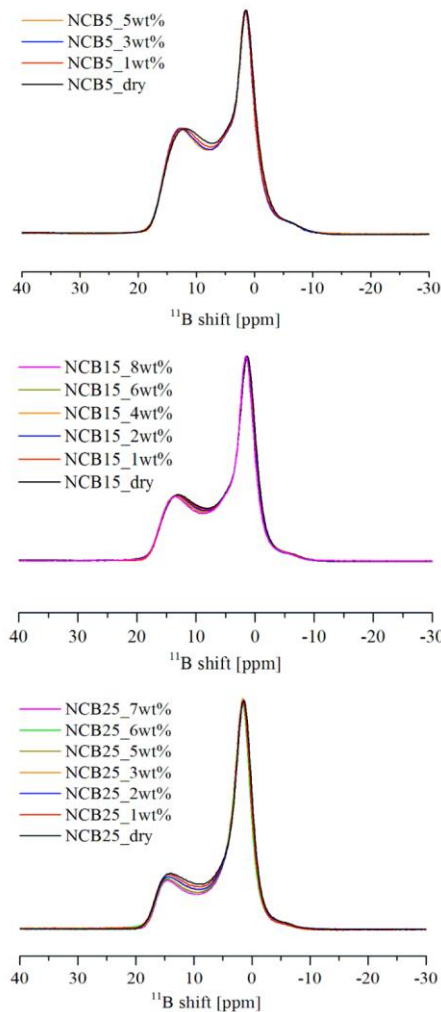
Fig. 3. ^{11}B MAS NMR spectra of hydrous borate glasses normalized to the intensity of the resonance at 0 ppm (BO$_4$).

4. Discussion

4.1 Analyses of Band Structures in the Near-Infrared

A question is whether the bands at 4750 and 4900 cm^{-1} originate from OH groups or H_2O molecules. To answer this question the spectra were normalized to the peak height of the 4600 cm^{-1} band facilitating the determination of differences in peak shapes (Fig. 4). Spectra show broadening of the bands at 4100 cm^{-1} and 4600 cm^{-1} with increasing H_2O content, in particular for NCB15 and NCB25. It is obvious that the intensities of neither the band at 4750 cm^{-1} nor the band at 4900 cm^{-1} correlate to the molecular H_2O band at 5200 cm^{-1}. Thus, we conclude that both bands represent OH groups bond to boron.
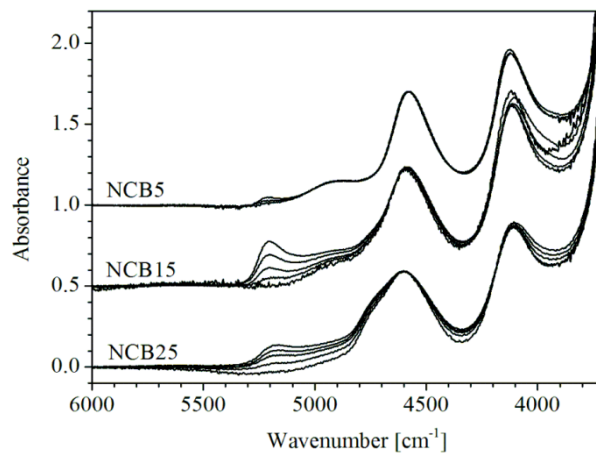
Fig.4. NIR spectra of hydrous NCB5, NCB15 and NCB25 glasses, normalized to same peak height at 4600 cm^{-1}.

The NIR spectra of the borate glasses show similar features as hydrous boron containing silicate glasses reported in the studies of Romano et al. [60] and Schmidt et al. [59]. In the latter study a shoulder at ~ 4650 cm^{-1} on the high frequency wing of the main OH combination band in the system $NaAlSi_3O_8$-B_2O_3-H_2O was assigned to BO_3-OH. Arguments for doing so are the increase of intensity of the shoulder with increasing boron content and the dominance of trigonal boron (92-98%) indicated by ^{11}B-NMR spectroscopy.

On the other hand, in our glasses the MIR spectra are more consistent with an assignment of the band near 4600 cm^{-1} to tetrahedral boron. This peak can be assigned to a combination of the fundamental OH stretching vibration at 3500 cm^{-1} with a lattice vibration near 1100 cm^{-1}, where tetrahedral coordinated boron is typically observed. In doing so, one need to take into consideration that the combination bands originate mainly from weakly H-bonded hydrous species, i.e. contributions of the fundamental OH stretching vibration bands at high wavenumbers [61]. For instance, for soda lime silicate and alkali silicate glasses OH vibration modes at wavenumbers >3400 cm^{-1} are predominantly represented in the NIR spectra [46,61,62]. Hydrous glasses of the join $NaAlSi_3O_8$ - $NaBSi_3O_8$ show a peak at ~ 4750 cm^{-1} which was attributed to BO_4-OH since ^{11}B-NMR spectroscopy point to the dominance of tetrahedral boron in these glasses [59]. In our soda-lime borate glasses a shoulder of the main OH combination peak is developing with increasing network modifier content (from NCB5 to NCB25) at same wavenumber (Fig. 1). The correlation to alkali content supports the assignment of this band to BO_4-OH, consistent with the borosilicate glasses of [35]. In that case MIR spectra are not suitable to distinguish whether OH groups are bond to BO_3 or BO_4. A network vibration near 1200 cm^{-1} (between the regimes of BO_4 units and BO_3 units) would be expected to combine with the fundamental OH stretching mode near 3550 cm^{-1} to yield a wavenumber of ~ 4750 cm^{-1}.

In agreement with [35] the band at 4900 cm^{-1}, which grows with BO_3 abundance, is assigned to vibrations of BO_3-OH. This is also supported by the MIR spectra, i.e. the band 4900 cm^{-1} is interpreted to be a combination excitation of the OH stretching vibration band at ~ 3500 cm^{-1} and vibration modes of BO_3 units at ~ 1400 cm^{-1}.

4.2 Constraints for Spectra Evaluation

As discussed in the study of Withers and Behrens [63] on aluminosilicate glasses the choice of baseline is decisive for the determination of linear molar absorptions coefficients and hence for the calculation of water speciation. It is crucial that the definition of the baseline needs to have a high reproducibility. This includes that clear constraints are given to avoid subjective spectra evaluation. For instance, a flexi-curve baseline for our spectra would be heavily influenced by the choice of points to construct the baseline and it may be difficult to transfer the baseline from one spectrum to another.

The baseline chosen for our soda-lime borate glasses is defined by the extension of the flat absorption range between 6000 and 5300 cm^{-1} to 3500 cm^{-1}. The flank of the 3500 cm^{-1} peak is very steep so that it does not affect the spectrum beyond the maximum of the 4100 cm^{-1} band (Fig. 5). The baseline was found to have a high reproducibility for both low and high water bearing glasses. Since the largest extrapolation of the linear baseline is required for the 4100 cm^{-1} band, the derived absorbances have the largest error for this band.

Especially the 4900 and 4750 cm^{-1} peaks are strongly affected by overlapping with the peaks at 5200 and 4600 cm^{-1}, which make it difficult to determine the respective peak intensities. Hence, quantitative evaluation was only performed for the bands at 4100, 4600 and 5200 cm^{-1}, indicated by vertical lines in Fig. 5.
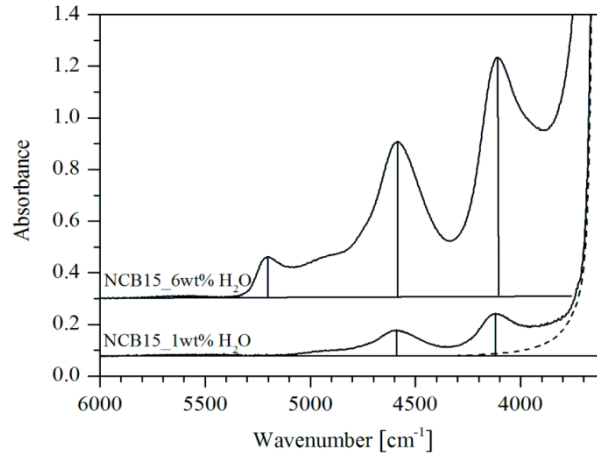
Fig. 5 NIR spectra of hydrous NCB15 glasses. Solid horizontal lines show the applied baseline chosen for these spectra. The band at 3400 cm^{-1} does not influence the combination vibrations as illustrated by the dashed line in the spectra. Solid vertical lines represent the wavenumber of peak maxima which were used for quantification of hydrous species ($\sim$ 4600 cm^{-1} for OH; $\sim$ 5200 cm^{-1} for H_2O) and total water ($\sim$ 4100 cm^{-1}).

4.3 Evaluation of the 4100 cm^{-1} Peak

The absorbance of the 4100 cm^{-1} peak scaled to sample thickness and density is proportional to H_2O content (measured with KFT) for NCB5, NCB15 and NCB25 (Fig. 6). This implies that OH groups as well as H_2O molecules contribute to this band. As visible in Fig. 6 the regression lines do not pass through the origin. This is probably due to the extrapolation of the linear baseline towards lower wavenumber. However, the offset is only marginal, despite the band at 4100 cm^{-1} is very close to the fundamental OH stretching mode at around 3500 cm^{-1}. This supports the assumption that the steep flank of the fundamental OH stretching bands does not noticeably affect the 4100 cm^{-1} band at its maximum.

The molar absorption coefficient for the band at 4100 cm^{-1} can be derived from the modified Lambert Beer law [63]:

$$\frac{1802 \cdot A_{4100}}{d \cdot \rho} = \varepsilon_{4100} \cdot cH_2O_{(t)} \tag{5}$$

where ε_{4100} is the linear molar absorption coefficient in $L \cdot mol^{-1} \cdot cm^{-1}$, $cH_2O_{(t)}$ is the total water content of the glasses measured with KFT, A_{4100} is the absorbance (peak height), ρ is the density in g/L and d is the sample thickness in cm. From the slopes given by Fig. 6 the following linear molar absorption coefficients ε_{4100} were obtained: (1.47 ± 0.07) $L \cdot mol^{-1} \cdot cm^{-1}$ for NCB5, (1.23 ± 0.03) $L \cdot mol^{-1} \cdot cm^{-1}$ for NCB15 and (1.03 ± 0.03) $L \cdot mol^{-1} \cdot cm^{-1}$ for NCB25. These values can be used for quantitative determination of total water in water-rich glasses.
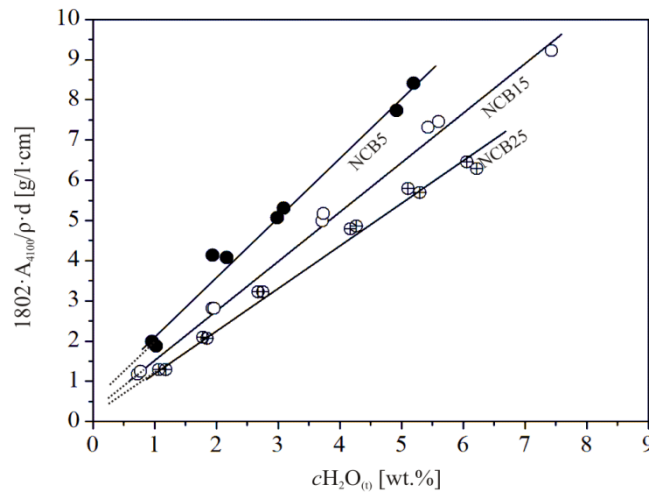
Fig. 6 Absorbance of the 4100 cm^{-1} absorption band normalized to density (ρ) and sample thickness (d) as a function of the H_2O content determined with KFT $cH_2O_{(t)}$ in NCB5, NCB15 and NCB25 glass. For each hydrous sample data of both ends of a glass cylinder are plotted.

4.4 Determination of Water Species Concentration

The OH combination band is composed by at least three different peaks. The individual contents of OH subspecies cannot be determined with the available data. Thus, the total OH content was determined using the absorbance at the peak maximum around ~ 4600 cm^{-1}. Determination of content of water species requires the knowledge of the density ρ in g/L for each hydrated glass,

the sample thickness d in cm, the absorbance A of the peak of the corresponding water species (listed in Tab. 2) and the linear molar absorption coefficient ε in $L \cdot mol^{-1} \cdot cm^{-1}$:

$$cH_2O_{mol} = \frac{1802 \cdot A_{5200}}{d \cdot \rho \cdot \varepsilon_{5200}} \tag{6}$$

$$cOH = \frac{1802 \cdot A_{4600}}{d \cdot \rho \cdot \varepsilon_{4600}} \tag{7}$$

where cH_2O_{mol} refers to the content of dissolved molecular water and cOH to the content of dissociated water in the glasses, both are given in wt.%. The total H_2O content in the glasses is represented by the sum of both contributions. Combining Eq. (6) and (7) with this constraint, the linear molar absorption coefficient can be derived from:

$$\frac{1802 \cdot A_{5200}}{d \cdot \rho \cdot cH_2O_{(t)}} = \varepsilon_{5200} - \frac{\varepsilon_{5200}}{\varepsilon_{4600}} \frac{1802 \cdot A_{4600}}{d \cdot \rho \cdot cH_2O_{(t)}} \tag{8}$$

where $cH_2O_{(t)}$ is the total H_2O content measured with KFT. For doing so, three basic assumptions are required as discussed in e.g. [43,64]. (1) The linear molar absorption coefficients are constant over the range of H_2O contents investigated. (2) All water species are represented by the NIR combination bands. (3) The ratio of different subspecies is constant.

If the absorbances normalized to density, thickness and H_2O content of the glasses show a linear relationship, the intercepts of the graph with the axis give the linear molar absorption coefficient ε for the corresponding water species (Fig. 7). It is worth noting that for OH groups ε corresponds to an effective absorption coefficient since the total water content is linked to the absorbance of the subspecies responsible for the band at ~ 4600 cm^{-1}. This is a common

approach which has been used for instance for the determination of total water contents of soda lime silicate glasses [65].

Data for very low water contents (< 1 wt.%) partially deviate (marked as grey data points in Fig. 7) from the trend given by samples with high water content. A possible explanation is a change in glass structure from dry to hydrous glasses. However, it is out of the scope of the present paper to investigate this phenomenon in detail.

Since the content of molecular water in NCB glasses is relatively low even in the high H_2O-bearing glasses, a large extrapolation to the y-axis is required, resulting in a large uncertainty for ε_{5200}. On the other hand, the absorption coefficient for the absorption band at 4600 cm^{-1} is very well defined.

Consistent with simple silicate and aluminosilicate glasses [40,43,44,66] the linear molar absorption coefficient ε_{4600} for the NCB glasses decreases with increasing alkali content from (1.47 ± 0.08) L·mol^{-1}·cm^{-1} for NCB5 to (0.99 ± 0.13) L·mol^{-1}·cm^{-1} for NCB15 and (0.92 ± 0.08) L·mol^{-1}·cm^{-1} for NCB25. In contrary, no clear trend is visible for ε_{5200}. In comparison with NCB5 and NCB25 the ε_{5200} of NCB15 glass is significant higher (Fig. 7). On the other hand the differences between the calculated water species contents (Eq. 6,7) for the three borate glasses is rather small (Fig. 8), i.e. OH groups are always strongly dominating.
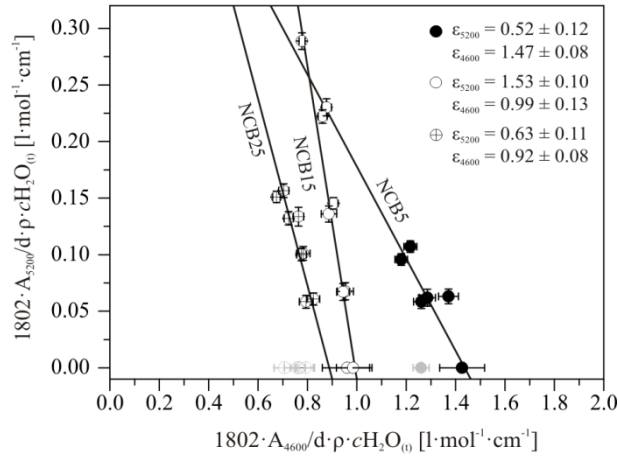
Fig.7. Calibration plot for the determination of the linear molar absorption coefficient of the NIR absorption bands at 5200 and 4600 cm^{-1} in NCB5, NCB15 and NCB25 glasses. The absorption coefficients ε for each composition were determined from the intercepts with the axes and are shown in the plot. Data marked with grey dots were excluded for the determination of absorption coefficients, see text for details.

In contrast to borate glasses, NIR calibrations for quantification of water species are available for many different silicate and aluminosilicate glasses. Whereas OH groups are the dominating water species in silicate glasses at relatively low H_2O contents (< 3 wt.%) [46,47,66] they are the predominant species in borate glasses at any H_2O content (Fig. 8). For instance in soda-lime silicates same amounts of molecular and dissociated water are present at ~ 4 wt.% H_2O content [46]. In contrast ~ 90% dissociated water and only ~ 10% of the molecular water are present in the NCB glasses (Fig. 8). Even at high H_2O contents (> 5 wt.%) OH groups are the dominant species in NCB5, NCB15 and NCB25 glasses. Below 2 wt.% total H_2O content no molecular water species is present in any of the three borate glasses.

These findings are consistent with studies on borosilicate glasses in which OH groups are increasingly stabilized with increasing boron content [59,60]. But in contrast to borate glasses a larger fraction of molecular water species is present at higher water contents. For instance, at ~ 8 wt.% H_2O same amounts of molecular water and dissociated H_2O are present in $NaBSi_3O_8$ glass

[40]. These findings demonstrate that bridging oxygens between borate groups and silicon tetrahedra are more difficult to hydrolyze than bridging oxygens between two adjacent borate groups.
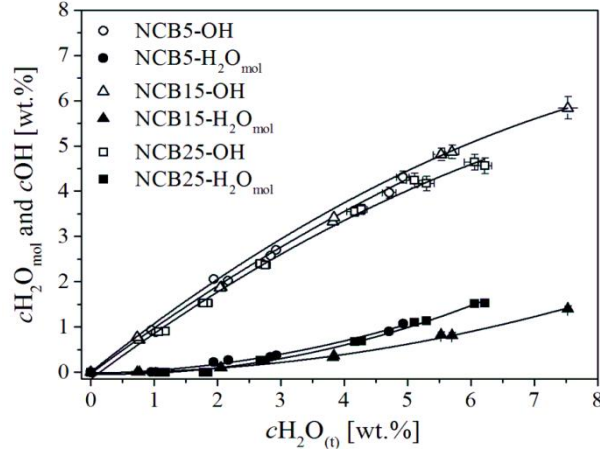
Fig. 8. Water speciation as the function of total H_2O content in NCB5, NCB15 and NCB25 glass.

The speciation of H_2O is frozen in at the glass transitions during cooling e.g. [46,48]. The glass transition temperature strongly decreases with addition of water (Tab. 2) and thus the data visible in Fig. 8 represent different temperatures. Provided that the equilibrium constant K for water speciation (Eq. 3) is independent of total H_2O content, these data allow conclusions about the temperature dependence of water speciation in the melt. In this approach, a basic assumption is that the speciation data can be directly related to the fictive temperature T_f of the glasses, which is determined by the specific cooling history in IHPV experiments. Studies on aluminosilicate glasses demonstrate the reliability of this approach [41,42].

The temperature dependence of K for various melt compositions is plotted in Fig. 9. Data for the silicates [69], aluminosilicates [42,70–75] and for borosilicates [59] are shown for comparison. In the study of Behrens and Yamashita [69] the higher values for the silicates in comparison to aluminosilicates were related to the effect of NBOs which promote the stabilization of OH groups. In the case of borates, which are virtually free of NBOs, weakly bonded oxygen between boron groups are responsible for the stabilization of OH groups. From the slope m of the straight

lines shown in Fig. 9 the standard enthalpy ΔH^0 for the water speciation reaction was calculated

as $\Delta H^0 = R \cdot m$ with R = 8.3144 J·mol^{-1}·K^{-1}. For NCB15 and NCB25 the ΔH^0 is well constrained

by the experimental data while for NCB5 the derived value has to be considered as an estimate

since it is based on two samples only. The ΔH^0 values of (7.2 ± 0.1) kJ/mol for NCB25, (14.7 ±

0.1) kJ/mol for NCB15 and 3.8 kJ/mol for NCB5 are significantly lower than reaction enthalpies

for silicates and aluminosilicates (25-35 kJ/mol) [42,69–75]. This trend is probably caused by

weak bonding of bridging oxygen between boron polyeder. The ΔH^0 of the borosilicate glass is

between the values for silicate, aluminosilicates and borate glasses (19.9 kJ/mol) [59].
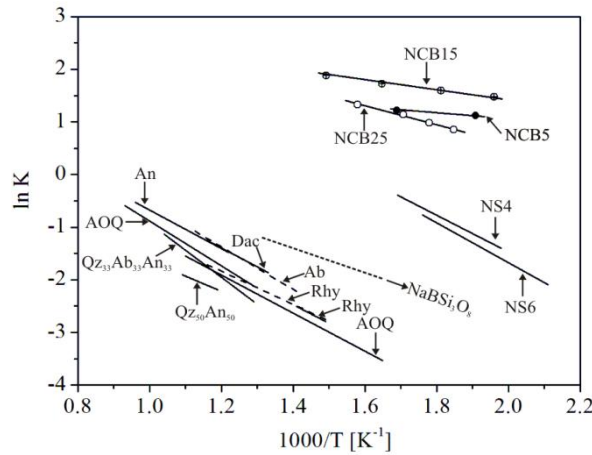
Fig. 9. Comparison of equilibrium constants for water speciation in silicate, aluminosilicate, borosilicate and borate glasses/melts. Data for comparison was taken from [42,59,69–75]. Explanation of abbreviations: Rhy=rhyolite, AOQ=$Na_{0.39}K_{0.31}Al_{0.69}Si_{3.31}O_8$, Dac=dacite, An=andesite; Ab=$NaAlSi_3O_8$, Qz$_{33}$Ab$_{33}$An$_{33}$=$Na_{0.5}Ca_{0.25}AlSi_3O_8$, Qz$_{50}An_{50}$=$Ca_{0.5}AlSi_3O_8$, NS4=$Na_2O-4SiO_2$, NS6=$Na_2O-6SiO_2$.

4.5 Influence of water on boron speciation

The relative abundance of tetrahedral boron in the glasses N_4 = $BO_4/(BO_4 + BO_3)$ was

determined using the fitted areas of the corresponding resonance in the ^{11}B MAS NMR spectra.

Based on the internal consistency of our data shown in Fig. 10, the precision of N_4 determination

is estimated to be better than 2%. However, it should be noted that the estimated areas do not directly represent the relative amounts of trigonal and tetrahedral boron in the samples due to different quadrupolar interaction parameters of both species [76]. The pulse response of a quadrupolar nucleus is strongly dependent on the relation of quadrupolar interaction (C_Q,) to the radio frequency (rf)-field. BO_4 shows no quadrupolar interaction with neighboring oxygens while quadrupolar parameters for BO_3 derived from fitting the spectra of the borated glasses are in the range of $C_Q = 2.4 - 2.8$ MHz and $\eta = 0.0 - 0.2$. Furthermore, in MAS experiments the quadrupolar interaction results in residual second-order effects often degrading spectral resolution. These effects depend strongly on magnetic field strength [77]. At high magnetic field strength the signals of BO_3 and BO_4 are separated and quadrupolar interaction for BO_4 is depressed. At low magnetic field strength both signals are superimposed, and the fraction of BO_4 may be systematically overestimated.

This may partially explain deviations of our data determined at a magnetic field strength (9.4 T) to data published in Smedskjaer et al. [57] for NCB glasses with same nominal composition using a magnet with 21.8 T. The measured fraction of BO_4 in the Smedskjaer et al. [57] study is lower by 5.3 % for NCB15 and 7.4% for NCB25 compared to our data. Another contribution to the differences between both data sets originates from different pressure histories. Whereas the NCB glasses in [57] represent the N_4 value of glasses synthesized at ambient pressure, NCB glasses in our study were synthesized at pressures of 500 MPa. Smedskjaer et al. [10] reported N_4 being about 2% higher for NCB25 glasses compressed at 500 MPa compared to glasses synthesized at ambient pressure. Small differences in chemical composition between the studies (only nominal compositions are given in [10,57]) may also contribute to the differences in N_4. Thus, the overall overestimation of BO_4 in our measurements is estimated to be in the order of 4%.

Although there is a systematic overestimation of BO_4 in our data, the relative changes in boron speciation are nevertheless well reproduced. A linear increase of N_4 with sodium content is observed (Fig. 10), consistent with published data for other borate glasses [37,78]. This trend cannot be extrapolated towards high network modifier concentrations. Experimental data and calculations based on the random pair model of Gupta [79] reported in Smedskjaer et al. [57] indicate a maximum value of N_4 for the NCB system for about 35 mol% $Na_2O + CaO$ (Fig. 10). Compared to alkalis, on a molar basis the influence of water on the boron coordination is approximately ten times lower (Fig. 10). The dependence on water content is similar for NCB5 and NCB15, but slightly more pronounced for NCB25. For instance, N_4 increases from 24.8 to 25.7% for NCB5 (5 wt.% $H_2O \cong 15$ mol% H_2O), from 42.3 to 44.6% for NCB15 (6 wt.% $H_2O \cong$ 17 mol% H_2O) and from 53.4 to 57.5% for NCB25 (6 wt.% $H_2O \cong 17$ mol% H_2O).

Much larger effects on boron speciation upon hydration were found for borosilicate glasses. In $NaBSi_3O_8$ glass the fraction of $BO_3/(BO_3+ BO_4)$ deceases from 12.5% to 5% with the addition of 4 wt.% H_2O to the anhydrous glass (personal communication). Substitution of aluminum for boron in these glasses triggers the effect of water on the boron speciation. In $NaAl_{0.75}B_{0.25}Si_3O_8$ glass the ratio of $BO_3/(BO_3+ BO_4)$ decrease from 40% to 12.5% comparing the anhydrous glass and the 4 wt.% H_2O containing glass.
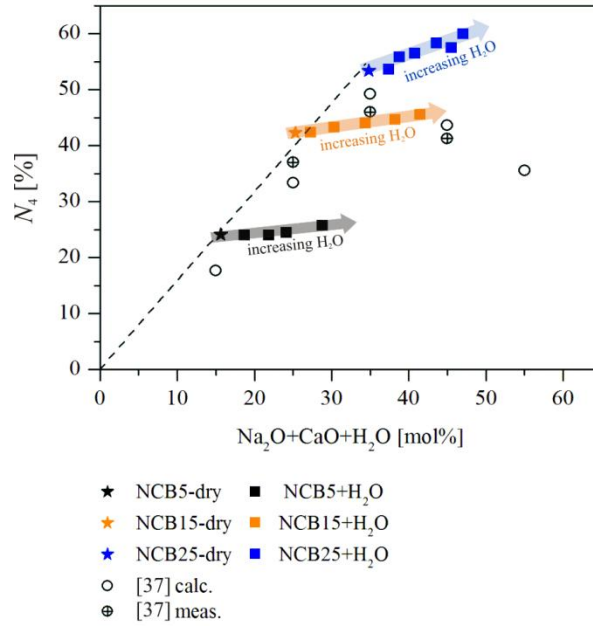
Fig. 10. Fraction of tetrahedrally coordinated boron vs. $Na_2O+CaO+H_2O$ content for NCB5, NCB15 and NCB25 glass. H_2O contents represent average values of both sides of a glass cylinder. The dashed line is a linear regression through our data for dry glasses. The arrows show the effect of H_2O content for each of the three base compositions. Data from Smedskjaer et al. [57] for the dry borate glasses at ambient pressure are shown. Note the decrease in N_4 when Na_2O+CaO exceeds 35 mol%.

A crucial question is whether the observed trends of rising N_4 upon hydration is due to a charge compensating role of protons similar to that of alkalis, or to a decreasing T_f resulting from hydration. A higher T_f value favors the right hand side in Eq. 1, means the transformation of BO_4 units to BO_3 units and NBOs [4,9,37,80]. Stebbins and Ellsworth [80] and Sen et al. [4] investigated the influence of T_f on boron speciation in sodium borate glasses (containing 5 to 30 mol% Na_2O) and borosilicate glasses (20 mol% Na_2O, 20 mol% B_2O_3 and 60 mol% SiO_2). They found that changes of the boron speciation as a function of T_f is small in compositions with low NBO contents. On the other hand a significant effect of T_f on boron coordination was observed in the borosilicate glasses which contain higher fractions of NBO.

The influence of changing T_g with hydration on boron coordination was also discussed in the study of Schmidt et al. [5]. It was observed that the boron speciation is not changing with

increasing boron content in the glasses although this decreases significantly T_g. They conclude that the variation of T_g has little effect on the boron coordination in the respective compositions. In our glasses, incorporation of water results in a dramatic decrease in fictive temperature (Tab. 2) which may easily explain the small increase in BO_4. Hence, a stabilizing effect of H_2O on boron tetrahedral appears to be of minor importance for these borate glasses. The slightly higher dependence of N_4 on water content in NCB25 compared to NCB5 and NCB15 can be explained by a small fraction of NBO in this glass. Based on the random pair model of Gupta [9], Smedskjaer et al. [57] suggest that NBOs first begin to form when the content of Na_2O and CaO exceeds 33 mol%. The results of Stebbins and Ellsworth [80] point to larger effect of T_f on boron speciation in compositions containing NBOs.

5. Conclusions

The structural investigation of H_2O-bearing soda-lime borate glasses was subject in the present study. NIR spectra show that OH groups are the predominant water species and no significant differences in water speciation for NCB5, NCB15 and NCB25 were observed. In addition to the main OH absorption band at 4600 cm^{-1}, we observed additional B-OH species in NIR spectra at 4750 cm^{-1} and 4900 cm^{-1}. Through the combination of information from NIR and MIR spectra we attribute these bands to BO_4-OH and BO_3-OH vibration modes respectively.

From ^{11}B MAS NMR spectra we could see that the influence of H_2O on boron speciation is significantly lower than the influence of alkalis. The small increase in relative abundance of tetrahedral boron upon hydration can be explained by the dramatic change in glass transition temperature. A slightly larger effect of water on boron coordination in the glass with highest alkali content (NCB25) is attributed to a small fraction of non-bridging oxygen in this glass.

Chapter 1B[1]

Water, the other Network Modifier in Borate Glasses

Abstract

In the present study we have investigated whether the effect of water on properties of borate glasses resembles that of alkali oxide. Soda-lime-borate glasses with nominal compositions of x Na_2O, 10 CaO, (90-x) B_2O_3 (x = 5, 15 and 25 mol%) were doped with up to 8 wt.% H_2O by processing glass powder + distilled water in platinum capsules in an internally heated gas pressure vessel at 1523 K and 500 MPa. The water content of hydrous glasses was determined by Karl-Fischer titration and near-infrared spectroscopy. The glass transition temperature T_g. was derived from DTA and micropenetration experiments for which the effect of water loss at the surface of the hydrous glasses was studied. Heating glass samples at 10 K min^{-1} in the DTA resulted in T_g values which are close to T_{12} isokom temperatures confirming the equivalence of enthalpy relaxation and viscous relaxation for borate glasses. For all three glass series it is shown that T_g strongly decreases whereas the liquid fragility strongly increases upon addition of water. These findings reveal that H_2O primarily causes breaking of B-O-B bonds rather than supporting 4-fold coordinated boron as it is well-known for alkali oxides in this concentration range.

Contributions of the candidate

Scientific ideas: 50%   Analysis and interpretation: 65%

Experimental work: 50%   Paper writing: 35%

1. Introduction

Boron oxide glasses are soft materials with a low glass transition temperature due to only three-fold coordination of boron by oxygen. Addition of network modifiers such as alkali oxides and alkaline earth oxides results in a strengthening of the glass structure due to the change in boron coordination from trigonal to tetrahedral. The increased interconnection in the network causes an increase in viscosity and, therefore, an increase in the glass transition temperature. This conversion dominating at low temperatures and network modifier contents up to about 25 mol% is known as the "boron anomaly". At higher fractions of alkali oxides and at higher temperatures non-bridging oxygens (NBO) are increasingly formed in competition with tetrahedrally coordinated boron, which leads to a decrease in viscosity (see e.g. [81]). Upon compression borate glasses show a transformation of the coordination number of boron from three to four [7,82,83] while fast quenching (high fictive temperature) favors four-fold coordinated boron [4,9,80,84]. This boron coordination is reported to resist (up to 1440 min) upon annealing close to the glass transition range ($0.9T_g$) [10]. For longer times and higher temperatures, changes in density indicate structural relaxation on time scales of viscous flow [85].

In silicate and aluminosilicate systems it is well known that the incorporation of both water and alkali oxides reduce the viscosity of the melt e.g. [12,14,86,87],. However the effect of water is much stronger than alkali [14,87]. Shelby and McVay [87] studied sodium trisilicate glasses with water concentrations up to 0.185 wt.% and reported on a definite relationship between the size of the added ion (H^+, Li^+, K^+, Rb^+ and Cs^+) and the effect of that addition on the rheological behavior of the glass. For higher water contents speciation of H_2O is evident, i.e. water dissolves in silicate glasses besides as OH groups also as H_2O molecules. The fraction of molecules are found to increase in soda-lime-silicate glasses with total water content continuously, while OH groups appear to saturate at a level of approx. 1.5 wt.% [46]. The effect of both species on viscosity of silicate glasses has been identified using a three-component model [45,88]. Although

OH groups seems to reduce viscosity 3-5 times stronger than H_2O molecules [45,89], the contribution of the latter cannot be neglected and hinders a direct comparison with alkali on a level above 0.2 wt.% total water.

The situation is different in the case of hydrous soda-lime-borate glasses since OH groups dominate water speciation over the entire range of accessible compositions (up to 8 wt.% total water) [90]. In contrary to alkali oxides, the incorporation of H_2O in the glasses produces only minor increase in the abundance of four-fold coordinated boron. Thus, the present paper aims in shedding light on the rheological properties of soda lime borate glasses with particular focus on the role of water. For doing so, we determined glass transition temperatures as function of Na_2O and H_2O content of the glasses using differential thermal analysis (DTA). To interpret the observed trends in terms of melt viscosity, micropenetration experiments were performed on the three different nominally dry glasses and on one series of glasses with same anhydrous composition but with different water content. A crucial aspect of studies on hydrous glasses at ambient pressure conditions is to verify that water loss during heating has not a noticeably impact on the data. Infrared spectroscopy on post-experimental glasses and combination of DTA with thermogravimetry (TG) and mass spectrometry (MS) was applied to recognize changes in water content of the samples.

2. Experimental and analytical methods

2.1 Anhydrous glasses

Three anhydrous soda-lime-borate glasses with nominal compositions x mol% Na_2O (x = 5, 15, 25), 10 mol% CaO, and 90-x mol% B_2O_3 (NCBx) were prepared from Na_2CO_3, $CaCO_3$ and H_3BO_3 powders following the procedure described in detail in [90].

The composition of the three glasses was analyzed by inductively coupled plasma optic emission spectroscopy (ICP-OES, 715-ES VARIAN) and electron micro probe analysis (EMPA,

CAMECA SX100). In the case of EMPA measurements, the B_2O_3 content of the glasses was estimated by difference of the total of measured oxides to 100 wt.%. For details on the measurement conditions see Bauer et al. [90]. Averaging data of both analytical methods yields composition in mol% of 5.50 Na_2O, 10.15 CaO, 84.36 B_2O_3 for NCB5, 15.22 Na_2O, 10.19 CaO, 74.60 B_2O_3 for NCB15, and 25.43 Na_2O, 10.16 CaO, 64.41 B_2O_3 for NCB25.

2.2 Hydrous and compressed glasses

For syntheses of hydrous glasses containing up to 8 wt.% H_2O, glass powder and distilled water were filled stepwise in turn in a platinum capsule (diameter: 6 mm, length: 25-30 mm) to facilitate homogeneous distribution of water in the glass. To produce anhydrous compressed glasses only the starting glass powders were loaded into platinum capsules. By subsequent compaction of the material in the capsule using a steal piston a cylindrical shape of glass bodies was achieved. After sealing the capsules with a PUK welding device (PUK[3] professional plus, Co. Lampert), possible weight loss due to a leakage was checked by placing the capsules in a drying furnace at 373 K.

All syntheses were performed in internally heated pressure vessel (IHPV) using argon as pressure medium at 500 MPa and 1423 K for 14-20 hours. A detailed description of the apparatus is given in Ref. [50]. For all syntheses similar pressure was chosen to eliminate pressure induced differences in the glass structure and properties. For each run two capsules were placed in the hot spot of the sample holder between the two furnace-controlling K-type thermocouples (Ni-CrNi). The temperature of the samples was controlled by a third thermocouple located in the middle of the hot spot zone. The maximum variation in temperature was ±10 K and pressure accuracy is within ±50 bars. In order to preserve pressure-induced structural changes and the volatiles in the glass, the samples were isobarically quenched (by switching of the furnace) using an automatic pressure controller. This leads to a cooling rate of ~

200 K min^{-1} through the temperature region of glass transition. All glass cylinders after high pressure synthesis were clear and no crystals or bubbles could be observed. Due to the hygroscopic character of the glasses, exposure to water was avoided and oil was used for sawing and polishing of the samples e.g. for preparation of thin-sections. All samples were stored in a desiccator with P_2O_5 as desiccant.

2.3 Analysis of water content and speciation

The total water content $cH_2O_{(t)}$ of hydrated glasses was determined by Karl-Fischer-titration (KFT). In addition, near-infrared (NIR) spectroscopy was used to measure the concentration of H_2O-molecules, cH_2O_{mol}, and water dissolved in form of OH groups, cOH, in these glasses. To quantify $cH_2O_{(t)}$ for nominally dry glasses the fundamental OH stretching vibration band in the mid infrared was evaluated.

Glass sections polished on both sides were prepared for infrared spectroscopy. Thickness was determined using a digital micrometer (Mitutoyo) with a precision of $\pm$ 2 µm. IR spectra were recorded using a Fourier Transform Infrared (FTIR) spectrometer (Bruker IFS88) coupled with an IR microscope (Bruker IR scope II) equipped with a mercury-cadmium-tellurium (MCT) detector. In the mid infrared (MIR) a globar light source and a KBr beamsplitter were applied. Spectra were collected in the range of 600 to 6000 cm^{-1} with a spectral resolution of 4 cm^{-1}. 50 scans were accumulated for background (air) and sample measurements. A slit aperture between the objective and the detector limited the analyzed sample volume. In the focus plane, the area selected by the slit was typically (100 x 100) µm^2. In the near infrared (NIR) a tungsten light source and a CaF$_2$ beam splitter was applied. Spectra were measured in the range of 2000 – 11000 cm^{-1} with a spectral resolution of 2 cm^{-1}. 100 scans were accumulated for each spectrum. In the focus plane, the area selected by the slit was (100 x 100) µm^2 for routine measurements. In order to improve spatial resolution, in measurements of profiles in glasses after micropenetration

experiments a focus area of (30 x 120) μm^2 was adjusted with the long side being aligned parallel to the edge of the sample. Data of $cH_2O_{(t)}$, cH_2O_{mol} and cOH of the glasses are included in Tab. 1 and 2.

2.4 Differential thermal analysis

The glass transition temperature, T_g, was determined by differential thermal analysis (DTA) using a thermobalance TAG 24 (Setaram, Caluire, France). Measurements were conducted in flowing synthetic air (45 ml min^{-1}) on bulk or powdered samples (15-20 mg) placed in open Pt-crucibles. The sample mass was recorded with an accuracy of $\pm$ 0.01 mg. Simultaneous analysis of evolved gases was performed using a mass spectrometer (Balzers Quadstar 421) coupled to the DTA apparatus by a heated (453 K) quartz glass capillary. The multiple ion detection (MID) modus was applied selecting mass numbers (m/e) of 17 and 18 for water (OH, H_2O) or 44 for CO_2.

Because T_g can be affected by water losses during DTA analysis, four repeated heating-cooling cycles at 10 K min^{-1} were performed for each sample and the maximum cycle temperature was limited to T_g + 50 K. For NCB glasses melted under pressure, the first DTA run was performed to equilibrate the thermal and pressure histories, i.e. this run represents the fictive temperature T_f of the glass. The second, third and fourth heating cycles were then used to determine the glass transition temperature for cooling and heating at 10 K min^{-1} under ambient pressure.

According to Mazurin [54,55] and Yue [91] the glass transition temperature T_g was determined during heating from the crossover temperature of two tangents aligned to the decreasing flank and base line of the endotherm, respectively. Figure 1 shows the DTA signal for four subsequent heating cycles of the standard glass DGG-I, which was used as reference. T_g was 816 $\pm$ 2 K and this isokom temperature correspond to the certified viscosity of log η = 12.02 $\pm$ 0.09 (viscosity η in Pa·s) [92].
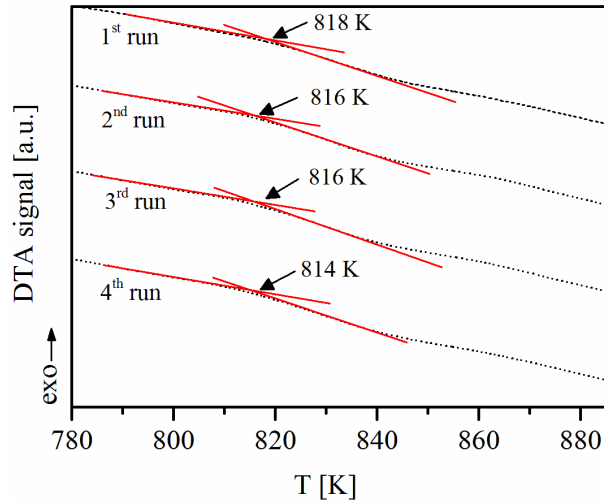
Fig. 1. DTA signals of four heating cycles and illustration of determination of T_g by the tangent method for DGG-I standard glass. Crossover temperature and tangent construction is shown for each run. Data are plotted with an offset for clarity.

2.5 Sphere penetration viscometry

Penetration measurements were performed on a vertical dilatometer (Bähr VIS 404) by force control in the range from 1–4 N for the nominally dry NCB5, NCB15, NCB25 glasses and for two hydrated NCB15 glasses. The pushing rod is equipped with a sapphire micro-sphere (radius $r = 0.75$ mm). Cylindrical samples with a diameter 3–4 mm and a height of 1–3 mm were sliced from the anhydrous and hydrated glasses. Coplanar surfaces were prepared by grinding and polishing of the cylinder faces. Sample thickness was typically 2 mm. The experiments were carried out at ambient atmosphere in a temperature range from 572 to 801 K. The T_g value determined by DTA was chosen as target temperature for the first experiment with each glass. Water vapor pressure was not controlled during experiment. Temperature was controlled with S-type thermal elements ($\pm$ 0.1 K) located close (2–3 mm) to the glass surface at the upper face of the cylinder. The thermal gradient along the cylinder axis was less than $\pm$ 1 K mm^{-1} indicating a temperature accuracy of less than about $\Delta T = \pm 3$ K. A linear variable displacement transducer

continuously recorded the indentation depth of the sphere into the glass. The shear viscosity η was calculated according to [93].

$$\eta = \frac{9Ft}{32\sqrt{(2rL^3)}} \qquad (1)$$

with η = Newton viscosity, F = applied force, t = time, r = radius of the sphere, and L = indentation depth. The system is calibrated by the standard glass G1 of the Physikalisch-Technische Bundesanstalt (PTB) [94]. Repeated measurements at same temperatures during a course of micro-sphere penetration experiments with nominally dry soda lime borate glasses resulted in an uncertainty in viscosity of $\pm$ 0.05 log units.

In order to study the possible effect of water loss on viscosity of the hydrous glasses, an experiment of three temperature steps was performed while the load was applied constantly on the NCB15-5wt.%n-I glass (Fig. 2, see Tab. 2 for sample code). After heating to $T_{(I)}$ = 577.5 K at 15 K min^{-1}, a hold of ~ 100 min was applied to allow for temperature equilibration, i.e. the time was significantly longer than the relaxation time for the melt (I). Subsequently the temperature was raised by 10 K to $T_{(II)}$ = 587 K at 5 K min^{-1} and held for another 200 min (II). As a last step, the temperature was lowered to $T_{(III)}$ = 577.5 K again and dwelled for 200 min (III). The increase in viscosity from the first to the third step was approximately $\Delta\eta \approx 0.6$ log units. After the experiment, a section was cut and polished perpendicular to the surface for IR spectroscopy. NIR spectra measured close to the top, in the center and close to the bottom of the sample give evidence for a water loss during experiment (Fig. 3a). Evaluation of the spectra to obtain the concentration of both hydrous species in the glasses follows Bauer et al. 2015 [90]. A zone depleted in both OH and H$_2$O was formed on both sides of the sample NCB15-5wt.%n-I, with a thickness of about 120 μm (Fig. 3b). It is worth noting that water loss was less significant for sample NCB15-2wt.%n-I, i.e. OH contents ~40 μm away from the upper and the lower surface were only 10% lower than in the center.

To avoid possible complexity in data interpretation due to water loss, viscosity of hydrated glasses was determined from the first heating step only. At higher temperatures holds to allow for equilibrium viscous flow were shorter (50 min (log ≈11.5) and 30 min (log ≈10.5)). The error in viscosity due to loss in water during first hold was estimated to 0.2 log units for all temperatures. For all experiments a linear stress strain-rate relation was obtained indicating pure Newtonian flow of the NCB glasses below the threshold limit of shear thinning [95].
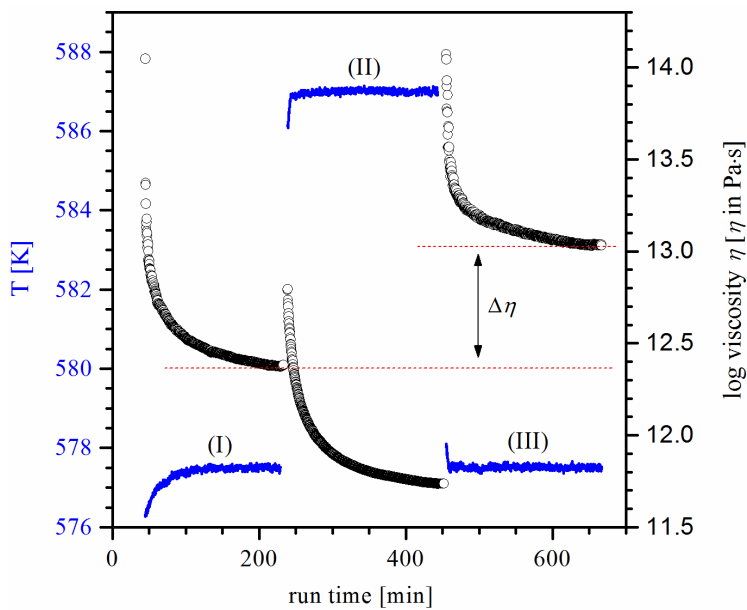
Fig. 2. Readout of a micro-sphere penetration experiment of the hydrous glass NCB15_5wt.%n-I while performing three temperature steps: $T_{(I)}$ = 577.5 K, $T_{(II)}$ = 587 K and $T_{(III)}$ = 577.5 K. Temperature: blue line, left ordinate, logarithm of viscosity: black line, right ordinate. Note the increase in viscosity $\Delta\eta$ between step I and III due to water loss.
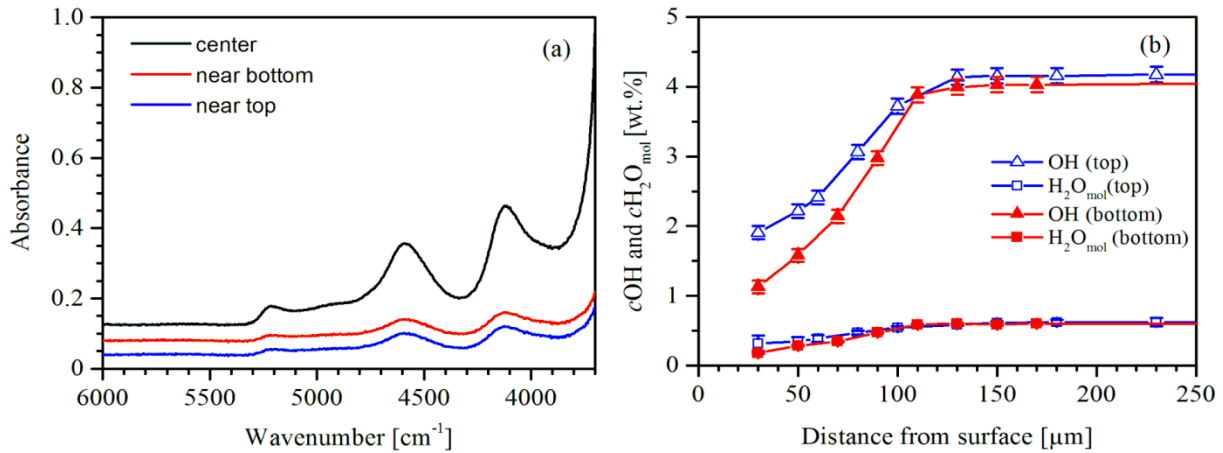
Fig. 3 (a) Near-infrared spectra recorded in the center, near to the top and bottom (distance from the surface 40 μm each) of sample NCB15_5wt.%n-I after a series of micro-sphere penetration experiments. The band at 4160 cm^{-1} is an unassigned mode correlated to cH$_2$O$_{(t)}$, the band at 4590 cm^{-1} is a combination mode of OH groups and the band at 5210 cm^{-1} is a combination mode of H$_2$O molecules [24]. (b) Profiles of hydrous species in sample NCB15-5wt.%n-I perpendicular to the former surfaces. The top of the sample was in contact with the sphere of the indenter, the bottom was lying on a ceramic plate. Note the similarity of both profiles and the decrease in concentration of both hydrous species towards the surfaces of the samples. Lines are intended as visual guides.

3. Results

3.1 Infrared spectroscopy

MIR spectra of nominally dry glasses produced in the IHPV are shown in Fig. 4a. Similar spectra were obtained for the air-melted glasses (not shown). Comparison with spectra of glasses containing ca. 1 wt.% H$_2$O (Fig. 4b) gives evidence that only the asymmetric band with maximum near 3500 cm^{-1} is directly related to the water content of the glasses. Bands below 3000 cm^{-1} are attributed to vibrations of the borate network. For instance, the band at 2800 cm^{-1} is most likely the first overtone of the intensive band of trigonal boron near 1400 cm^{-1} (see Fig. 1a in [90]). The OH stretching vibration features show some differences to the spectra published in Fig. 1b of [90]. These differences originate from contributions of water absorbed in the potassium bromide pellets to the spectra published in the former study. The spectra recorded on glass plates in this study do not contain such artifacts and resemble spectra of aluminosilicate

45

glasses [15–17]. Means, OH groups in borate glasses are only involved in weak hydrogen bonding, in contrast to alkali silicate glasses which exhibit strong bands at low wavenumber (i.e. at 2800, 2300 and 1750 cm^{-1} [47,61] originating from interaction of OH groups with non-bridging oxygen.
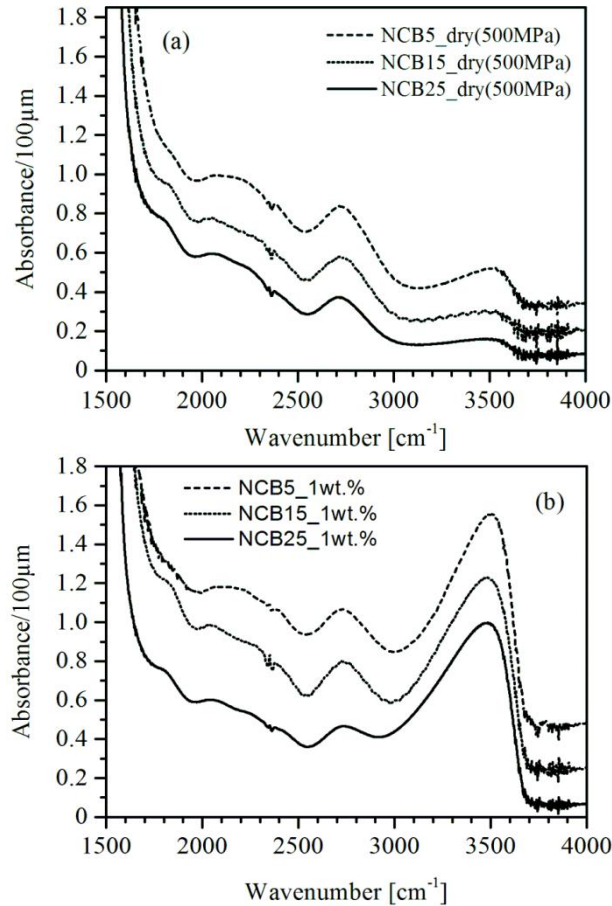
Fig. 4. MIR spectra of (a) nominally dry glasses and (b) glasses containing ~1 wt.% H$_2$O synthesized at 500 MPa pressure. The asymmetric band with maximum at 3500 cm^{-1} is due to fundamental OH stretching vibrations while bands at lower wavenumber originate from network vibrations. Features at 2350 cm^{-1} are artifacts caused by different CO$_2$ concentrations in the IR beam during background and sample measurements.

The water content of the nominally dry glasses was determined using the absorbance of the band at 3500 cm^{-1}. Since this band is superimposed to network vibration bands at its low wavenumber flank, we followed the recommendation of the International Commission on Glass (ICG) to define the peak height (absorbance) for this band [65]. The ICG proposed to use the difference of

the absorbance at the peak maximum (A_{3500}) minus the absorbance recorded at 4000 cm^{-1} (A_{4000}) as a measure of the peak height for soda lime silicate glasses. Soda lime silicate glasses show also strong overlap of the OH stretching vibration band with network vibration bands so that the baseline of the OH stretching vibration band cannot be reliably constrained. Prerequisite for determination of $c_{H_2O_{(t)}}$ from infrared spectra using the Lambert-Beer law

$$c_{H_2O_{(t)}} = \frac{1802 \cdot A_{3500}}{d \cdot \rho \cdot \varepsilon_{3500}}$$

(2)

is the knowledge of the density ρ, the sample thickness d and the linear molar absorption coefficient ε. The molar absorption coefficient for the band at 3500 cm^{-1} was determined using thin sections of glasses containing up to 2 wt.% H_2O. Density and water content of these glasses are reported in Bauer et al. 2015 [90]. A compilation of data used in the calibration is given in Tab. 1. Based on these data, average values of ε_{3500} were calculated and applied to the water-poor glasses. With increasing sodium content ε_{3500} decreases from (94.2 ± 1.9) L·mol^{-1}·cm^{-1} for NCB5 to (77.5 ± 4.6) L·mol^{-1}·cm^{-1} for NCB15 and (66.5 ± 3.5) L·mol^{-1}·cm^{-1} for NCB25. The calculated water contents of nominally dry glasses are included in Tab. 2. It is striking that the water content of the air-melted glasses strongly increases with decreasing alkali content from 0.044 wt.% for NCB25_dry (0.1MPa) to 0.122 wt.% for NCB5_dry (0.1MPa). This trend reflects the stabilization of the borate network by formation of tetrahedrally coordinated boron. Additionally, it can be seen that the compressed nominally dry glasses contain slightly higher $c_{H_2O_{(t)}}$ than the air-melted glasses. This is due to water adsorbed on the glass powder surface before loading into the platinum capsules.

Tab. 1 Calibration of the absorption coefficients for the 3500 cm^{-1} band. I or II at the end of the sample name refers to analysis of pieces cut from both ends of a glass cylinder. Numbers in parentheses give uncertainty of the last digit. Error of absorbance is 0.010. Errors of the absorption coefficients were calculated by error propagation.

	cH$_2$O$_{(t)}$ (KFT)	density	d	A$_{3500}$-A$_{4000}$	ε_{3500}
	[wt.%]	[g/L]	[µm]		[L·mol^{-1}·cm^{-1}]
NCB5_1wt.%-I	0.96(3)	2201(4)	139(4)	1.503	92.4 ± 4.5
NCB5_1wt.%_-I	1.03(6)	2201(4)	126(5)	1.519	96.0 ± 5.0
NCB15_1wt.%-I	0.77(5)	2366(5)	67(2)	0.527	77.4 ± 10.7
NCB15_1wt.%-II	0.73(7)	2366(4)	53(2)	0.43	84.0 ± 14.6
NCB15_2wt.%-I	2.06(7)	2351(3)	72(2)	1.422	73.1 ± 3.8
NCB15_2wt.%-II	2.04(8)	2351(3)	57(2)	1.142	75.7 ± 4.8
NCB25_1wt.%-I	1.18(5)	2466(5)	99(4)	0.992	62.2 ± 4.7
NCB25_1wt.%-II	1.07(5)	2466(5)	101(3)	0.977	66.0 ± 5.0
NCB25_2wt.%-I	1.85(5)	2464(5)	77(2)	1.315	67.2 ± 3.7
NCB25_2wt.%-II	1.78(8)	2464(5)	83(2)	1.425	70.8 ± 3.7

3.2 Glass transition temperature

Glass transition temperatures, T_g, determined by DTA are summarized in Tab. 2. For any given water concentration, T_g is maximal and minimal for NCB15 and NCB5, respectively. Further, in all three NCB glasses, dissolution of water in the borate glass structure leads to a decrease in T_g. No systematic shift of T_g was observed during repeated DTA runs. This behavior is visualized exemplarily by Fig. 5 for the hydrous glasses NCB5_1wt.%-I, NCB15_4wt.%-I, and NCB25_7wt.%-I. The thermal stability of hydrous glasses during DTA measurements was further confirmed by only minor mass loss after thermal treatment. Except for sample NCB5-5wt.%-I, the total mass loss was < 1%. Figure 6 shows that the minor mass loss of the hydrous glasses can by assigned to water species since ion currents of mass 18 (H$_2$O) and 17 (OH) were approximately 10 times larger than for mass 44 (CO$_2$). Some of the DTA samples contained larger glass pieces suitable for post-experimental investigation by IR spectroscopy. These measurements confirm minor loss of water from hydrous NCB15 and NCB25 samples during the experiments. Typically, molecular H$_2$O concentration was slightly higher in the post-

experimental samples compared to the starting materials. This finding indicates re-equilibration of water speciation at the relatively low temperatures of DTA experiments.

Since the first upscan was used to equilibrate for the different thermal and pressure histories of the glasses the corresponding temperature was assigned to an apparent fictive temperature T_f in Tab. 2. After the first upscan all glasses were relaxed at ambient pressure and passed the glass transition at a cooling rate of 10 K min^{-1}. Thus, memory of the high pressure and other cooling rates is lost in the data, which were used to define T_g. The mean values of T_g in Tab. 2 were calculated from the 2nd to 4th runs.

Tab. 2. Glass transition temperature, T_g, of 4 successive DTA heating cycles at 10 K min^{-1} and total mass loss after the 4th cycle for dry and hydrous NCBx (x = 5, 15, 25 mol% Na$_2$O) glasses. Sample code extensions: _wt.% = nominal water content, -I = refer to sample cut from both ends of a glass cylinder (see [90]), n = new batch. Water contents before and, if available, after experiments are also given. Error in the last digit is given in parentheses. *IR measurements on nominally dry glasses are based on the peak height of the band at 3500 cm^{-1}. Hydrous glasses were analyzed by NIR spectroscopy using combination bands at 4600 cm^{-1} (OH groups) and 5120 cm^{-1} (H$_2$O molecules). Initial water contents of hydrous glasses are already reported in [90].

	Initial water content										Water content after DTA	
	KFT cH$_2$O$_{(t)}$ [wt.%]	IR cOH [wt.%]	IR cH$_2$O$_{mol}$ [wt.%]	T_f 1st upscan [K]	T_g 2nd upscan [K]	T_g 3rd upscan [K]	T_g 4th upscan [K]	T_g mean [K]	Total mass loss [%]	IR cOH [wt.%]	IR cH$_2$O$_{mol}$ [wt.%]
NCB5_dry (0.1MPa)	-	0.122(5) *	-	728	712	713	716	714(2)	0.00	-	-
NCB5_dry (500 MPa)	-	0.143(10) *	-	710	696	699	695	697(2)	0.09	-	-
NCB5_1wt.%-I	0.96(3)	0.93(3)	0.00(2)	648	653	654	654	654(1)	0.34	-	-
NCB5_3wt.%-I	2.93(8)	2.70(7)	0.37(1)	-	601	589	594	595(6)	0.81	-	-
NCB5_5wt.%-I	4.93(10)	4.31(13)	1.07(4)	531	525	523	525	524(1)	1.43	-	-
NCB15_dry (0.1MPa)	-	0.079(10) *	-	775	776	775	-	776(1)	0.04	-	-
NCB15_dry (500 MPa)	-	0.093(10) *	-	770	771	773	770	771(2)	0.46	-	-
NCB15_2wt.%n-I	1.90(10)	1.78(9)	0.00(2)	-	-	-	-	-	-	-	-
NCB15_2wt.%-I	2.06(7)	1.88(3)	0.09(2)	675	669	671	669	670(1)	0.14	1.83(4)	0.09(2)
NCB15_4wt.%-I	3.82(8)	3.33(8)	0.33(2)	608	605	608	607	607(2)	0.06	3.58(8)	0.46(2)
NCB15_5wt.%n-I	4.90(10)	4.10(7)	0.62(2)	-	-	-	-	-	-	-	-
NCB15_6wt.%-I	5.53(12)	4.81(14)	0.82(7)	560	552	551	554	552(2)	0.13	-	-
NCB15_8wt.%-I	7.53(10)	5.84(25)	1.40(6)	509	510	510	511	510(1)	0.33	6.35(13)	1.64(3)
NCB25_dry (0.1MPa)	-	0.044(3) *	-	762	760	761	759	760(1)	0.03	-	-
NCB25_dry (500 MPa)	-	0.087(8) *	-	758	747	749	748	748(1)	0.31	-	-
NCB25_1wt.%-I	1.18(05)	0.91(1)	0.00(2)	696	696	696	697	696(1)	0.44	-	-
NCB25_2wt.%-I	1.85(07)	1.53(2)	0.00(2)	669	666	665	665	665(1)	0.32		-
NCB25_3wt.%-I	2.86(08)	2.40(5)	0.26(1)	637	633	633	633	633(1)	0.07	2.54(5)	0.39(2)
NCB25_5wt.%-I	4.17(13)	3.55(11)	0.68(2)	592	586	587	586	586(1)	0.06	3.27(3)	0.72(2)
NCB25_6wt.%-I	5.30(12)	4.17(16)	1.13(4)	567	561	562	564	562(2)	0.00	3.91(8)	1.20(2)
NCB25_7wt.%-I	6.22(11)	4.56(17)	1.51(5)	544	542	542	540	541(1)	0.09	4.51(9)	1.63(3)
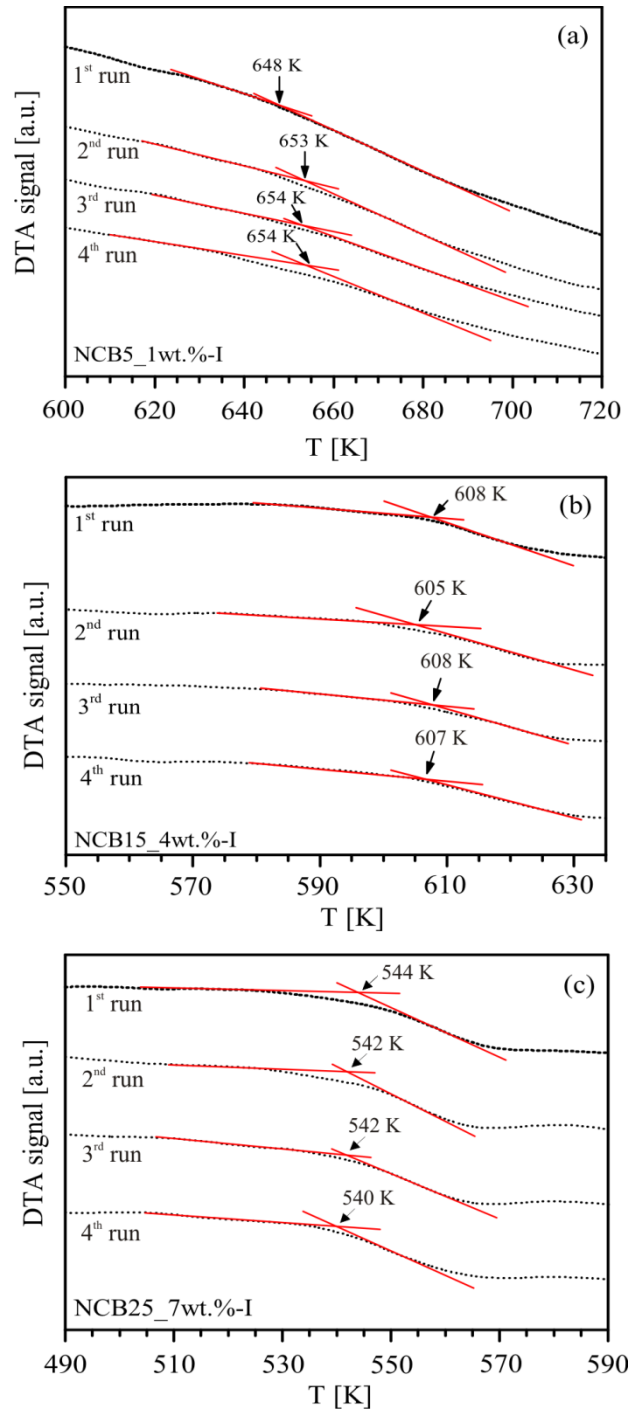
Fig. 5 Repeated DTA runs (heating and cooling at 10 K/min) of the hydrous soda-lime borate glasses (a) NCB5_1wt.%-I, (b) NCB15_4wt.%-I, and (c) NCB25_7wt.%-I. Crossover temperature and tangent construction is shown for each run.
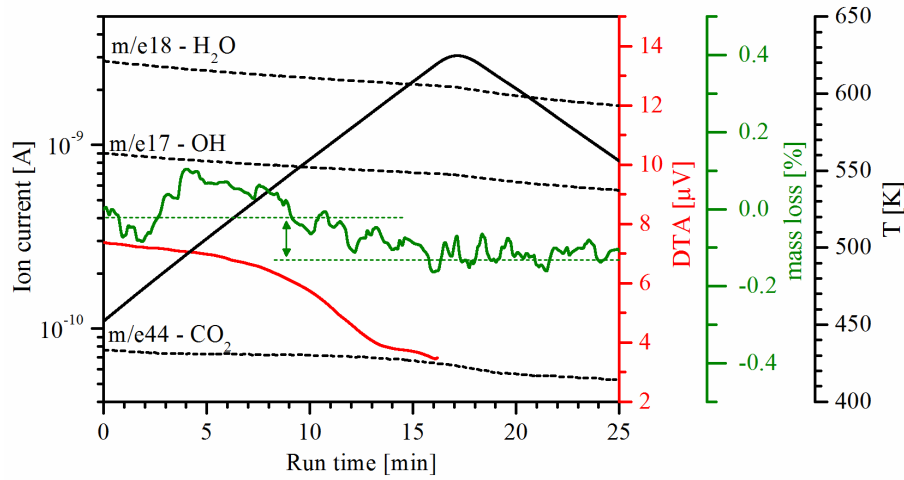
Fig. 6. DTA signal of the glass transition endotherm and corresponding mass loss as well as the ion currents of the mass channels m/e17, m/e18 and m/e44 of the first upscan of glass NCB15_6wt.%-I.

3.3 Viscosity

The viscosity in the glass transition range was measured for the anhydrous soda-lime borate glasses and for two hydrated glasses with 15 mol% Na_2O and $cH_2O_{(t)}$ = 1.9 and 4.9 wt.% (Tab. 3). Figure 7 shows that viscosity increases in the order 5, 25, 15 mol% Na_2O for the anhydrous glasses, while for the hydrous glasses viscosity decreases with increasing water content. For the relative small interval of the glass transition range (approximately 3 decades) the temperature dependence of the viscosity is described by the Arrhenian equation log $\eta = A + B/T$ with the kinetic fragility (steepness index) $m = A$-12. The Arrhenian parameters A and B are summarized together with the steepness index m and the isokom temperature T_{12} for which the Newtonian viscosity is 10^{12} Pa s ($T_{12} \approx T_g$) in Tab. 3.
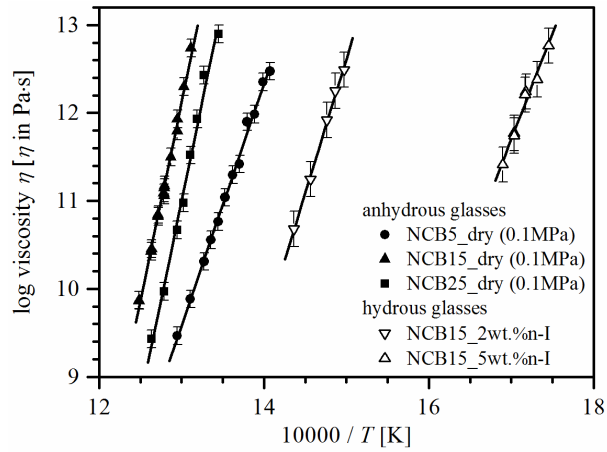
Fig. 7. Arrhenian representation of the temperature dependence of viscosity of the dry soda-lime borate glasses NCB5_dry(0.1MPa), NCB15_dry(0.1MPa), NCB25_dry(0.1MPa) and for two hydrated glasses NCB15_2wt.%n-I and NCB15_5wt.%n-I of cH$_2$O$_{(t)}$ = 1.90 and 4.90 wt.%, respectively. Lines are best linear fit of the equation log $\eta = A + B/T$ through the data.

Tab. 3 Viscosity of dry soda-lime borate glasses NCB5_dry(0.1MPa), NCB15_dry(0.1MPa), NCB25_dry(0.1MPa) and for two hydrated glasses NCB15_2wt.%n-I and NCB15_5wt.%n-I of $cH_2O_{(t)}$ = 1.90 and 4.90 wt.%, respectively. Arrhenian parameter A, B, kinetic fragility m (m = 12-A) and isokom temperature T_{12} (η (T_{12}) = 10^{12} Pa·s) of fitting the equation log $\eta = A+B/T$ through the data (η in Pa·s and T in K). Numbers in parentheses give uncertainty of the last digit.

	NCB5_dry(0.1 MPa)		NCB15_dry(0.1 MPa)		NCB25_dry(0.1 MPa)		NCB15_2wt.%n-I		NCB15_5wt.%n-I	
	T	log η	T	log η	T	log η	T	log η	T	log η
	710.6	12.47	762.6	12.74	743.5	12.90	667.9	12.49	572.9	12.77
	715.0	12.35	767.6	12.30	753.5	12.43	672.7	12.25	577.5	12.38
	720.2	11.99	772.3	11.93	758.2	11.93	677.3	11.92	582.1	12.24
	724.9	11.90	772.4	11.80	762.9	11.52	686.6	11.25	582.4	12.21
	729.7	11.42	777.1	11.50	767.7	10.98	696.2	10.68	586.9	11.74
	734.2	11.30	781.7	11.18	772.6	10.67			587.0	11.77
	739.2	11.04	781.8	11.15	782.0	9.97			591.7	11.41
	743.8	10.76	781.9	11.06	791.5	9.43				
	748.8	10.56	782.2	11.09						
	753.4	10.31	786.5	10.84						
	763.0	9.88	786.6	10.82						
	772.3	9.47	791.5	10.46						
			791.7	10.43						
			801.0	9.87						
			801.2	9.87						
A	-26.1(7)		-46.4(9)		-48(2)		-33(1)		-29(3)	
$B \times 10^{-4}$	2.74(5)		4.50(9)		4.52(19)		3.06(9)		2.41(17)	
m	38.1(7)		58.4(9)		60(2)		45(1)		41(3)	
T_{12} (K)	720		771		756		676		584	

4. Discussion

4.1 DTA versus viscosity measurement

The glass transition temperatures derived from DTA measurements are in excellent agreement (deviation less than 5 K) with the temperatures at which the viscosity equals 10^{12} Pa·s for NCB15 glasses with water contents up to 2 wt.% (Fig. 8). This finding confirms that the equivalence of enthalpy relaxation and viscous relaxation, which is well established for silicate melts [91,96,97], applies also to soda lime borate melts.

The deviation of the viscosity data for the melt containing about 5 wt.% dissolved water from the trend can be explained by water loss during viscosity measurement. Post-experimental analyses show that water loss was negligible during DTA measurement for that sample. From the deviation to the trend line it can be estimated that about 0.5 wt.% H_2O was lost in the sample volume probed by the sphere before and during the corresponding time period of micropenetration.

The evolution of T_g with water content shows the typical trend found for numerous aluminosilicates, i.e. a steep decrease of T_g at low $cH_2O_{(t)}$ and flattening of the curve at high $cH_2O_{(t)}$. Thus, the effect of water on glass transition in borate glasses is particularly pronounced at low water contents. Based on the trend line we infer that addition of 0.1 wt.% of water to a dry NCB15 melt reduces T_g by approximately 6 K.
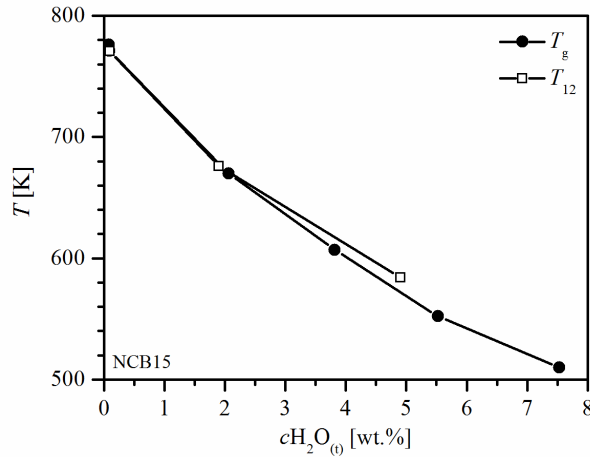
Fig. 8 Comparison of T_g from DTA measurements with T_{12} from viscosity measurements. Lines are intended as visual guides.

4.2 Effect of water vs. alkali on glass transition

Figure 9 shows T_g and T_{12} versus the total molar fraction of network formers (Na_2O + CaO + H_2O) of the nominally dry and hydrous soda-lime-borate glasses under study (NCBx, x = 5, 15 and 25 mol% Na_2O). In order to extend the concentration range, T_g and T_{12} data of dry and hydrous boron oxide glasses (x = 0) from Ref. [98] and of anhydrous NCB glasses with x > 25 from Refs. [57,99] are included in Fig. 9. It can be seen that for anhydrous glasses the expected course of the "boron anomaly" with a maximum at about 30 mol% network modifier is established. The corresponding change in the boron coordination from 3 to 4 in the NCB5, NCB15 and NCB25 glasses was shown in a previous paper by NMR measurements [90].

As water content increases a pronounced drop in T_g and T_{12} is evident for all glasses under study. Also for pure B_2O_3 glasses a decrease in the glass transition with increasing $cH_2O_{(t)}$ was observed [81,98]. Although anhydrous glasses have different T_g values caused by different sodium content, the decrease of T_g by increasing water content is nearly the same for all three NCB glasses (see e.g. dashed water concentration iso-lines in Fig. 9 and Fig. 10). It is obvious that water does not significantly influence boron coordination as known for alkaline ions. There appears to be no strengthening of glass structure by a change of coordination of boron by oxygen

when water is inserted. This can be confirmed by the results of our previous paper [90] where only a very slight increase of boron coordination with increasing water content was measured. Therefore, the addition of water predominantly causes the formation of NBO in the network. This is further confirmed by the dashed water concentration iso-lines in Fig. 9. The iso-lines were constructed by employing the ΔT_g values of Fig. 10 for each series of hydrous glasses and inserting the data on the trend lines indicated by arrows in Fig. 9. The iso-lines for 3.4 and 5.8 mol% water-bearing glasses show almost the same course of the "boron anomaly" as for the anhydrous glasses. With increasing water content the maximum shifts towards larger total amount of network modifiers in which the shift approximately corresponds to the water content.

To shed light on the role of water on viscosity of hydrated NCB, its steepness index m is analyzed. Figure 11 shows that these glasses obey the trend established for hydrous silicate glasses in a previous study [100]: Water, which is predominantly dissolved as OH groups decreases the liquid fragility. To revisit this relation for an enlarged data basis of hydrous melts, literature data of the Newtonian viscosity in the systems (H_2O)-Na_2O-B_2O_3-SiO_2 [100], (H_2O)-Na_2O-CaO-SiO_2 [100,101], (H_2O)-Na_2O-SiO_2 [87], and (H_2O)-SiO_2 [102,103] are also plotted in Fig 11. Thus, also for NCB glasses the dependence of m on the water concentration can be approximated by a straight line of the type $m = a - b \cdot \log cH_2O_{(t)}$ with the fitting parameters $a = 47.8 \pm 0.8$, $b = 9.6 \pm 0.9$ $cH_2O_{(t)}$ in wt.%). It should be noted, that this trend is only valid within the investigated range of $cH_2O_{(t)}$, where water is presumably present as OH. Spectroscopy reveals that dissolution of water as molecules starts already at $cH_2O_{(t)} \approx 0.5$ wt.% in soda-lime-silicate glasses [46] and at $cH_2O_{(t)} \approx 1.5$ wt.% in hydrous silica glasses [103]. In contrast, for the soda-lime-borate glasses of this study, predomination of OH groups occurs even at very high $cH_2O_{(t)}$ (>7.5 wt.%). Furthermore, Fig. 11 shows that the slope of the lines increase with increasing fragility of the glass systems under consideration.

57

On the other hand, the effect of water molecules on liquid fragility is less clear. For hydrous silicate glasses it is reported that water molecules although strongly decreasing viscosity only weakly influences kinetic fragility [100]. This apparent contradiction could be possibly explained in terms of the mechanism adopted in explaining surface stress relaxation phenomena utilized as a novel glass strengthening method in Ref. [104]. According to [104,105], two water molecules inside of large voids of a silica network may break into OH^- and H_3O^+. The excess proton of the hydronium ion (H_3O^+) can jump to other water species or through the silica network. Bridging oxygen's, in particular those being strained, are prone for free proton absorption and can temporarily form energetically favourable bridging OH groups before jumping to a new site [104,106–108]. Such process results in a change of Si-O-Si bond angle, a change observed in silica glass associated with surface structural stress relaxation. It seems plausible to assume that such mechanism can also affect viscosity due to local stresses involved in viscous flow.

If one assumes the same trend also for the other glass types, i.e. that water molecules only weakly influences kinetic fragility [100], no change in the steepness index within the shaded area of Fig. 11 (hydrous glasses with predomination of H_2O molecules), a value between 15 and 37 is expected for the fragility of pure water. This assumption would lead to the result that pure water is a relative strong liquid at $T_g/T = 1$, which is in agreement with the proposition that pure water is strong near the glass transition but becomes fragile at higher temperatures showing a strong-to-fragile transition in the temperature range $T_g/T = 0.6$–0.8 [109,110].

In order to quantify the effect of the two different water species (OH groups and H_2O molecules) on the decrease of the glass transition temperature, a three component model was proposed, which predicts T_g of a water-bearing glass as a weighted combination of contributions of the dry glass, OH groups and H_2O-molecules [88]. Using the reduced glass transition temperature

$T_g/T_g{}^{GN}$ where $T_g{}^{GN}$ is the glass transition temperature for a dry glass containing 0.02 wt.% total water, T_g of different glass compositions can be compared [45]:

$$\frac{T_g}{T_g{}^{GN}} = \frac{1.01 \cdot c_G + 0.22 \cdot A \cdot cOH + 0.22 \cdot B \cdot cH_2O_{mol}}{c_G + A \cdot cOH + B \cdot cH_2O_{mol}} \qquad (3)$$

where c_G (= 1- $cH_2O_{(t)}$, cH_2O_{mol} and cOH are the corresponding weight fractions ($c_i = C_i / 100\%$ with C_i listed in Tab. 2) of anhydrous glass and water dissolved as H_2O molecules and OH groups, respectively. A and B are adjustable parameters, which express the influence of hydroxyl and molecular H_2O on $T_g/ T_g{}^{GN}$. Figure 12 shows that the reduced glass transition temperature is shifted to higher water content for hydrous borate glasses, which indicates that molecular water is less influential in borate glasses and vice versa OH groups are more efficient. The difference can be derived also from the ratio A/B, which is 6.5 and 2.6 in hydrous borate and silicate glasses, respectively.
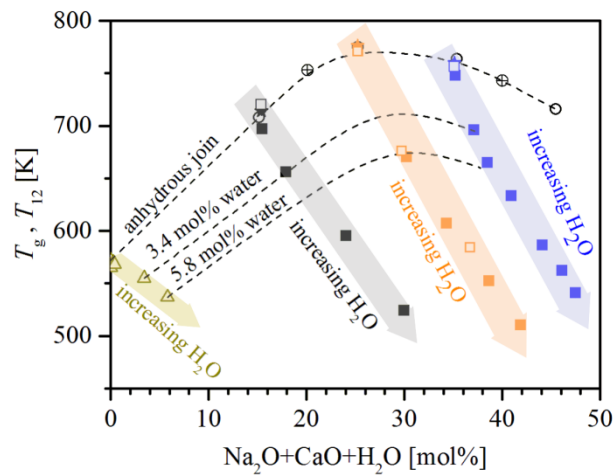
Fig. 9 Glass transition temperature T_g (solid stars and squares) and T_{12} (open squares) vs. summarized molar fraction $Na_2O + CaO + H_2O$ for dry and hydrous NCB5, NCB15, and NCB25 glasses (grey, orange and blue arrows, respectively). Water contents are based on IR data before experiment. Literature data: Dry soda-lime-borate glasses with x = 5, 15, 25, 35 [57] (open circle) and x = 10, 30 [99] (cross circle) as well as dry and hydrous boron oxide (x = 0) [98] (open triangle).
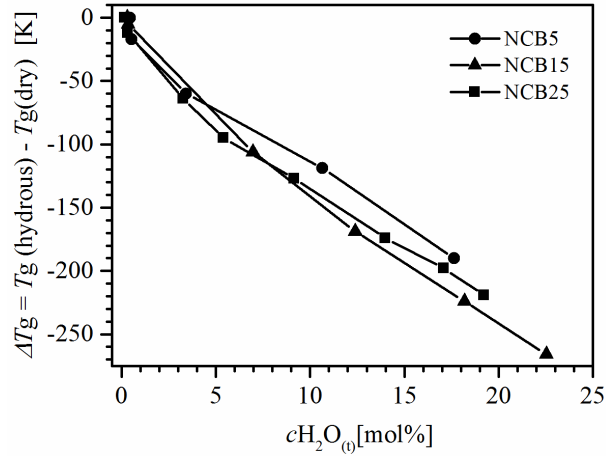
Fig. 10 Decrease in the glass transition temperature ΔT_g for NCBx glasses with increasing water content $cH_2O_{(t)}$. Water contents are based on IR data before experiment.
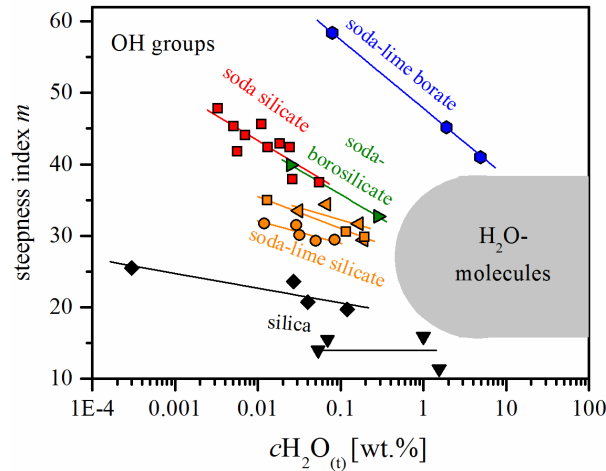
Fig. 11. Steepness index m vs. water content $cH_2O_{(t)}$. Data of hydrous glasses: (H_2O)-Na_2O-CaO-B_2O_3 (NCBx, this work, blue hexagon, Tab. 3), (H_2O)-Na_2O-B_2O_3-SiO_2 (green triangle, [100]), (H_2O)-Na_2O-CaO-SiO_2 (orange circle, [101]; orange square and orange triangle [100]), (H_2O)-Na_2O-SiO_2 (red square, [87]), and (H_2O)-SiO_2 (black diamond, [102]; black triangle, [103].

Lines are best fit of the equation $m = a - b \cdot \log cH_2O_{(t)}$ through the data. For hydrous borate glasses the adjustable parameters a and b are 47.8 and 9.6, respectively. For other glasses see Ref. [100]. Grey area: Hydrous glasses in which water is predominantly dissolved as H_2O molecules.
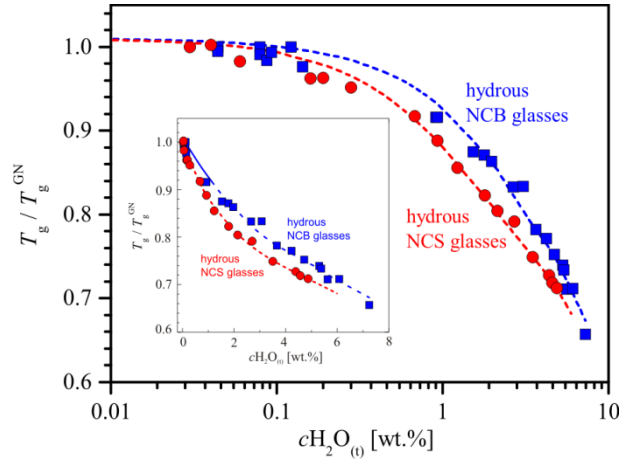
Fig. 12. Reduced glass transition temperature T_g/T_g^{GN} of the soda-lime borate (NCB) glasses of this study and for soda-lime silicate (NCS) glasses of Ref. [89] versus total water content $cH_2O_{(t)}$ in logarithmic scales (Insert: $cH_2O_{(t)}$ in linear scales). Lines are fit of Eq. (2) through the data with A = 11.7 and B = 1.8 (NCB) and A = 21.0 and B = 8.0 (NCS). Note: In accordance with Ref. [45] we set $T_g^{GN} = T_g(cH_2O_{(t)} = 0.02$ wt.%) and assumed that for the glasses NCB5_dry (0.1MPa), NCB15_dry (0.1MPa), NCB25_dry (0.1MPa) the reduced glass transition temperature is unity. In case of NCS glasses of Ref. [89] we set $T_g/T_g^{GN} = 1$ for the sample FG0a with $cH_2O_{(t)} = 0.03$ wt.%.

5. Conclusion

Glass transition temperatures of soda lime borate glasses strongly decrease upon hydration. This behavior is opposite to what is known as the boron anomaly, i.e. the increase of T_g when alkali oxide is added to boron oxide glass. The findings show that, in contrary to alkali cations, protons are unable to support tetrahedrally coordinated boron within the borate network. Thus, incorporation of H_2O in borate glasses mainly causes breaking of B-O-B bonds resulting in a reduction of viscosity and the glass transition temperature. The strong increase in the liquid fragility of hydrous borate glasses which reflects a less stability of their short-range order against temperature-induced structural degradation appears to be in line with the predominate mechanism of a water-induced B-O-B breakage.

A similar behavior can be expected for other boron-bearing glasses, e.g. borosilicate glasses. Glasses with water contents of several wt.% as studied in this paper are not common in industrial

glass production. However, water-rich regions can be locally formed in glasses, for instance near the surface by corrosion and near the tip of cracks where water is easily absorbed. For these hydrous regions one would expect a much lower glass transition temperature and by that a strongly extended ability for stress accommodation. However, the impact of a modified surface glass structure on fatigue and practical strength is beyond the scope of this study and will be addressed in a future investigation.

Chapter 2A[1]

Structural Investigation of Hydrous Borosilicate Glasses

Abstract

The structural properties of a borosilicate glass with nominal 16 mol% Na_2O, 10 mol% B_2O_3 and 74 mol% SiO_2 and water contents between 0 and 8 wt.% H_2O (0-22 mol% H_2O) were investigated with IR, Raman and ^{11}B MAS NMR spectroscopy. In addition to the pronounced OH stretching vibration band of weakly H-bonded species at 3580 cm^{-1} the MIR spectra show a triplet at 2900, 2350 and 1750 cm^{-1}, similar as observed in water-bearing silicate glasses. These bands are assigned to OH groups and water molecules which are strongly H-bonded, to non-bridging oxygen.

Water species contents determined from absorption bands in the NIR at 5200 cm^{-1} (molecular H_2O), 4700 cm^{-1} (B-OH), and 4500 cm^{-1} (Si-OH) indicate that hydroxyl groups dominate up to ~6 wt.% total H_2O. Based on the absorption coefficients known from literature for silicate and borate glasses the B-OH/Si-OH ratio is estimated to be ≈ 0.8.

As indicated by density, Raman and NMR data the incorporation of water has strong structural impacts in particular at low water contents up to 3 wt.% H_2O. While the nominally dry glasses still contain a significant fraction (12%) of three-fold coordinated boron, all boron is four-fold coordinated in hydrous glasses.

Raman spectroscopy indicates that the addition of water results preferentially in the formation of silicon tetrahedra with only two bridging oxygen (Q^2) while the abundance of silicon tetrahedra with three bridging oxygen (Q^3) remains constant. Contributions of species with and without bonding to BO_4 tetrahedra can be separated in the Raman spectra for both Q^2 and Q^3 species.

Comparison to the NMR data suggests that BO_4 tetrahedra are preferentially connected with Q^3 species, stabilizing these species against depolymerization upon further water addition.

_____

[1]A modified version of this Chapter was submitted to the Journal of Non-Crystalline Solids in Nov. 2016, Structural investigation of hydrous sodium borosilicate glasses, U. Bauer, H. Behrens, S. Reinsch, E. I. Morin, J. F. Stebbins.

1. Introduction

Borosilicate glasses were intensively investigated in the past because of their wide range of technical glass applications as e.g. optical glasses or as container material of nuclear waste. Special features of such glasses are e.g. high chemical durability and thermal-shock resistivity.

With the addition of alkalis or alkaline-earth oxides to boron containing glasses, boron initially present as trigonal planar groups (BO_3) is charge compensated by the additional oxygen and thus four-fold coordinated boron (BO_4) species is generated. At high alkali or alkaline-earth contents, the excess oxygens act as non-bridging oxygens (NBO) and result in a depolymerization of the network and the conversion from BO_4 to BO_3. Temperature and pressure also affects the boron coordination and hence causes changes e.g. in density, thermal expansion and mechanical properties of the glass [4,7,10,80,85,111–115].

Glasses of technical relevance typically contain much less than one weight percent H_2O (e.g. < 0.1 wt. % H_2O in silicate and borosilicate < 1 wt.% H_2O in borate and phosphate glasses). High water contents of several weight percent are common in natural systems as volcanic glasses, but are usually of minor importance for industrial glass production. However, such high water contents may become of interest for water-related fatigue of glasses since water easily can be absorbed and accumulated for instance at crack tips or near the glass surface and lead to corrosion.

The influence of water on glass properties in boron-bearing glasses is poorly investigated compared to silicate and aluminosilicate glasses. Water and alkalis both depolymerize the melt structure and thus reduce the viscosity of the melt [11,12], whereby the effect of water is stronger compared to alkalis, e.g. [14]. It is known that water in glasses is present as two main species: as molecular water and as water dissolved in form of OH groups [14,15,16,17]. The fraction of the two different water species present in silicate and aluminosilicate glasses, respectively compared to borate glasses are very different. Whereas OH groups are dominating

only at moderate water contents (< 4 wt.% H_2O) in silicate glasses [46,47,74], they are the dominant species up to ~8 wt.% H_2O in aluminoborosilicate glasses [34] and are predominantly present in borate glasses even for water contents $\geq$ 8 wt.% H_2O [90], reflecting a trend of increasingly stabilized OH groups with rising boron content.

In soda lime borate glasses it was recently found that the effect of water on the stabilization of boron in tetrahedral coordination is ten times lower compared to that of alkalis, probably because protons are much more localized compared to alkalis [90]. For aluminoborosilicate glasses a slightly larger influence of water on B speciation was discovered [5].

In this study ^{11}B MAS NMR, Raman, MIR and NIR spectroscopy are applied to improve the knowledge about the role of water in the borosilicate glass network. Kinetic aspects of these glasses obtained from measurements of the glass transition temperature, viscosity and internal friction are discussed in a forthcoming paper.

2. Experimental and analytical methods

2.1 Starting materials

For the synthesis of borosilicate glass containing nominal 16 mol% Na_2O, 10 mol% B_2O_3 and 74 mol% SiO_2 powder mixtures of Na_2CO_3, B_2O_3 and SiO_2 were melted in a 2.4 liter platinum crucible at 1603 K for 3.5 hours in an induction furnace. During the last 40 min at 1603 K the melt was stirred 20 min in the lower part and 20 min in the upper part of the platinum crucible to facilitate homogenization. Subsequently the temperature was raised to 1673 K. After 1 hour the melt was poured into a preheated graphitized steel mold. The obtained glass ingots were transferred into a furnace preheated at 893 K and subsequently cooled in the switched-off furnace during the night for stress relaxation. The composition of the NBS start glass was analyzed by inductively coupled plasma-optic emission spectrometry (ICP-OES, 715-ES

VARIAN). ~50 mg sample material were dissolved by microwave digestion using 4 ml 85% H_3PO_4, 3 ml 65% HNO_3 and 1 ml 40% HF. The specified contents are based on three individual analyses (16.00 ± 0.21 mol% Na_2O, 9.97 ± 0.11 mol% B_2O_3 and 74.03 ± 0.30 mol% SiO_2). The NBS start glass was crushed with a steal mortar to powder which was subsequently used for the synthesis of hydrous and compressed glasses.

2.2 Hydrous and compressed glasses

For syntheses of hydrous glasses, glass powder and distilled water were filled stepwise in turn in a platinum capsule (diameter: 6 mm, length: 25–30 mm) to facilitate homogeneous distribution of water in the glass. To produce anhydrous compressed glasses only the starting glass powder was loaded into the platinum capsules. By subsequent compaction of the material in the capsule using a steel piston a cylindrical shape of glass bodies was achieved. After sealing with a PUK welding device (PUK3 Professional Plus, Co. Lampert), the capsules were checked for possible leakage by measuring the weight loss after storage in a drying furnace at 373 K.

Syntheses were performed in an internally heated pressure vessel (IHPV) at 500 MPa and 1423 K for 14–20 h using argon as pressure medium. In each run 2-3 capsules were placed in the hot spot zone of the sample holder between the two furnace-controlling K-type thermocouples (Ni-CrNi). The temperature of the samples was monitored by a third thermocouple located in the middle of the hot spot zone. The maximum variation in temperature during the synthesis was ±10 K, and pressure accuracy is within ±50 bars. In order to preserve pressure induced structural changes and to avoid water loss of the glasses, samples were isobarically quenched using an automatic pressure controller (normal quench, NQ) when switching off the furnace. This leads to a cooling rate in the regime of T_g of ~8 K/s for NBS0-500MPa, NBS0.5 and NBS1, ~6 K/s for NBS3 and ~3.5 K/s for NBS5. The sample containing 8 wt.% H_2O was quenched much faster (~200 K/s) through the range of glass transition using a rapid quench (RQ) sample holder since

the sample was partially crystallized in a first trial when using the NQ procedure. A detailed description of the RQ method for IHPV is given in Berndt el al.[50].

All glass cylinders were clear and no crystals or bubbles were observed after high pressure synthesis. This implies that synthesis conditions were volatile-undersaturated, means H_2O solubility in the borosilicate glass is significantly above 8 wt.% at 1423 K and 500 MPa. For IR and KFT measurements glass pieces were cut from each end of the glass body to test for homogeneous distribution of water (Tab. 1). Exposure of glasses to water was avoided and oil was used for sawing and polishing samples, e.g. for preparation of thin sections for spectroscopy. In following, the number in the sample name refers to the nominal water content and roman numerals are used to distinguish glasses pieces cut from both ends of the glass body.

2.3. Analysis of water content and speciation

The total water content $cH_2O_{(t)}$ of the glasses was determined by pyrolysis and subsequent Karl-Fischer Titration (KFT). The analysis procedure for the borosilicate glasses was the same as reported in Bauer et al. 2015 [90]. A detailed description of the method is given in [43,47,51–53].

IR spectra were collected on sections polished on both sides using a Fourier Transform Infrared (FTIR) spectrometer (Bruker IFS88) coupled with an IR microscope (Bruker IR scope II) equipped with a mercury-cadmium-tellurium (MCT) detector. Absorption spectra in the mid-infrared (MIR) were recorded to investigate fundamental OH stretching vibrations and to determine $cH_2O_{(t)}$ of nominal dry glasses. A KBr beam splitter and a globar light source were use, and spectra were recorded in the range of 600 to 6000 cm^{-1} with a spectral resolution of 2 cm^{-1}. 50 scans for sample and background (air) measurements were accumulated. A slit aperture between the objective and the detector was used to limit the analyzed sample volume. In the focus plane, the area selected by the slit was typically (100 x 100) μm^2.

To determine different water species contents of H_2O molecules (cH_2O_{mol}) and water dissolved in form of OH groups (cOH) near-infrared (NIR) spectra were collected using a tungsten light source and a CaF_2 beam splitter in combination with the MCT detector. Spectra were measured in the range of 2000 - 11000 cm^{-1} with a spectral resolution of 4 cm^{-1} and 100 scans were accumulated for each spectrum. As in the case of measurements in MIR an area of (100 x 100) μm^2 in the focus plane was selected. At least three spectra for each sample were measured to check the reproducibly of the collected spectra and the homogeneity of water distribution in the glass. Additional samples produced for dynamic mechanical analysis (DMA) are also included in our spectroscopy study (indicated by DMA in Tab. 1). Here, NIR spectra were collected on bulk samples using a 2 mm aperture and an Indium SB D 413 detector. An aperture plate of 2 mm in diameter was chosen to limit the analyzed sample volume. The spectral resolution in the NIR was 2 cm^{-1} and 100 scans were accumulated for background and sample measurements. The thickness of the glass sections and bars were measured using a digital micrometer (Mitutoyo) with a precision of $\pm$ 2 μm. The average thickness of each sample is listed in Tab. 1,2.

2.4 NMR spectroscopy

^{11}B MAS NMR spectra were collected on a 14.1 T Varian spectrometer using a Varian/Chemagnetics T3 probe with 3.2 mm zirconia rotors. The spinning speed was 20 kHz, the recycle delay was 8s, and a radio frequency pulse length of 0.275 μs was used, which corresponded to a (solid) rf tip angle of 21°. [11]B chemical shifts were reported in parts per million (ppm) relative to 1.0 M boric acid at 19.6 ppm. Fits were done with either multiple Gaussians or two quadrupolar lineshapes for BO_3 with the DMFIT program, using two Gaussians for the BO_4 peak, and correcting for spinning sidebands. Both fitting procedures resulted in similar N_4.

2.5 Raman

Raman spectra of hydrous and anhydrous NBS glass samples were collected in the frequency range between 300 and 1700 cm^{-1} on a confocal Bruker Senterra micro-Raman spectrometer equipped with an Olympus BX 51 microscope and an Andor DU420-OE CCD camera. Unpolarized spectra were obtained at ambient conditions, using the 532 nm laser excitation line with 20 mW power, under the 20x magnification of an Olympus SWD (short working distance) objective for 40 s with 3 times acquisition repetitions. An aperture with 50 x 1000 μm^2 was chosen and the instrumental precision was within ±3 cm^{-1}. Measurements were conducted on polished samples with 2-3 mm thickness a few microns below the surface. The spectra were only background corrected and neither corrections for temperature nor frequency were applied since "thermal effects" affect the spectra only below 300 cm^{-1} and contributions from excitation line are very small [116]. Curve fitting was performed using OriginPro2016G.

3. Results and discussion

3.1 Band assignment in the mid-infrared

Information about differences in hydrogen bond strength can be derived from the region of fundamental OH-stretching in the mid-infrared. Fig. 1(a) shows MIR spectra of nominal dry glasses (NBS0-0.1MPa, NBS0-500MPa) and glasses containing 1 and 3 wt.% H_2O respectively. The spectra of hydrous NBS glasses resemble on spectra of silicate glass, e.g. [15,18,53] and show a characteristic absorption peak at 3580 cm^{-1} which is attributed to OH stretching vibrations of weakly H-bonded hydrous species. The sharp band developing at 1635 cm^{-1} with increasing water content is due to bending vibrations of H_2O molecules (Fig. 1(b)) [14,40].

Additional features related to vibrations of water species could be identified in subtraction spectra in which the spectrum of nominal dry NBS0-0.1MPa glass was subtracted from water

containing glasses. In the subtraction spectra the contributions of network vibrations in the range between 1500 and 2000 cm^{-1} are removed. Broad absorption bands at ~2900, ~2350, and ~1750 cm^{-1} in subtraction spectra of NBS glass (Fig. 1b) resemble features of water-bearing silicate glasses sometimes referred to as the ABC triplet [47,61]. According to [61] these bands do not represent different water species expiring different degrees of hydrogen bonding but result from different vibrations of the same type of species. It is noteworthy that the ABC triplet is not a specific property of OH groups but occurs for H_2O molecules as well [47,117].
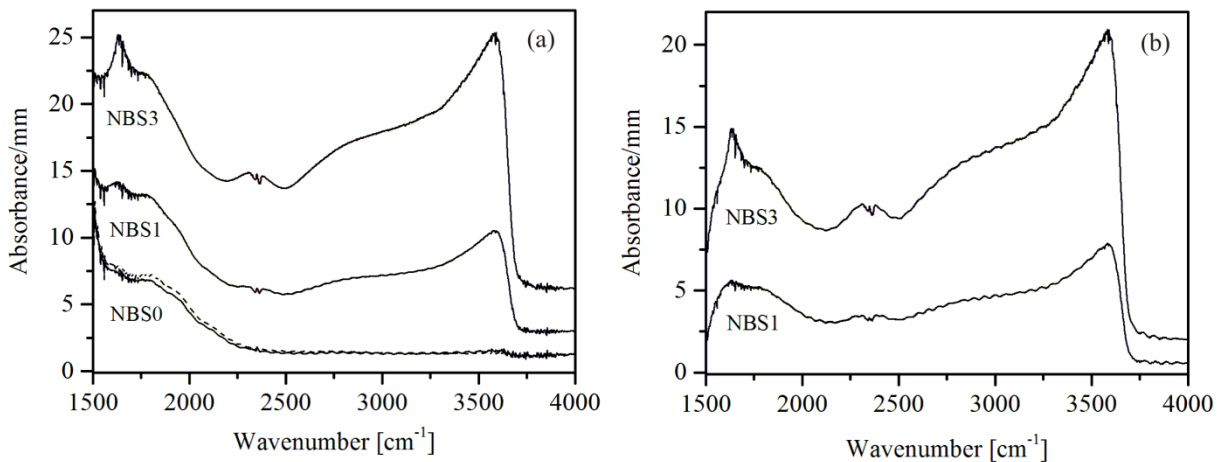
Fig. 1. (a) MIR spectra of nominally dry NBS0-0.1MPa (dotted line) and NBS0-500MPa samples as well as NBS1 and NBS3. The spectra are normalized to the same thickness and are shifted for clarity. (b) Subtraction spectra of NBS1 and NBS3. The weak features at 2350 cm^{-1} are caused by differences of CO_2 contents between a background and a sample measurement.

3.2 Band assignment in the near-infrared

NIR spectra for hydrous NBS glasses with nominal water contents of 1, 3, 5, and 8 wt.% H_2O are shown in Fig. 2. A spectrum of a nominal dry NBS glass is shown for comparison. Four main band features can be observed at ~4000, 4500, 4700 and 5200 cm^{-1}, and their intensities are rising with increasing water content. Bands at 5200 and 4500 cm^{-1} are assigned to the combination of stretching and bending vibrations of H_2O molecules and OH groups attached to silicon (Si-OH), respectively [14,17,40,118]. In borosilicate glasses a peak near 4700 cm^{-1} was reported in the study of Schmidt [59] who attributed the peak to hydroxyl groups connected to

boron in tetrahedral configuration (B-OH). This is in accordance with the findings in soda lime

borate glasses [90]. The interpretation of the absorption band near 4000 cm^{-1} is not that clear. It

was attributed to combination modes of strong Si-OH bonds [119], to molecular water [48] or to

vibrations involving both species, molecular water and OH groups [17]. Fig. 2(b) shows that the

normalized absorbance of the band near 4000 cm^{-1} is correlated with the total water content in

borosilicate glasses. Since the intensity of this band is comparable to other combination bands in

the NIR, the band is most likely a combination of OH stretching vibration with a low

wavenumber mode in which hydrous species are involved.
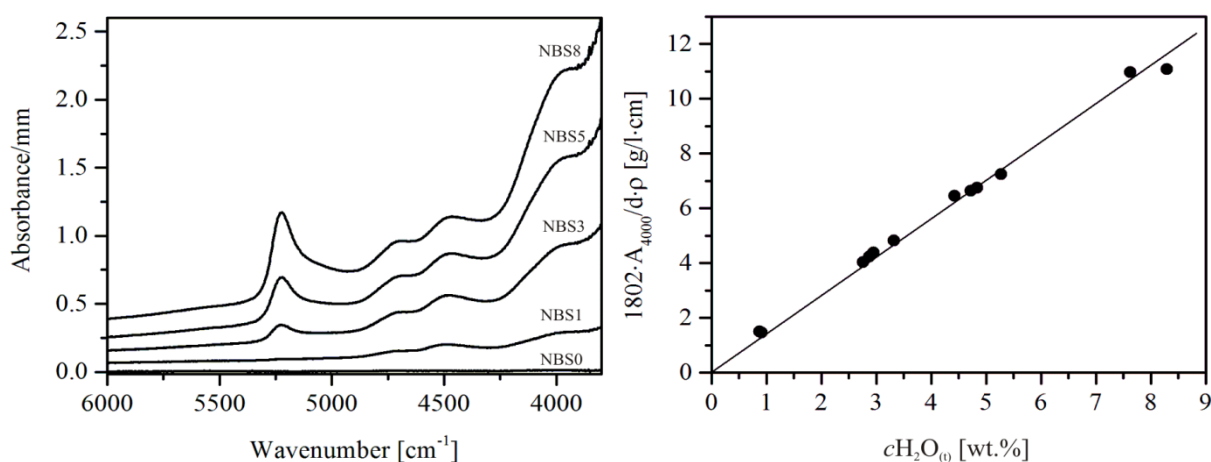
Fig. 2. (a) Selected NIR spectra of NBS glasses. The spectra are normalized to the sample thickness. (b) Absorbance of the peak at 4000 cm^{-1} normalized to sample thickness and density plotted vs. the total water content.

3.3 Quantitative evaluation of IR spectra

3.3.1 Water contents of nominal dry glasses

For the determination of total water contents of nominal dry glasses the absorbance of the band

at 3580 cm^{-1} in the mid-infrared range was used. This band is superimposed by other OH

stretching contributions as mentioned above and hence only little constraints for the construction

of a baseline are given. Therefore, the absorbance at 4000 cm^{-1} was taken as a characteristic

background value following the recommendation of the Technical Committee (TC14) of the

International Commission of Glass (ICG) [65] based on soda-lime silicate glass. By using the Lambert-Beer law and the knowledge of the density ρ, the sample thickness d and the linear molar absorption coefficient ε the total water content of nominal dry glasses can be obtained:

$$c_{H_2O_{(t)}} = \frac{1802 \cdot A_{3580}}{d \cdot \rho \cdot \varepsilon_{3580}} \qquad (1)$$

The linear molar absorption coefficient ε_{3580} was derived from two fragments of NBS1 with slightly different water contents (see Tab. 1). By averaging these values a linear molar absorption coefficient of $\varepsilon_{3580=}$70.6 ($\pm$1.6) l·mol^{-1}·cm^{-1} was determined, comparable to values determined for polymerized aluminosilicate glasses [120]. Spectra of NBS3 glasses were not included in the calibration since the absorbance of the 3580 cm^{-1} is too high to allow reliable quantification. The derived water contents of nominal dry glasses are shown in Tab. 2. Compared to the dry sample melted at 0.1 MPa, the high pressure sample exhibit only a slightly higher water content ($c_{H_2O_t}$ = 0.010 ($\pm$0.001) wt.% for NBS0-0.1MPa, $c_{H_2O_t}$ = 0.029 ($\pm$0.001) wt.% for NBS0-500MPa). This implies that the NBS glass powder used in the high pressure synthesis is not sensitive to adsorbed water.

3.3.2 Quantification of water species contents

Usually flexicurve or tangent baselines are applied to near-infrared spectra. As discussed in the study of Withers and Behrens [63] and Ohlhorst et al. [66] the choice of baseline type heavily influences subsequent spectra evaluation and hence quantification of water species contents. Therefore, we used different types of baseline corrections to test for high reproducible application to low and high water-bearing glasses. Compared to a flexicurve baseline we found that a straight line defined by the flat absorption region in the frequency range between 6000 and 5400 cm^{-1} is better constrained especially for both OH bands and exhibits a high reproducibility

over the range of investigated water contents. This procedure was also applied to hydrous borate glasses investigated in our previous study [90] and to borosilicate glasses studied by Schmidt [59]. Examples of the applied baseline correction are shown in Fig. 3.
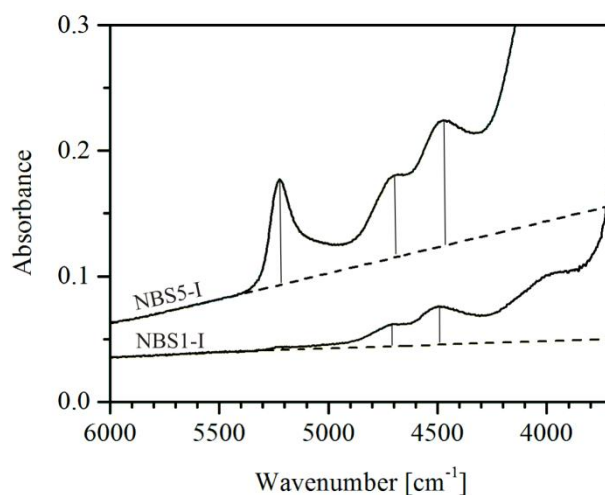
Fig. 3. NIR spectra of hydrous NBS glasses (1 and 5 wt.% H_2O). Dashed lines show the baseline applied to the spectra. Solid vertical lines represent the peak positions of peak maxima which were used for the quantification of water speciation (5200 cm^{-1} for H_2O_{mol}, 4500 cm^{-1} and 4700 cm^{-1} for OH).

The quantification of water speciation in our hydrous NBS glass series is based on the peak at 5200 cm^{-1} for molecular water and the bands at 4500 and 4700 cm^{-1} which represent the amount of hydroxyl groups bond to Si and B, respectively. Determination of the contents of Si-OH and B-OH requires the knowledge of the individual absorption coefficients for these bands. These values can be determined only when independent information of the relative abundance of both OH species is available or if the ratio of peak intensities varies strongly with water content. As shown in Fig. 4 the absorbance at 4700 cm^{-1} (A_{4700}) is proportional to that at 4500 cm^{-1} (A_{4500}) at least up to total water contents of 5.3 wt.%. Deviations at higher water contents may be an artifact of baseline correction. Thus, the total OH content can be quantified using either the absorbance of one of the OH peaks (i.e. A_{4500}) or sum of both peaks ($A_{4500+4700}$). We have tested

74

the consistency of both approaches and the associated errors in determination of species concentrations.
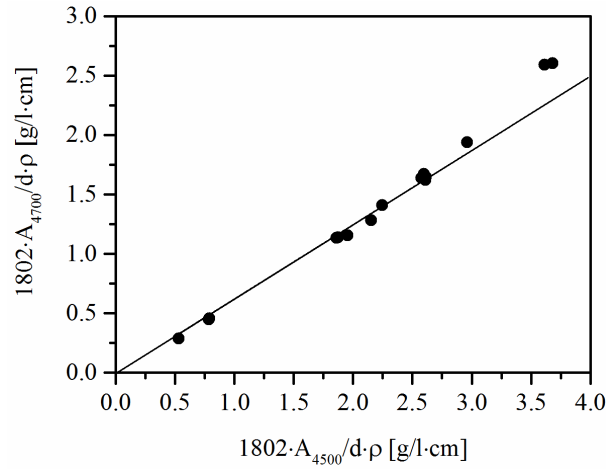
Fig. 4. Absorbance of the 4700 cm^{-1} absorption band normalized to density and sample thickness is plotted as a function of the normalized absorbance of the 4500 cm^{-1} peak. The linear fit include samples with water contents between 0.5 and 5 wt.%.

Water species contents can be calculated from the modified Lambert-Beer law:

$$cH_2O_{mol} = \frac{1802 \cdot A_{5200}}{d \cdot \rho \cdot \varepsilon_{5200}} \qquad (2)$$

$$cOH = \frac{1802 \cdot A_{4500}}{d \cdot \rho \cdot \varepsilon_{4500}} \qquad (3)$$

or, when using the sum of both OH bands

$$cOH = \frac{1802 \cdot A_{4500+4700}}{d \cdot \rho \cdot \varepsilon_{4500+4700}} \qquad (4)$$

where cH_2O_{mol} refers to the content of dissolved molecular water and cOH to the content of dissociated water in the glasses, both are given in wt.%. d is the sample thickness in cm. For

water contents between 1 and 8 wt.% H_2O the dependence of density ρ (in g/l) on water content (in wt.%) can be described by the linear relation $\rho = 2541\ (\pm 7) - 19.0\ (\pm 1.6) \cdot cH_2O_{(t)}$ (Fig. 5). This equation applies only to high pressure glasses. Samples relaxed at ambient pressure have densities 1 - 2 % lower. Additionally, samples with low water contents show systematic deviation from this trend which points to structural changes in the glasses, see below. However, for the determination of species concentration this deviation is of minor importance and species concentrations can be determined with a precision of 2 % using the density relationship.
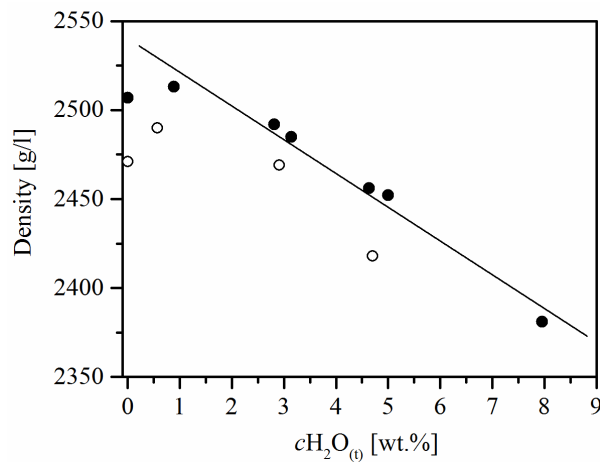
Fig. 5. Densities of anhydrous and hydrous high pressure NBS glasses as a function of water content are marked with filled symbols. Densities of anhydrous and hydrous relaxed NBS glasses are marked with empty symbols. The constants for the linear equation to calculate densities were obtained by least square regression of the density data of hydrous high pressure samples. Error bars are smaller than the symbols.

Assuming that the absorption coefficients are constant over the range of H_2O contents investigated, the linear molar absorption coefficient can be derived combining Eq. (2) and (3):

$$\frac{1802 \cdot A_{5200}}{d \cdot \rho \cdot cH_2O_{(t)}} = \varepsilon_{5200} \cdot \frac{\varepsilon_{5200}}{\varepsilon_{4500}} \cdot \frac{1802 \cdot A_{4500}}{d \cdot \rho \cdot cH_2O_{(t)}} \tag{5}$$

where $cH_2O_{(t)}$ is the total H_2O content measured by KFT. A similar equation is obtained by combining Eq. (2) and (4) when using the sum ($A_{4500+4700}$).

The absorption coefficients determined from both approaches are $\varepsilon_{5200} = 1.01$ (± 0.04) $l \cdot mol^{-1} \cdot cm^{-1}$ and $\varepsilon_{4500} = 0.98$ (± 0.06) $l \cdot mol^{-1} \cdot cm^{-1}$ in the case of the single band method and $\varepsilon_{5200} = 1.08$ (± 0.05) $l \cdot mol^{-1} \cdot cm^{-1}$ and $\varepsilon_{4500+4700} = 1.52$ (± 0.04) $l \, mol^{-1} \cdot cm^{-1}$ for the two band method (Fig.6). Information about the proportions of B-OH and Si-OH in NBS glasses can be derived from the peak heights at 4500 and 4700 cm^{-1}, if reasonable estimates of the absorption coefficients are available.

$\varepsilon_{4500+4700}$ for NBS is similar to the absorption coefficient of the Si-OH band in a rhyolite glass ($\varepsilon_{4500(Rh)} = 1.52$ (± 0.08) $l \cdot mol^{-1} \cdot cm^{-1}$ [63]) and the absorption coefficient of the B-OH band derived from different soda-lime borate glasses ($\varepsilon_{4600(NCB)} = 1.12$ (± 0.13) $l \cdot mol^{-1} \cdot cm^{-1}$ [90]) using a similar baseline correction. The NIR absorption coefficients for aluminosilicate glasses depend strongly on the degree of polymerization [120], and within this group of glasses rhyolite has the largest structural similarity to NBS glass. In borate glasses the peak position of the B-OH band is slightly lower than in the borosilicate glass, but non-bridging oxygen which have major impact on the absorption coefficient of the NIR combination bands due to H-bonding, are absent in borate glass. Hence, we suggest that ε_{4600} of borate glass is a good proxy for B-OH bonds in borosilicate as well. With this pre-requisites we can estimate the ratio of B-OH/Si-OH as:

$$\frac{B-OH}{Si-OH} = \frac{A_{4500}/\varepsilon_{4500(Rh)}}{A_{4700}/\varepsilon_{4600(NCB)}} \tag{6}$$

The B-OH/Si-OH ratio of 0.83 ± 0.06 implies only a slightly higher fraction of Si-OH over B-OH.
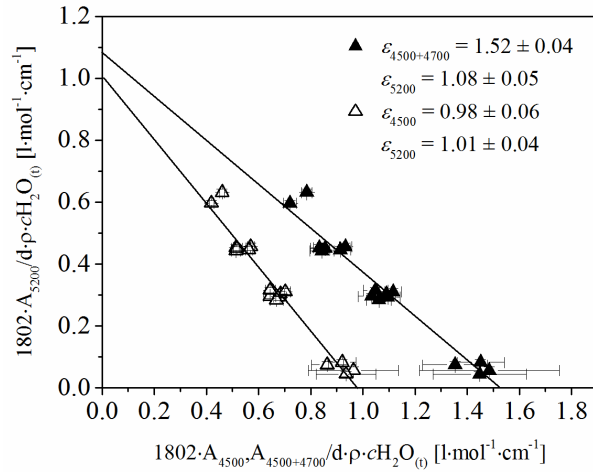
Fig. 6. Calibration plot for the determination of the linear molar absorption coefficient of the NIR absorption bands from hydrated NBS glasses. Empty triangles refer to data using the absorbance at 4500 cm^{-1}. Filled triangles based on the sum ($A_{4500+4700}$). The absorption coefficients ε_{4500} and $\varepsilon_{4500+4700}$ respectively in l·mol^{-1}·cm^{-1} were determined from the intercepts with the axes and are shown in the plot.

Solid and dashed curves in Fig. 7 represents water species contents determined from the single OH band evaluation vs. the two OH bands method, respectively. Only small differences at water contents ≥ 5wt.% can be observed between both evaluation methods. In the case of the single band equal amounts of dissociated and molecular H_2O are present at 6 wt.% total water, using the two band method this occurs at 7 wt.% H_2O_t. However, these differences are within the uncertainty of the linear molar absorption coefficients.

The water species distribution is similar to that in silicate glasses [46,117]. In contrast 80% of dissolved water is dissociated in soda-lime borate glasses [90] at around 7 wt.% H_2O, suggesting that OH groups are stabilized by boron [59].
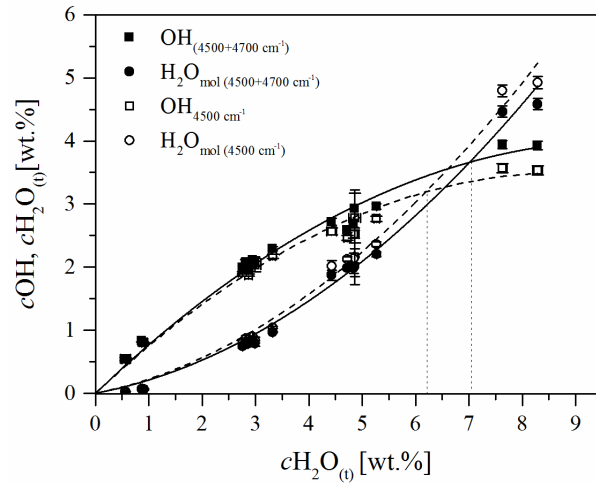
Fig. 7. Water species concentration ($c_{H_2O_{mol}}$ and cOH) as a function of total water content ($c_{H_2O_{(t)}}$) measured with KFT in NBS glasses. Black solid lines and symbols display the water species contents determined from the two band method. Grey dashed lines and symbols show the species contents based on the evaluation of the 4500 cm^{-1} peak only. Dashed vertical lines display the total water content at which equal amounts of H_2O_{mol} and OH groups are present.

Tab.1. Sample characterization of hydrous NBS glasses and spectroscopic data of NIR measurements.

	KFT					IR									
	$c\mathrm{H_2O_{(t)}}$	T_f	T_g	ρ	d	Peak position			A_{5200}	A_{4500}	A_{4700}	cOH	$c\mathrm{H_2O_{mol}}$	$c\mathrm{H_2O_{(t)}}$	further analysis
	[wt.%]	[K]	[K]	[g/l]	[mm]	[cm^{-1}]	[cm^{-1}]	[cm^{-1}]	[mm^{-1}]	[mm^{-1}]	[mm^{-1}]	[wt.%]	[wt.%]	[wt.%]	
NBS1-I	0.91 ± 0.04	722	721 ± 2	2513 ± 3	0.262	5230	4707	4490	0.003	0.171	0.242	0.81 ± 0.001	0.06 ± 0.01	0.87 ± 0.01	SPV
NBS1-II	0.87 ± 0.05				0.266				0.003	0.169	0.237	0.83 ± 0.001	0.07 ± 0.01	0.90 ± 0.01	
NBS3-I	2.87 ± 0.07	613	602 ± 2	2492 ± 3	0.267	5228	4704	4485	0.032	0.363	0.497	1.95 ± 0.02	0.79 ± 0.04	2.74 ± 0.04	
NBS3-II	2.76 ± 0.08				0.271				0.03	0.327	0.452	1.99 ± 0.01	0.75 ± 0.04	2.74 ± 0.04	
NBS5-I	4.84 ± 0.10	529	551 ± 2	2456 ± 3	0.278	5224	4704	4482	0.083	0.481	0.644	2.69 ± 0.05	1.98 ± 0.08	4.67 ± 0.08	
NBS5-II	4.43 ± 0.09				0.285				0.077	0.435	0.584	2.72 ± 0.05	1.87 ± 0.08	2.59 ± 0.08	
NBS0.5b-I	0.56 ± 010	n.a.	n.a.	2490 ± 3*	2.200	5216	4702	4493	0.01	0.162	0.292	0.55 ± 0.02	0.03 ± 0.001	0.58 ± 0.02	DMA, Raman
NBS0.5b-II	0.57 ± 0.07								0.008	0.16	0.288	0.54 ± 0.02	0.02 ± 0.001	0.57 ± 0.02	
NBS3b-I	2.99 ± 0.11	n.a.	n.a.	2469 ± 3*	2.198	5226	4698	4483	0.251	0.597	0.192	2.09 ± 0.08	0.79 ± 0.04	2.88 ± 0.09	DMA, Raman
NBS3b-II	2.82 ± 0.08								0.259	0.586	0.19	2.07 ± 0.08	0.81 ± 0.04	2.88 ± 0.09	
NBS5b-I	4.86 ± 0.11	n.a.	n.a.	2418 ± 3*	2.056	5223	4696	4471	0.596	0.752	0.155	2.92 ± 0.30	2.01 ± 0.29	4.93 ± 0.42	DMA, Raman
NBS5b-II	4.54 ± 0.08								0.652	0.794	0.152	3.11 ± 0.32	2.20 ± 0.31	5.31 ± 0.45	
NBS3c-I	3.32 ± 0.05	575	570 ± 3	2485 ± 3	0.282	5223	4687	4482	0.034	0.069	0.043	2.29 ± 0.03	0.97 ± 0.01	3.26 ± 0.03	NMR, SPV
NBS3c-II	2.95 ± 0.05				0.287				0.029	0.066	0.039	2.12 ± 0.03	0.83 ± 0.01	2.95 ± 0.03	
NBS5c-I	4.72 ± 0.06	536	530 ± 2	2452 ± 3	0.294	5223	4696	4474	0.081	0.091	0.056	2.59 ± 0.04	1.98 ± 0.03	4.57 ± 0.05	NMR, SPV
NBS5c-II	5.27 ± 0.05				0.297				0.086	0.103	0.067	2.96 ± 0.04	2.20 ± 0.04	5.17 ± 0.06	
NBS8c-I	7.63 ± 0.08	465	465 ± 2	2381 ± 3	0.295	5223	4700	4468	0.18	0.131	0.093	3.94 ± 0.07	4.46 ± 0.09	8.41 ± 0.11	NMR, Raman
NBS8c-II	8.29 ± 0.09				0.292				0.183	0.128	0.092	3.93 ± 0.07	4.58 ± 0.09	8.51 ± 0.11	

Numbers in the sample name refer to the nominal water content. Letter b characterizes samples synthesized for DMA and letter c indicates samples which were also analyzed by NMR spectroscopy. I or II in the sample name refers to glass pieces from both ends of the sample used to check homogeneity of water distribution. The fictive temperature T_f of the synthesized glasses and the glass transition temperature T_g were determined with DTA using a glass piece from the center part of the sample. Average and standard deviation of three heating cycles is given for T_g. Densities (ρ) were determined via the buoyancy method by measuring the sample weight in air and in ethanol. Errors are ± 2 µm of thickness (d) and ± 0.003 for absorbances. Peak positions are average values with estimated errors of ± 5 cm^{-1}. n.a.= not analyzed. c_{OH} is calculated using the sum $A_{4500+4700}$. SPV=sphere penetration viscometry. See text for details. * Density was measured on glasses which were relaxed at ambient pressure during DMA.

Tab. 2. Sample characterization of nominal dry NBS glasses and spectroscopic data of MIR measurements.

	T_f	T_g	ρ	d	A_{3585}	$cH_2O_{(t)}$	further analysis
	[K]	[K]	[g/l]	[mm]	[mm^{-1}]	[wt.%]	
NBS0(0.1MPa)	850	847 ± 2	2471 ± 3	0.082	0.008	0.010 ± 0.001	DMA, NMR, Raman, SPV
NBS0(500MPa)-I	837	838 ± 2	2507 ± 3	0.062	0.034	0.033 ± 0.001	Raman
NBS0(500MPa)-II				0.069	0.032	0.025 ± 0.001	
NBS1-I	722	721 ± 2	2513 ± 3	0.065	0.479	0.74 ± 0.03	SPV
NBS1-II				0.063	0.491	0.79 ± 0.03	
NBS0(500MPa)c-I	830	827 ± 1	2505 ± 3				NMR
NBS0(500MPa)c-II							

For notes see Tab.1

3.4 Boron speciation

The [11]B MAS spectra show well separated resonances of BO_3 and BO_4 species (Fig. 8(a)). BO_4 groups are responsible for the dominating resonance around -2 ppm, while the minor resonance at ~13 ppm is due to BO_3 groups. According to [121–123], the BO_4 resonance contains two contributions arising from BO_4 surrounded by four Si atoms (at -2 ppm) and BO_4 surrounded by three Si atoms and one B (at 0 ppm) [121–123]. Thus, the increase of the isotropic chemical shift of the BO_4 resonance from -2 ppm to 0 ppm upon water addition may indicate an increasing number of BO_4 with second-neighbor boron atoms.

The fraction of $BO_4/(BO_3+BO_4)$ based on signal area is denoted as N_4. The sample NBS0-500MPa synthesized with a cooling rate of ~500 K/min (N_4= 88 (±2) %) exhibits a slightly lower N_4 value compared to the NBS glass with same nominal bulk composition, same pressure treatment and a cooling rate of 40 K/min ($N_4 = $ 93.1 (±0.5) %) studied by Wondraczek et al. [7]. The difference is larger than expected from the dependence of N_4 on cooling rate determined by [7] (increase of N_4 by ~1% for a decrease in cooling rate from 40 K/min to 4.5 K/min). As visible in Fig. 8(b,c) the pressure treatment at 500 MPa has only minor effect on

boron speciation in dry NBS glass. This finding contrasts with results of Wondraczek et al. [7] who reported an increase of N_4 from 89.3 ($\pm$0.5) % to 94.2 ($\pm$0.5) % for a pressure increase from 0.1 to 500 MPa. Deviations to the study of Wondraczek et al. [7] can be due to the use of different pressure vessels and different NMR spectrometer as well as differences in the spectra evaluation.

N_4 is plotted as a function of total water content in Fig. 8(b) and increases from 88 ($\pm$ 2) % in the dry compressed sample to 98 ($\pm$ 2) % upon addition of 3 wt.% water. Also at higher water contents virtually all boron is present in tetrahedral configuration. The evolution of N_4 with water content can be correlated to the density data shown in Fig. 6. The deviation from linearity in the density plot at low water contents indicates drastic structural changes up to 3 wt.% H_2O. This can be related to depolymerization of the network through the incorporation of H_2O which enables the formation of the preferential four-fold coordination state of boron. Thus, a densification of the structure can be achieved. Melt depolymerization is also visible in the strong decrease of the fictive temperature of the glasses with increasing water content (Tab. 1). Another possibility to influence N_4, which was often used in literature, is the variation of T_f by changing the cooling rate [4,7,80,112,115]. Consistent with our observations lowering of T_f was found to increase N_4.

In comparison to the NBS glass a less pronounced increase of N_4 with the addition of H_2O was found in soda-lime borate glasses [90] and in boron-containing sodium aluminosilicate glasses [5]. In the sodium-poor NCB5 glass (5 mol% Na_2O, 10 mol% CaO, 85 mol% B_2O_3) N_4 remains almost constant after addition of 3 wt.% H_2O (increase from 24.1% to 24.4%) while for the sodium-rich NCB25 glass (25 mol% Na_2O, 10 mol% CaO, 65 mol% B_2O_3) a more pronounced increase from 53.4% to 56.4% was noted. In boron-containing sodium aluminosilicate glasses with an excess of Al+B to Na sodium is preferentially used to stabilize aluminum in tetrahedral coordination and boron is almost exclusively in trigonal coordination [5]. Adding 4.4 wt.% water to the dry glasses N_4 only increases from 2% to 6%. The increase

of N_4 can be at least in part the results of a decrease in fictive temperature of the glasses. Stebbins and coworker [80,124] found a strong influence of T_f on BO_4 in borosilicate glasses but no effect for borate glasses. They suggest that the higher NBO content in the borosilicates is responsible for the significant BO_4 increase in contrast to the polymerized borate glasses.

We consider two possible scenarios to explain the large increase of N_4 in the borosilicate glass, whereby it has to be clearly distinguished between the influence of initial NBO content and the effect of OH groups on the glass structure. Addition of small amounts of water lead to a break-up of the network by formation of OH groups as described above. This break-up facilitates for the sodium cations the accessibility to the negatively charged NBOs, present already in the initial glass but hindered to coordinate with alkali by structural constraints. Clustering of NBOs around network modifiers was observed in molecular dynamic simulation [125,126] and confirmed by NMR analysis on aluminoborosilicate glasses [127]. But OH groups may also be directly involved in the coordination polyhedra of alkalis, thus indirectly stabilizing BO_4 groups adjacent to the alkalis.
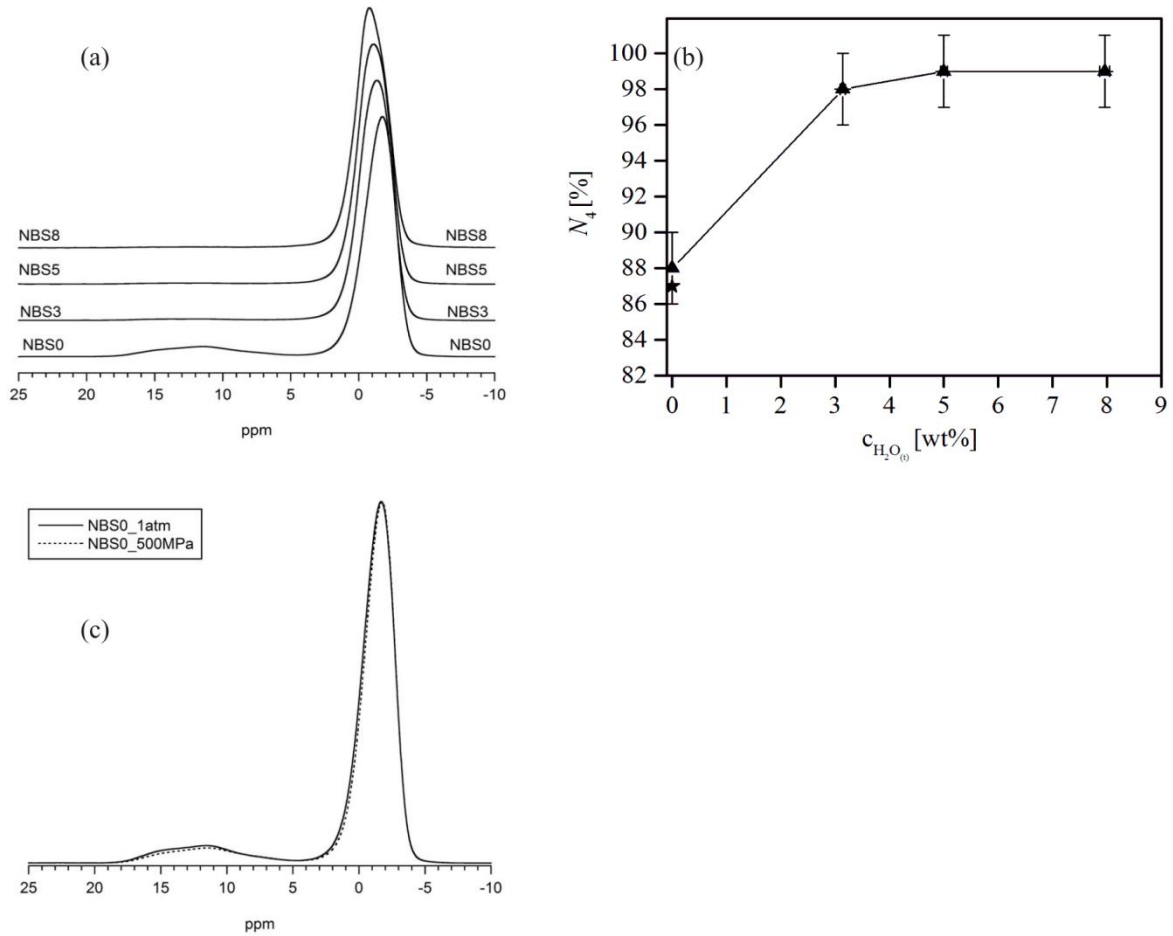
Fig. 8.(a) ^{11}B MAS NMR spectra of hydrous and anhydrous glasses synthesized at 500 MPa. (b) N_4 as a function of water content. The N_4 value of the uncompressed NBS glass (NBS0-0.1MPa) is marked with an star. (c) Comparison of the ^{11}B MAS NMR spectra of the compressed and uncompressed NBS glass.

3.5 Raman spectroscopy

The Raman spectra can be divided into three frequency regimes at 300-700 cm^{-1}, 700-1300 cm^{-1} and 1300-1700 cm^{-1} (Fig. 9). Bands below 600 cm^{-1} are attributed to Si-O-Si bending modes, coupled with tetrahedral O-Si-O bending vibrations, consistent with spectra of silicates [116]. The sharp peak at 630 cm^{-1} is assigned to breathing modes of danburite like rings which consist of two BO$_4$ tetrahedra and two SiO$_4$ tetrahedra [128].

Information about the degree of depolymerization of silicate tetrahedra can be derived from the Si-O stretching region around 1100 cm^{-1}. The number i of bridging oxygens per silicon

tetrahedra is often used to define Q^i species. Correspondingly, a Q^4 species stands for a tetrahedron composed of four bridging oxygen, while Q^0 describes an isolated tetrahedron.

In borosilicate glasses with boron contents above 25 mol% significant band features have been observed between 1300 and 1700 cm^{-1} which are associated with stretching of B-O$^-$ (O$^-$ = NBO) within large borate groups [129,130]. None or only very weak band features at around 1350 cm^{-1} are present in NBS glasses which contain only 10 mol% B_2O_3. This implies that boron is homogeneously distributed in the network and larger boron cluster are absent.
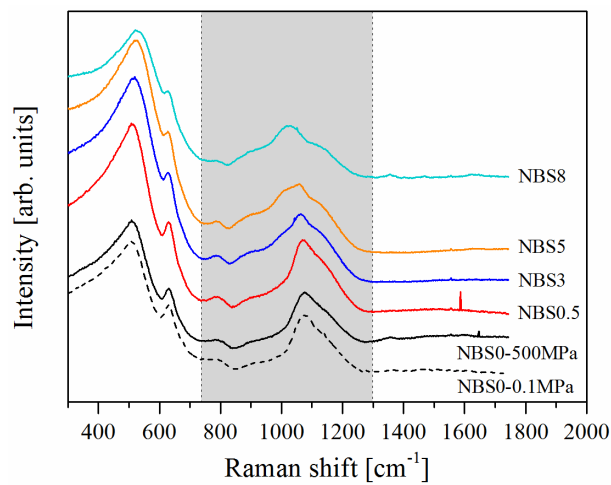
Fig. 9. Uncorrected Raman spectra of hydrous and anhydrous NBS glasses. Spectra are shifted for clarity. The grey area shows the Si-O stretching region which was deconvoluted for the determination of Q species.

For simplicity we have chosen a linear baseline to correct for the background in the range of Si-O stretching (Fig. 10). A comparison of a linear and spline baseline showed that spectra are essentially unaffected by the type of baseline in this region.
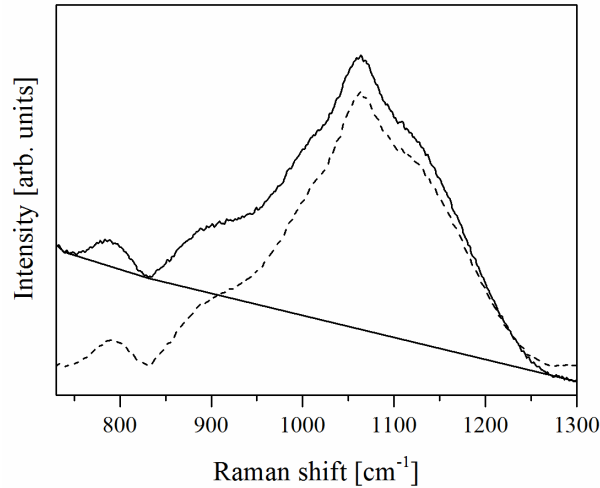
Fig. 10. Example of baseline correction of Raman spectra for NBS3 glass. The spectrum represented by the solid line show the uncorrected Raman spectrum with the applied linear baseline. The dashed line is the baseline corrected spectrum.

A quantitative evaluation of Raman spectra in terms of Q species is often difficult, since the intensities of the bands depend on the molecular polarizability [131] of the vibrating system, and hence on the composition of the material. In first approximation the fractions of the areas (A_{Q^i}) of the deconvoluted Raman spectrum between 730 and 1350 cm^{-1} are assumed to represent the Q species distribution. Following the spectra deconvolution of dry and hydrous $Na_2Si_4O_9$ glasses [117] and hydrothermally altered alkali borosilicate glass [132] we fitted the spectra of the NBS glasses with six Gaussians centered at about 800, 900, 950, 1000, 1065 and 1130 cm^{-1} (Fig. 11) to determine the Q species distribution.

The band features of dry NBS glass in the Si-O stretching region exhibit strong similarities to dry $Na_2Si_4O_9$ glass reported in [117]. Small shifts of peak positions towards lower wavenumbers can be explained by the presence of Si-O-B connections. It is worth noting that the full width of half maximum (FWHM) of the band at ~1125 cm^{-1} attributed to Q^4 species is wider for the dry NBS glass (FWHM=127) than for the dry $Na_2Si_4O_9$ glass (FWHM≈95). The larger FWHM can be related to the presence of both, Si-O-Si and Si-O-B connections. However, because of the poorly resolved band features around 1125cm^{-1} individual Gaussians

for different Q^4 species are not well constrained, especially in the dry glasses and the glasses with low water content. Therefore, we include only one fit curve for the Q^4 species in the spectra deconvolution.

At water contents ≥ 3 wt.% the features in the Si-O stretching region of NBS glass differ significantly from hydrous $Na_2Si_4O_9$ glasses [117]. Whereas the band at 1100 cm^{-1} is dominating for all water contents up to 10 wt.% in the tetrasilicate glasses, a band at ~1000 cm^{-1} increases rapidly on expense of the 1065 cm^{-1} band in hydrous NBS glasses. Following the Q species assignment of $Na_2Si_4O_9$ glass [117] and hydrothermally altered alkali borosilicate glass [132] we attribute this two features to two different Q^3 species, $Q^{3'}$ and $Q^{3''}$. The bands at ~880 and 920 cm^{-1} present in dry and hydrous NBS glasses rise continuously with increasing water content, and we relate those bands to different Q^2 species ($Q^{2'}$ and $Q^{2''}$) consistent with the designation of $Q^{3'}$ and $Q^{3''}$ species. Based on the stronger bonds of Si-O-Si relative to Si-O-B the depolymerized species at the higher wavenumber ($Q^{3''}$, $Q^{2''}$) are expected to belong to the Si-O-Si species, whereas Si-O-B are expected to occur at lower wavenumber ($Q^{3'}$, $Q^{2'}$).

In a study on hydrous sodium tetrasilicate glasses a peak near 900 cm^{-1} was interpreted as Si-OH related vibration, since this peak is only present in the hydrous glasses but absent in anhydrous glasses [117]. As the peaks at ~880 and 920 cm^{-1} are observed in hydrous as well as in dry NBS glasses an assignment to Si-OH or B-OH is not supported. The distinct peak at 800 cm^{-1} in NBS glasses show the opposite trend as the band at ~880 cm^{-1} and decreases rapidly with increasing water content which was also observed in hydrous $Na_2Si_4O_9$ glasses [117]. This peak was interpreted as cage-like vibrations of Si atoms mainly in Q^4 tetrahedra, representing directly the decrease of network connectivity with the addition of water [117].
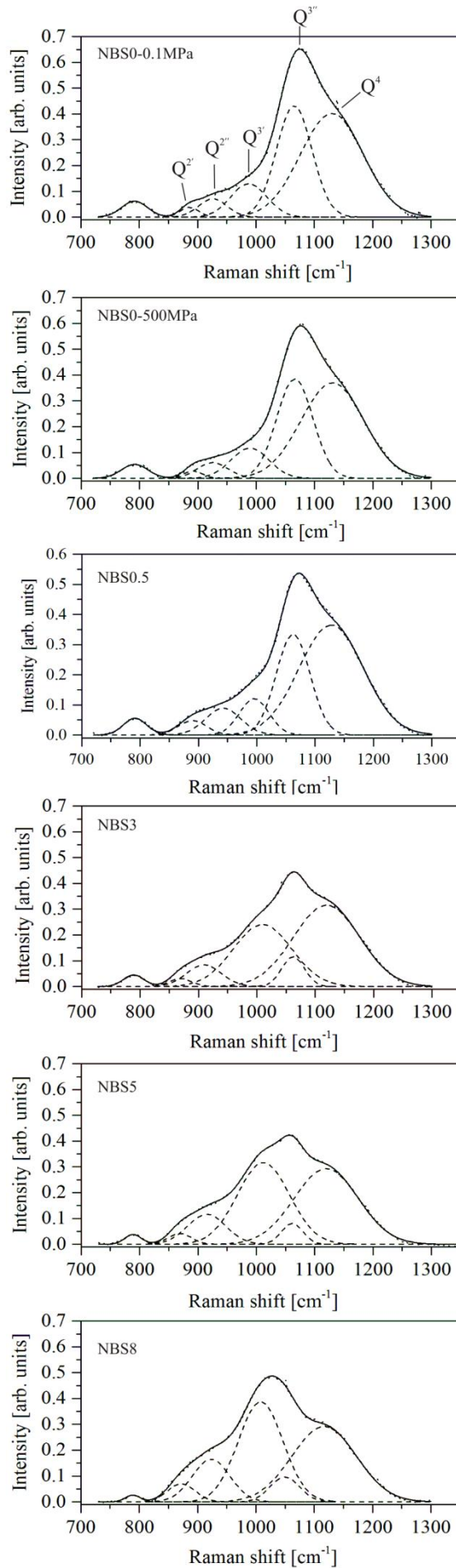
Fig. 11. Deconvoluted Raman spectra of hydrous and anhydrous NBS glasses in the Si-O stretching region.

As illustrated in Fig. 12 the area associated with Q^4 (A_{Q^4}) species decreases continuously from ~51% in nominal dry NBS glasses to ~40% in NBS8 to the same degree as the sum of $A_{Q^{2'}}$ and $A_{Q^{2''}}$ ($= A_{Q^2_{(t)}}$) increases from 5.5% in nominal dry NBS glasses to 17% in NBS8. $A_{Q^{3'}}$ strongly increases up to ~3 wt.% H_2O, and levels than off. An opposite trend is observed for $A_{Q^{3''}}$ so that the sum of $A_{Q^{3'}}$ and $A_{Q^{3''}}$ ($A_{Q^3_{(t)}}$) remains almost constant over the range of water contents (40.4% for nominal dry NBS glasses, 42.4% for NBS8).

The trends of $A_{Q^{3'}}$ and $A_{Q^{3''}}$ correlate well with the observation that structural changes occur primarily at low water contents as suggested by the density data. Moreover, the strong increase of $A_{Q^{3'}}$ with the addition of 3 wt.% H_2O and the subsequent stagnancy with further water addition resembles strongly the trend of N_4 with water addition (Fig. 8(b)). Therefore, $Q^{3'}$ is assigned to a SiO_4 tetrahedron with one NBO connected to two other SiO_4 tetrahedra and one BO_4 unit while $Q^{3''}$ is assigned to a SiO_4 units with one NBO connected to three other SiO_4 tetrahedra. This is consistent with the expectation that the peak at lower wavenumber is caused by the species connected to BO_4. Assignment of $Q^{2'}$ and $Q^{2''}$ is analogous to the Q^3 species, means the low wavenumber band results from connection to a BO_4 tetrahedron. This picture of Q species distribution points towards a preferential linkage of BO_4 to SiO_4 tetrahedra with one NBO. On the other hand, in the case of Q^2 species there appears to be a preference for the species without bonding to BO_4. Water does not affect noticeably this trend.

Moreover, the fact that the sum of both areas of $Q^{3'}$ and $Q^{3''}$ is almost constant over the range of water contents investigated point to a depolymerization mechanism which is mainly based on a direct conversion from Q^4 to Q^2 units through the reaction with water. This finding contrasts with observations on $Na_2Si_4O_9$ glass, in which Q^3 is produced on expense of Q^4 upon incorporation of H_2O [117]. At high water contents >5wt.%, Q^4 species are not involved

in the water dissolution mechanism in $Na_2Si_4O_9$ glass but Q^3 species are transformed into Q^2 species.
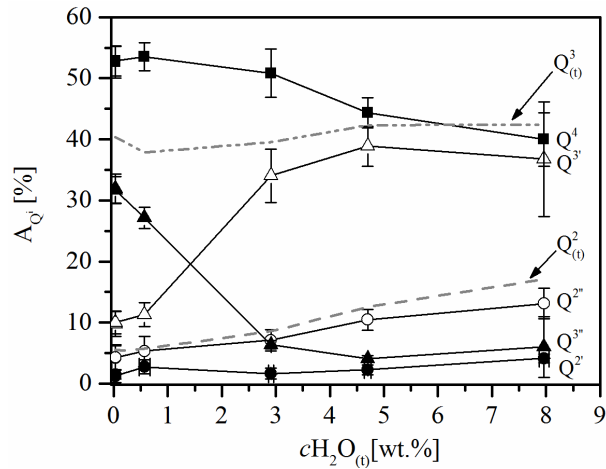
Fig. 12. A_{Q^i} as a function of total water content in hydrous and anhydrous NBS glasses. Q species in % represent the relative fractions of the areas under the Raman spectrum in the frequency range between 730 and 1300 cm^{-1}.

$A_{Q_{(t)}^3}$ and $A_{Q_{(t)}^2}$ are the sums of $A_{Q^{3'}} + A_{Q^{3''}}$ and $A_{Q^{2'}} + A_{Q^{2''}}$ respectively and are illustrated by the dashed-dotted and the dashed lines.

To characterize the degree of depolymerization of melts, the ratio of non-bridging oxygen per tetrahedron (NBO/T) is often used. It can be calculated from the Q species distribution obtained from Raman measurements via

$$\frac{NBO}{T} = \frac{\sum_{o}^{i}[(4-i) \cdot Q^i]}{\sum(Q^i)} \qquad (7)$$

Another determination of NBO/T is possible via NIR measurements using NBO/T of 0.17 for the anhydrous NBS glass (calculated from the remaining sodium content after BO_4 charge compensation) and assuming that each OH is equivalent to one additional NBO. Fig. 13 shows the development of NBO/T as a function of the water content based on the Raman and NIR data. The trend of NBO/T upon addition of water is similar for both methods, but the NBO/T value determined by Raman spectroscopy has an offset by ~0.35. The value of 0.53

derived from the Raman data for the dry glass would mean that on the average one NBO occur in each second tetrahedron. This value is much higher than NBO/T calculated from starting composition based on chemistry, and clearly shows the difficulty of precise quantification of Q species in our NBS glasses via Raman spectroscopy. Based on these findings a higher scattering cross section for the depolymerized Q species can be inferred. However, the derived evolution of Q species with water content is consistent with the density and the NMR data. Therefore, we conclude that the interpretation of the Raman spectra allows at least a semi-quantitative statement about the Q species distribution.
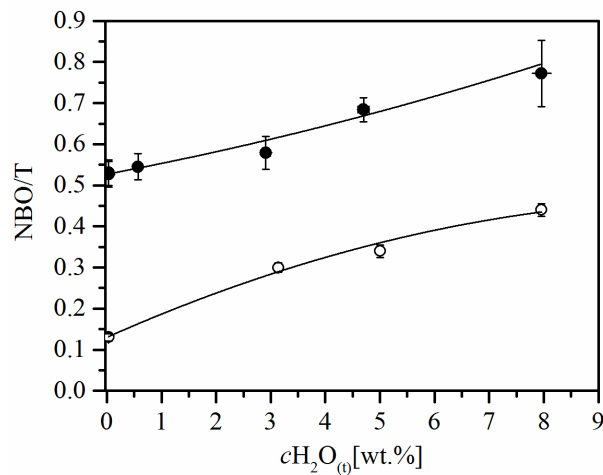
Fig. 13. Number of non-bridging oxygens per tetrahedra vs. total water content. Raman data (full dots), NIR data (empty dots) based on the calculation of NBO formation after BO_4 charge compensation. The solid lines are polynomial fits and are intended as visual guides.

4. Conclusion

A detailed characterization of the anhydrous and hydrous NBS glass structure and the role of NBOs and OH groups on network structure was provided in the present study. NIR analysis showed that the dissociated water species dominate up to 6 wt.% H_2O with roughly equal portions of Si-OH and B-OH. The break-up of oxygen bridges by formation of OH groups

lead to large structural modifications at water contents $\leq$ 3wt.% H_2O as indicated by the density data, Raman and NMR spectroscopy.

The findings obtained from hydrous and anhydrous borate- and borosilicate glasses [5,80,90,124], clearly point to the importance of modifier cation to support the formation of tetrahedrally coordinated boron in hydrous glasses. If the coordination polyhedra of the modifier cations can be satisfied via NBOs or OH groups the formation of BO_4 upon water incorporation is promoted. Comparison to Raman observations indicates that BO_4 groups are preferentially bond to Q^3 species. In contrast to silicate glasses where both Q^4 and Q^3 species are affected by the attack of water, the depolymerization mechanism in NBS glasses is primarily based on the direct conversion from Q^4 to Q^2. Q^3 seems to be stabilized through the linkage to BO_4 tetrahedra. Determination of Q species contents based on the Raman spectra lead to an overestimation of depolymerized Q species in our NBS glasses which is probably a result of the higher scattering cross sections of those species. However, the observed trends are supported by the density and NMR data and provide important information of the structural rearrangements in borosilicate glasses.

Investigation of relaxation processes in hydrous borosilicate glasses are needed to improve the knowledge of the role of water on fatigue. These aspects will be discussed in continuative study.

Chapter 2B[1]

Relaxations Mechanisms in Hydrous Sodium Borosilicate Glasses

Abstract

Borosilicate glasses (16 Na_2O-10 B_2O_3-74 SiO_2, named NBS) with water contents between 0 and 22 mol% H_2O (0-8 wt.% H_2O) where investigated to improve the knowledge of the effect of water on relaxation mechanisms. Differential thermal analysis and sphere penetration viscometry, as well as internal friction measurements where applied to study network related relaxation mechanisms (α-relaxation) in the range of glass transition, as well as relaxation modes occurring at lower temperatures (β-, γ- relaxation).

Consistent with literature data of various silicate and aluminosilicate glasses a strong decrease of the glass transition temperature T_g is observed for low water contents ($\leq$ 1 wt.% H_2O), while the T_g decrease is less pronounced at higher water contents in NBS glasses. The T_g data based on DTA measurements and the isokom temperature T_{12} derived from viscosity measurements are in excellent agreement, confirming the equivalence of enthalpy and viscous relaxation for NBS glass.

The decrease of T_g with increasing water content of hydrous NBS glasses resemble the trend of aluminosilicate glasses with a similar degree of initial depolymerization, i.e. similar ratio of non-bridging oxygens per tetrahedron (NBO/T).

In silicate, borosilicate, aluminosilicate and borate glass compositions OH groups contribute considerably to the decrease of T_g, while molecular water plays only a minor role. The effect of water is particularly pronounced in polymerized aluminosilicates such as rhyolite glass but much weaker for soda lime borate glass and float glass.

93

Internal friction measurements reveal that the addition of water to NBS glass correlates with the appearance of a β-relaxation mode visible in the mechanical loss spectra. A discrimination between individual contribution of molecular water and OH groups to β-relaxation is possible at water contents above 3 wt.% H_2O. Superimposition of different relaxations modes in mechanical loss spectra indicate complex associated process of sub- T_g modes and network relaxation.

_____

[1]This chapter 2B is planned to be submitted to the Journal of Non-Crystalline Solids, Relaxation mechanisms in hydrous sodium borosilicate glasses, U. Bauer, S. Reinsch, H. Behrens, P. Kiefer, R. Müller, J. Deubener

1. Introduction

It is well known that water plays an important role for the depolymerization of natural silicate melts and glasses, where several weight percents of water can be dissolved due to elevated pressures [e.g. 1,2]. The investigation of water in industrial relevant glasses is also a crucial issue, since water can cause aging and fatigue [133,134,21] as well as compaction [135] and sub-critical crack growth [134,136]. For instance, water easily can be absorbed and accumulated at crack tips or near the glass surface and lead to corrosion. Sub-T_g relaxation processes play a major role for crack propagation, but are poorly investigated in glasses with high contents of structural bonded water [13]. In contrast, network relaxation in the range of T_g is well investigated for a wide range of hydrous and anhydrous silicate and aluminosilicate glasses [e.g. 9]. Considerable less information is available about relaxation processes in the range of glass transition for hydrous boron-bearing glasses.

It is known that water in glasses is present as two main species: as molecular water (H_2O_{mol}) and as water dissolved in form of OH groups [14–17]. In silicate and aluminosilicate glasses the strongest decrease of T_g occurs in the range of low water contents (≤ 2 wt.% H_2O), where OH groups are the predominant water species. At water contents above ~3 wt.% the content of hydroxyl groups apparently level off and the amount of molecular water rises strongly. This trend is a consequence of the decrease in fictive temperature of the glass with increasing water content, i.e. water speciation is frozen in at different temperatures.

To the best of our knowledge only three studies on the water speciation in hydrous borosilicate and boroaluminosilicate glasses with high water contents (up to 10 wt.% H_2O) are available [58,57, chapter 2A]. These studies revealed that OH groups are increasingly stabilized with increasing boron content. While molecular water is the dominant water species at water contents >7 wt.% H_2O in borosilicate and boroaluminosilicate glasses, only ~ 1 wt.% molecular H_2O was found in soda-lime borate glasses with 7.5 wt.% H_2O [90].

In the three component model of Tomozawa [88] the influence of water species and dry glass component was considered to model the decrease of the glass transition temperature with increasing water content. Deubener et al. [45] applied this model of the reduced glass transition temperature to a variety of different silicate and aluminosilicate glasses and showed that the effect of OH groups on T_g is by far stronger compared to that of molecular water in these compositions.

There is only rare knowledge about the influence of individual water species on sub-T_g relaxation mechanisms in oxide glasses [13]. Free and forced oscillation methods can be used (mostly torsion and bending of glass beams) to get insights into relaxation of the glass network and fast sub-T_g relaxation modes. These modes are often denoted as α-, β-, and γ- relaxation in the order of decreasing temperature [18,19,137]. Whereas the interpretation of α- and γ- relaxation modes is quite clear, the mechanisms responsible for β-relaxation is still under debate.

α-relaxation is characterized by a broad internal friction peak, dominating the mechanical loss spectra, and by large activation energies ($E_\alpha \approx$ 419-502 kJmol^{-1}) [20] which are in good agreement with those of viscosity at T_g. The γ- relaxation mode observed at temperatures $<$ 373 K ($T_\gamma/T_\alpha \approx 0.38$) [35] is commonly attributed to the motion of alkalis, since the range of activation energies ($E_\gamma \approx$ 63-105 kJmol^{-1}) [36] resemble activation energies of alkali diffusion (63- 84 kJmol^{-1}) [20].

The β-relaxation phenomena has been assigned to several different mechanisms including movements of non-bridging oxygens (NBOs) in alkali silicate glasses [19,20], a cooperative movement of equal or dissimilar mobile species such as alkali or alkaline-earth ions [21–26] or movements within a cluster of alkaline-earth cations [19]. In water-poor ($\leq$ 0.3 wt.% H$_2$O) phosphate, borate and silicate glasses β-relaxation was correlated with cooperative motions of alkali ions and neighboring protons [27–32].

β-relaxation phenomena in glasses with higher water contents, where significant amounts of molecular water is present are rarely investigated. In the study of Reinsch et al. [13] two distinct β-relaxation peaks in mechanical loss spectra were attributed to dynamics of OH groups and molecular water in hydrated silicate glasses ($\leq$ 1.9 wt% H_2O). The relaxation mode of H_2O_{mol} was found to be faster compared to OH groups and is probably caused by jumps of H_2O molecules between adjacent cavities in the network. It is worth noting that rotation of H_2O molecules around their bisector axis, another low temperature process in hydrous glasses identified by NMR spectroscopy and quasielastic neutron scattering, is too fast to contribute to the β-relaxation peak [33,34].

Our study is aimed to improve the understanding of the influence of water speciation on relaxation mechanisms in borosilicate glasses by the analysis of T_g, viscosity, and internal friction. The composition of the investigated borosilicate glass (16 mol% Na_2O, 10 mol% B_2O_3 and 74 mol% SiO_2) was chosen as representative for a technical glass since the borosilicate crown glass BK7 from Schott AG is very similar in composition. A detailed characterization of the anhydrous and hydrous borosilicate glass structure was published in Bauer et al. (submitted), including analysis of water speciation, boron speciation as well as Q^n-speciation (SiO_4 tetrahedron with n= number of bridging oxygen).

2. Experimental and analytical methods

2.1 Sample preparation

For the synthesis of the borosilicate glass a powder mixture of Na_2CO_3, B_2O_3 and SiO_2 was used. A detailed description of the synthesis is given in Bauer el al. 2016 (submitted). Samples with 0.2 wt.% H_2O was synthesized from base glass by remelting and water steam

bubbling in 110 ml alumina crucibles at 1753 K and 0.3 MPa in argon atmosphere for 3 hours. Subsequently the temperature was lowered and cooled with 3 K/min through the regime of (T_g ± 150 K) to avoid internal stress in the glasses. The procedure was described in the study of Reinsch et al. 2013 [13]. All samples with water contents ≥ 0.5 wt.% were synthesized in an internally heated pressure vessel (IHPV) at 500 MPa and 1423 K for 14–20 hours using the same procedure as given in Bauer et al. 2016 (submitted).

2.2 Differential thermal analysis

The glass transition temperature, T_g, was measured by differential thermal analysis (DTA) in air using glass pieces or powdered glass of 15 - 20 mg placed in Pt-crucibles (thermobalance TAG 24, Setaram, Caluire, France). The same measurement routine and data evaluation (tangent method) was applied to hydrous borate glasses, and T_g values were found to be in perfect agreement with isokom temperatures (T_{12}) at viscosities of 10^{12} Pa·s [90]. For each sample four heating and cooling cycles with 10 K min^{-1} were performed. The maximum temperature did not exceed T_g by more than 50 K. The first cycle represents the fictive temperature T_f of the glasses, since the cooling history of the samples reflects the status of quenching after IHPV synthesis. The following three cycles were used for the determination of T_g. Definition of T_f and T_g is based on the onset of the endothermic step in the DTA curve according to Mazurin [54,55]. The average T_g values for all investigated glasses are shown in Tab. 1.

In order to detect a possible loss of water of high water-bearing glasses, the thermal gravimetric (TG) signal was simultaneously recorded during DTA measurement. Additionally, a mass spectrometer (MS, Balzers Quadstar 421) was used for analysis of evolved gases, coupled to the DTA by a heated (453 K) quartz glass capillary. Neither a significant mass loss nor a distinct signal for water by mass spectroscopy could be detected.

The good reproducibility of T_g determination further supports a negligible water loss during the DTA procedure. The maximum error of temperature for this method is ±5 K.

2.3 Sphere penetration viscometry

Viscosity data were obtained by sphere penetration measurements. Cylindrical samples with diameters of ~6 mm and heights of 1-2 mm were sliced from the synthesized glasses. Coplanar surfaces were obtained by grinding and polishing the sample surfaces. Two samples for each water content were available for the viscosity measurements.

The vertical dilatometer (VIS 404, Bähr GmbH) is equipped with a pushing rod made of silica glass and a sapphire sphere (radius $r = 0.75$ mm). The force applied on the pushing rod was adjusted to 3.9 N. The temperature is controlled with an S-type thermocouple (Pt-PtRh) placed in the vicinity (2–3 mm) of the sample surface. The thermal gradient along the sample axis is less than ±1 K mm^{-1}. Considering the accuracy of thermal couples and measurement equipment, the maximum error on the temperature is ±5 K.

A linear variable displacement transducer continuously records the indentation depth of the sapphire sphere into the glass. The shear viscosity was calculated according to [138]:

$$\eta = \frac{3F}{16\sqrt{2rL}\,\dfrac{\delta l}{\delta t}} \tag{1}$$

with η = Newton viscosity, F = applied force, t = time, r = radius of the sphere, L = cumulative indentation depth and δl = indentation within a measurement interval δt.

The system is calibrated by the standard glass G1 of the Physikalisch-Technische Bundesanstalt (PTB) [94]. Viscosity data of the standard glass G1 were reproduced with a standard deviation of ±0.10 in log units.

The measurements were performed on a set of dry and hydrous NBS glasses (see Tab.2 for details). The temperature program of the anhydrous NBS glass and the glass with 1 wt.% H_2O

include several temperature steps (dwell times between 30-250 min) within a measurement run (Tab.2), since the low water-bearing samples are expected to be not sensitive to water loss at the chosen temperatures. As stated in Tab. 2 the first two runs were conducted on two different samples of each composition. Only in the case of NBS1 runs 3 and 4 are repeated measurements on the same samples used for run 1 and 2, respectively.

The temperature program for samples with higher water contents (NBS3c and NBS5c) was subdivided into only three steps (T2 = T1+10 K and T3=T1) with dwell times of 150 to 200 min for viscosities close to 10^{12} Pa·s, while for viscosities of 10^{11}-10^{10} Pa·s dwell times of 100 min were selected. This program was chosen to avoid on the one hand long exposure to elevated temperatures and therefore risk of water loss and on the other hand to check for any water loss after the viscosity measurement. For the first temperature step, a heating rate of 20 K min^{-1} was applied. For subsequent steps heating or cooling rates of 5 K min^{-1} were adjusted.

2.4 Dynamic mechanical analysis

Internal friction measurements were made by dynamic mechanical analysis (DMA). The used analyzer (Gabo Eplexor 150 N, Ahlden, Germany) was operated in asymmetric three-point bending mode performing temperature-frequency sweeps at 4 N static force and 2 N dynamic force. Dynamic force and displacement were measured with a 25 N force detector and an inductive displacement transducer, respectively. Dry and hydrous NBS glasses were measured from 173 K up to temperatures close to T_g. It was not possible to reach the glass transition temperature due to progressive viscous bending of the sample under the applied static load (see also discussion below). Loss data below 273 K could be affected by sample surface icing when operated in air. Such data were not further considered.

The mechanical loss spectra were evaluated with OriginPro2016. The spectra have been smoothed using a moving average of 15 data points. For clarity the lowest point of each spectrum was shifted to zero. Subsequently, the spectra were fitted with three Gaussians which was sufficient to reproduce well the measured data.

3. Results

3.1 Glass transition temperature

The first DTA upscan is still affected by the synthesis conditions and is therefore referred to as the fictive temperature T_f of the glass (Tab.1). The glass transition temperature of hydrous and anhydrous NBS glasses was determined by subsequent DTA measurements on relaxed samples (Tab.1) and based on the average of three heating cycles. Relaxation to 0.1 MPa pressure and to the heating/cooling rates typically used for T_g determination was achieved by the first DTA upscan/downscan. T_g and T_f data are already given in Bauer et al. (submitted) but are discussed here in more detail in view of relaxation processes in the glasses.

As visible from Fig. 1 no mass loss during the DTA measurement was detected. In addition the simultaneously recorded ion currents for the masses 18 (H_2O) and 17 (OH) show no changes during DTA measurement as well. The very good reproducibility of T_g values determined from three heating cycles also verifies that no significant water loss occurred during DTA.

The incorporation of water into the NBS glass structure leads to a strong decrease of T_g with increasing water content. The strongest decrease in T_g is observed for the addition of ~1 wt.% H_2O to the dry glass (Tab. 1, Fig. 5). With further increasing water content the decrease of T_g is less drastic.

Tab.1. DTA results and water contents of hydrous and anhydrous glasses.

	$c\mathbf{H_2O_{(t)}}$	T_f 1st run	T_g 2nd run	T_g 3rd run	T_g 4th run	T_g mean	further analysis
	[wt.%]	[K]	[K]	[K]	[K]	[K]	
NBS0(0.1MPa)[*]	0.010 ± 0.001	850	845	846	846	847 ± 2	SPV, DMA
NBS1	0.89 ± 0.05	722	721	723	720	721 ± 2	SPV
NBS3	2.82 ± 0.08	613	603	600	604	602 ± 2	
NBS3c	3.14 ± 0.05	575	568	570	573	570 ± 3	NMR, SPV
NBS5	4.64 ± 0.10	529	549	553	552	551 ± 2	
NBS5c	5.00 ± 0.06	536	528	531	530	530 ± 2	NMR, SPV
NBS8c	7.96 ± 0.09	465	467	470	466	465 ± 2	NMR, Raman
NBS0.2b[*]	0.23 ± 0.05						DMA
NBS0.5b-I	0.56 ± 0.10						DMA
NBS0.5b-II	0.57 ± 0.07						
NBS3b-I	2.99 ± 0.11						DMA, Raman
NBS3b-II	2.82 ± 0.08						
NBS5b-I	4.86 ± 0.11						DMA, Raman
NBS5b-II	4.54 ± 0.08						

Numbers in the sample name refer to the nominal water content. Letter b characterizes samples synthesized for DMA and letter c indicates samples which were also analyzed by NMR spectroscopy reported in the chapter 2A. I or II in the sample name refers to glass pieces from both ends of the sample used to check homogeneity of water distribution (length of the samples used for DMA: ~30 mm). $c\mathrm{H_2O_{(t)}}$ is the total water content measured with KFT (chapter 2A). The fictive temperature T_f of the synthesized glasses and the glass transition temperature T_g were determined with DTA using a glass piece from the center part of the sample. T_f was determined from the first cycle. Average and standard deviation of subsequent three heating cycles is given for T_g. SPV=sphere penetration viscometry.
[*]water contents of NBS0(0.1MPa) and NBS0.2b were determined from MIR analysis using the peak at 3580 cm^{-1} and the absorption coefficient determined in the chapter 2A of 70.6 l·mol^{-1}·cm^{-1}. Absorbance, density, samples thickness for NBS0(0.1MPa) are presented in chapter 2A. Density, sample thickness and absorbance of NBS0.2b is 2450 g/l, 0.0079 cm and 1.73 respectively.
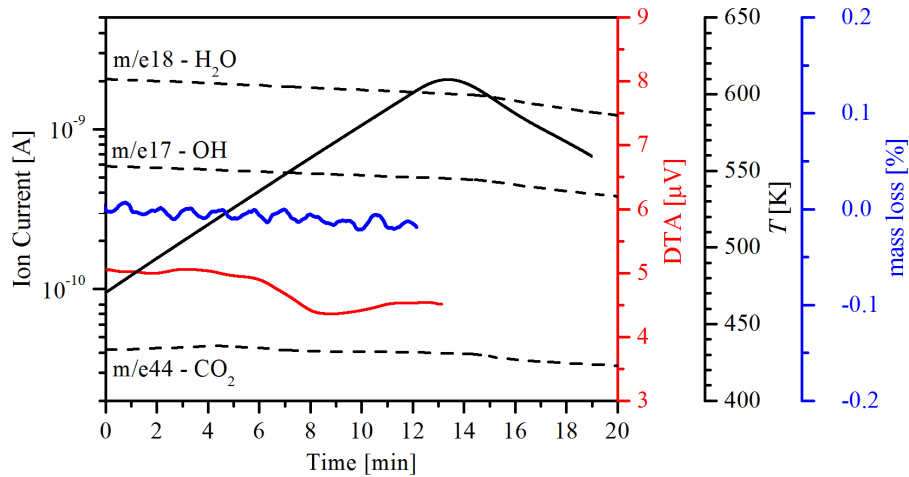
Fig. 1. Results of DTA-TG-MS measurements on sample NBS5. Black dashed lines show the ion currents of the mass channels m/e17 (OH), m/e18 (H_2O) and for comparison m/e44 (CO_2) during DTA measurement (red line). The solid black line represents the temperature evolution during experiment, and the blue line represents the mass change of the sample during the analysis.

3.2 Viscosity

The viscosity of anhydrous and hydrous NBS glasses with water contents up to 5 wt.% H_2O was measured in the range of $10^{10.60}$-$10^{12.75}$ Pa·s. The viscosity data of the anhydrous NBS glass exhibit a very good agreement of two measurement series (Tab.2; Fig. 3). Data for two samples of NBS1 processed in four measurement series are in perfect agreement. For instance, for NBS1 the viscosity in the first run is $10^{11.35}$ Pa·s at 730 K, $10^{11.37}$ Pa·s at 730 K in the second run, and $10^{11.30}$ Pa·s at 733 K in the last run. These data demonstrate high reproducibility of measurements and absence of water loss during high temperature treatment. The temperature program for the high-water bearing samples (NBS3c and NBS5c) comprises only three temperature steps to avoid any water loss during the measurement. Fig 2 shows the temperature and viscosity data for a micro-sphere penetration experiment of NBS5c measured at temperatures shortly above T_g.
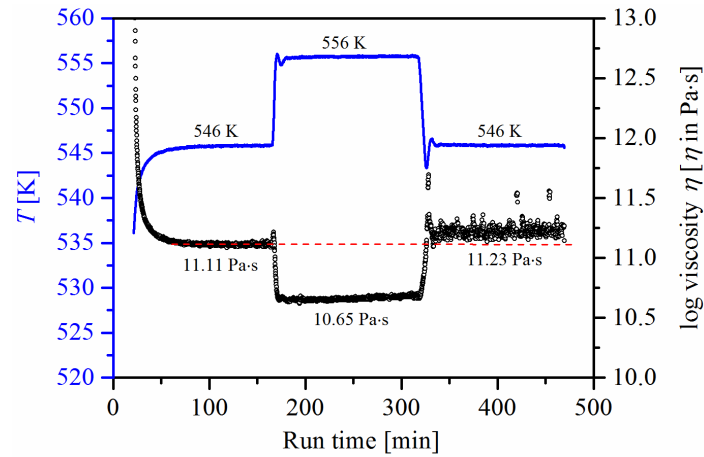
Fig. 2. Sphere penetration experiment of NBS5c. The temperature is marked with a blue line (left ordinate) ($T1$=546 K, $T2$=556 K, $T3$=546 K) The corresponding viscosities (11.11 Pa·s, 10.65 Pa·s and 11.23 Pa·s) are marked with black dots (right ordinate). The red line is indented as visual guide to facilitate the comparison of viscosities between the first and last temperature step.

Only a small increase in viscosity of ~0.1 log units between the first and the last temperature step (T1=T3) has been observed, indicating that only a marginal amount of water was lost during the viscosity measurement on this water-rich sample.

The dependence of viscosity on temperature is illustrated in Fig. 3. A strong decrease of the temperature T_{12}, at which viscosity equals 10^{12} Pas, is evident. In the measured temperature range the viscosity data for every water content can be well described by the Arrhenian equation for all glasses (see Fig.3):

$$\log \eta = A + B/T \qquad (2)$$

The Arrhenian parameter A and B as well as the derived T_{12} data are presented in Tab.2.
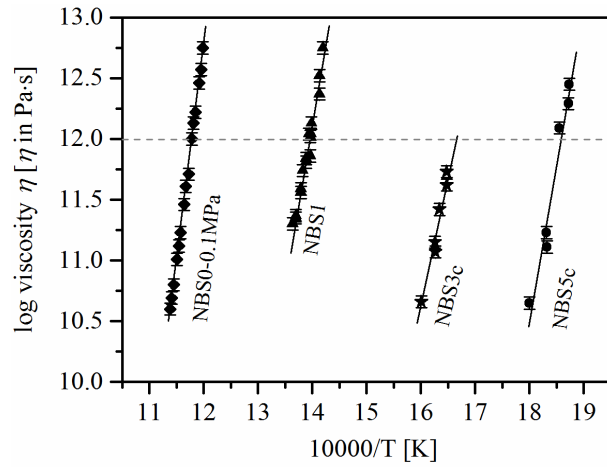
Fig. 3. Viscosity vs. reciprocal temperature of hydrous and anhydrous NBS glasses. Solid lines are the best linear fit of the equation log η = A+B/T through the data. The dashed line is indented for the determination of the isokom temperature T_{12} for which the Newtonian viscosity is 10^{12} Pa·s ($T_{12} \approx T_g$).

Tab.2. Viscosity data of nominal dry NBS glass (NBS0-0.1 MPa) and hydrous NBS glasses (NBS1, NBS3c and NBS5c).

| NBS0-0.1MPa			NBS1			NBS3c			NBS5c		
run	T [K]	log η [η in Pa·s]	Run	T [K]	log η [η in Pa·s]	run	T [K]	log η [η in Pa·s]	run	T [K]	log η [η in Pa·s]
1	834	12.75	1	715	12.04	1	615	11.07	1	534	12.45
	839	12.46		720	11.81		625	10.66		539	12.09
	844	12.22		725	11.56		615	11.15		534	12.29
	849	12		730	11.35						
	853	11.71		716	11.86	2	607	11.62	2	546	11.11
	859	11.46					612	11.42		556	10.65
	864	11.23	2	704	12.75		607	11.73		546	11.23
	869	11.01		715	12.13						
	874	10.8		720	11.84						
	879	10.6		725	11.59						
				730	11.37						
2	837	12.57		716	12.02						
	847	12.13									
	857	11.61	3	707	12.52						
	866	11.12		717	12.04						
	876	10.69									
			4	708	12.37						
				723	11.74						
				733	11.3						
A	-29.8 ± 0.5			-23.2 ± 1.7			-25.2 ± 3.7			-35.5 ± 5.0	
B x 10^{-4}	3.55 ± 0.04			2.52 ± 0.12			2.24 ± 0.22			2.55 ± 0.27	
T_{12}	850			716			600			538	

A and B are the Arrhenian parameters derived from the equation log η = A+B/T. T_{12} is the isokom temperature (see text for details).

3.3 Internal friction

Fig. 4 shows the smoothed mechanical loss spectra measured at f = 7.125 Hz of a nominal dry NBS glass and glasses containing between 0.23 and 4.70 wt.% H_2O.

In each mechanical loss spectrum the peak at highest temperature decreases significantly in temperature with the addition of water (Fig. 4), and only the low temperature flank is visible in the spectra. This issue based on instrumental limitation will be discussed below. In the spectrum of the nominally dry sample NBS0-0.1MPa a second peak at ~313 K can be seen. With the addition of water this peak slightly shifts towards higher temperatures and decreases significantly in its height until it diminishes at 0.50 wt.% H_2O. A broad shoulder of the high temperature peak develops at 650 K after the addition of 0.23 wt.% H_2O (Fig. 8). The height of this mode increases and it shifts towards lower temperature with further water addition.
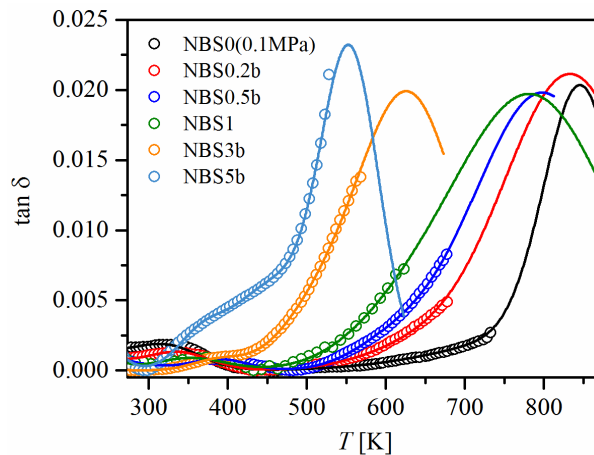

Fig. 4. Mechanical loss (tan δ) as a function of temperature for f = 7.125 Hz for the uncompressed nominal dry and hydrous NBS glasses. Symbols represents the measured data points. The cumulative fit curve is shown for better visualization (solid lines).

4. Discussion

4.1 α-relaxation in alkali-rich oxide glasses

T_g measured by DTA and the isokom temperature T_{12} for which the Newtonian viscosity is 10^{12} Pa·s derived from sphere penetration viscometry are in perfect agreement (Fig. 5). For comparison T_g and T_{12} data of different silicate [139,140], borate [90], and aluminosilicate glasses [141] are shown (Fig. 5). The latter are especially suited for comparison because of structural similarities, i.e. the coordination state of network forming species. In polymerized aluminosilicate glasses, such as albite and anorthite glasses, aluminum is predominantly coordinated by four oxygen with minor amounts of five-fold and six-fold coordinated aluminum [5,142–144]. With the addition of water the aluminum is still preferentially tetrahedrally coordinated, and only a minor increase of higher coordinated Al species has been found. [5,143–145]. As in the case of aluminosilicate and boroaluminosilicate glasses silicon favors strongly the four-fold coordination state in borosilicate glasses, regardless of the added water [5,145–147]. In contrast, a significant change of boron coordination has been observed with the addition of water to dry borosilicate glass [chapter 2A]. In the anhydrous NBS glass 88% of the boron is tetrahedrally coordinated. After the addition of 3 wt.% H_2O basically all boron is transformed into four-fold coordination.

The effect of H_2O on T_g in alkali-rich systems as phonolite [141] and NBS glasses is very similar as indicated by the parallel trends shown in Fig. 5. A stronger initial decrease of T_g upon hydration is visible for albite glasses compared to the phonolite glasses. As discussed in Bouhifd et al. [141] and previous studies on the effect of water on aluminosilicate glasses [e.g. 40,41], the influence of water on polymerized glasses as albite and rhyolite is more pronounced compared to aluminosilicate glasses containing some non-bridging oxygen (NBO) e.g. phonolite or dacite glasses. The degree of depolymerization in glasses is often

described by the ratio of non-bridging oxygen over tetrahedra cations (NBO/T). The NBO/T of the here considered glasses is calculated from the content of network modifier oxides ($Na_2O+CaO+K_2O+MgO$) and all network forming species (SiO_4, AlO_4, BO_4, BO_3) assuming that all Si and Al is exclusively tetrahedrally coordinated in these glasses. The dry albite glass with NBO/T = 0 is fully polymerized [141], while the phonolite glass with NBO/T = 0.19 exhibit a slightly higher degree of depolymerization [141]. The dry NBS glass with NBO/T of 0.13 is therefore in a very good agreement with the T_g data of aluminosilicate glasses. The T_{12} and T_g data of a polymerized rhyolite glass [139] and a more depolymerized dacite glass [140] support the correlation of an increased depolymerization for initially polymerized glasses. The T_{12} data of the rhyolite glass decrease stronger in the range up to 1 wt.% H_2O as the dacite glass.

The evolution of T_{12} vs. H_2O of float glass contrast this observation. Float glass is by far the most depolymerized glass composition (NBO/T= 0.77) [89] in comparison to the other glasses, but exhibit a similar strong decrease of T_{12} with water addition as the polymerized glasses (e.g. rhyolite or albite). Silicon is the only network former in float glass and is responsible for a rigid glass structure. On the other hand the influence of water on the glass transition temperature in glasses with weak connections as in the case of borate glasses or in glasses which consist of mixed network formers (e.g. Al+B or Al+Si) is comparatively less pronounced.
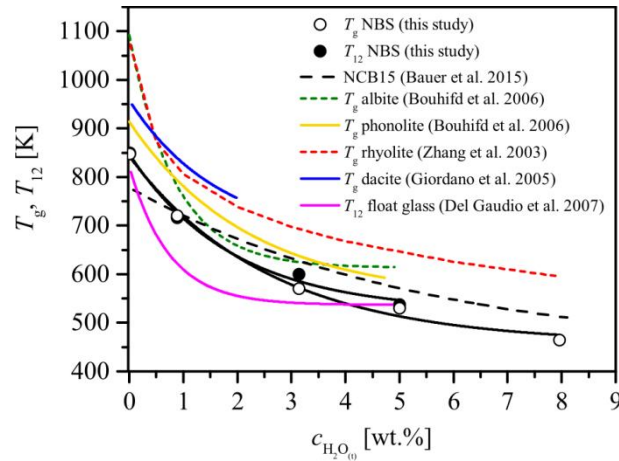
Fig. 5. Comparison of T_g determined by DTA with T_{12} data derived from viscosity measurements for NBS glasses. T_g data of albite and phonolite from Ref. [141] and T_g of soda-lime borate glasses from Ref. [90] as well as T_{12} and T_g data of rhyolite and dacite glasses respectively of Ref. [139] and Ref. [140] are plotted for comparison. Lines are exponential fits through the data.

4.2 Effect of glass composition and water speciation on network depolymerization

The type and the species of the network forming cations, as well as the initial degree of polymerization are important parameters for the evolution of depolymerization upon hydration (see previous section). Another parameter influencing the depolymerization of hydrous glasses is the water species distribution. The stabilization of hydroxyl groups or molecular water depends strongly on the composition of the oxide glass system. OH groups dominate only at water contents ≤ 3 wt.% in silicate [46] and aluminosilicate glasses [59,63] and are increasingly stabilized with rising boron content [59,90]. For instance, 80% of the dissociated water species and only 20% molecular water are present at 8 wt.% H_2O in soda lime borate glasses [90].

A three-component model to compare and to quantify the individual contributions of OH groups, molecular water and the dry glass on T_g was introduced by Tomozawa et al. [88]. Based on this model T_g of different glass compositions were compared in the study of

Deubener et al. [45] using the reduced glass transition temperature $T_g^* = \dfrac{T_g}{T_g^{GN}}$, where T_g^{GN} is

the glass transition temperature for a nominal dry glass containing 0.02 wt.% total water:

$$T_g^* = \frac{1.01 \cdot c_G + 0.22 \cdot A \cdot cOH + 0.22 \cdot B \cdot cH_2O_{mol}}{c_G + A \cdot cOH + B \cdot cH_2O_{mol}} \tag{3}$$

the weight fractions of the total water content of the anhydrous glass, of molecular water and OH groups of the hydrous glasses are expressed as c_G (=$1-cH_2O_{(t)}$), cH_2O_{mol} and cOH, respectively. A and B are parameters weighting the influence of hydroxyl groups and molecular water on the reduced glass transition temperature, respectively. Fig. 6 shows the reduced glass transition temperature as a function of the water content for selected silicate, borate, aluminosilicate and a borosilicate glass.
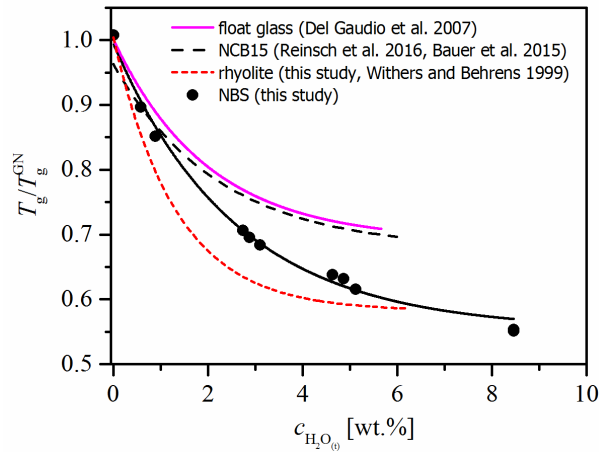

Fig. 6. Reduced glass transition temperature T_g / T_g^{GN} vs. water content of different alkali-rich oxide glasses. The weighting parameters A and B for the determination of the reduced glass transition temperature and corresponding literature are listed in Tab.3 for the different compositions.

Consistent with [45] the reduced glass transition temperatures of all glass compositions decrease considerable in the range of low water contents and decrease only marginal at water contents ≥ 2 wt.% H_2O. Whereas the evolution of T_g^* vs. H_2O for the borate glass and the float glass are rather similar, a distinct difference to the borosilicate and the ryholite glass can be observed. Deviation from a uniform fit curve of T_g^* vs. H_2O data of various silicate and aluminosilicate glasses was also visible in the data sets shown in [45]. Compositional differences in the T_g^* vs. H_2O plot are also indicated by differences of the water species weighting parameters A and B of the different compositions as presented in Tab.3.

Tab.3. Water species weighting parameters A (OH groups) and B (molecular water) for the calculation of the reduced glass transition temperature for different compositions.

	A	B	Ref.	Ref. of water speciation
Float glass	22.9	6.9	[89]	[89]
Soda-lime borate	11.7	1.8	[150]	[90]
Rhyolite	54.0	1.9	this study	[63]
NBS	30.2 ± 1.4	1.7 ± 2.0	this study	chapter 2A

The main contribution to decrease T_g^* arises from OH groups (A parameter) for all glasses. The highest value is determined for the fully polymerized rhyolite glass suggesting a very strong influence of OH groups in the depolymerization mechanism. While A varies strongly for the different considered compositions, the values determined for B representing the influence of molecular water are quite similar. A slightly higher contribution of molecular water on T_g^* has been found, but for all other composition molecular water does not play a crucial role for the decrease of T_g^*. In the case of borate glasses the fully polymerized network is only weakly connected and the decrease of T_g^* is comparatively less drastic.

4.3 Effect of H$_2$O on internal friction

Deconvolution of mechanical loss spectra into Gaussians is shown in Fig. 8 to separate and to analyze the different relaxation processes. The low temperature peak at ~313 K in the dry NBS glass is attributed to γ-relaxation which is in line with internal friction measurements on different silicate glasses [137,36,151]. The shift towards higher temperature and the decrease in height of this mode with the addition of water was also observed for hydrous soda-lime silica glass [13]. The peak at higher temperature (650 K) at first visible in the NBS glass with 0.23 wt.% is attributed to a β-relaxation process and correlates with the increasing water content consistent with the study of Reinsch et al. [13] on hydrous soda-lime silica glass. At 0.50 wt.% H$_2$O the γ- and β-relaxation modes are superimposed. Based on the development of the γ-relaxation mode it is expected to be absent at $\geq$ 2.91 wt.% H$_2$O.

In the study of Reinsch et al. [13] on soda-lime silicate glasses one β-relaxation peak was observed at water contents up to 0.24 wt.%, whereas a second β-relaxation peak arises at water contents >1 wt.%. The one at higher temperature was attributed to OH groups (β_{OH}) and the one at the lower temperature flank to a mode related to the increasing amount of molecular water (β_{H2O}). In the case of soda-lime silicate glasses it can be clearly distinguished between these two β-relaxation modes, whereas in the mechanical loss spectra of the NBS glasses we observe one broad β-relaxation peak at water contents <3 wt.%. Upon further water addition it is possible to identify a second β-relaxation mode and consistent with [13] we attribute this mode to (β_{H2O}).
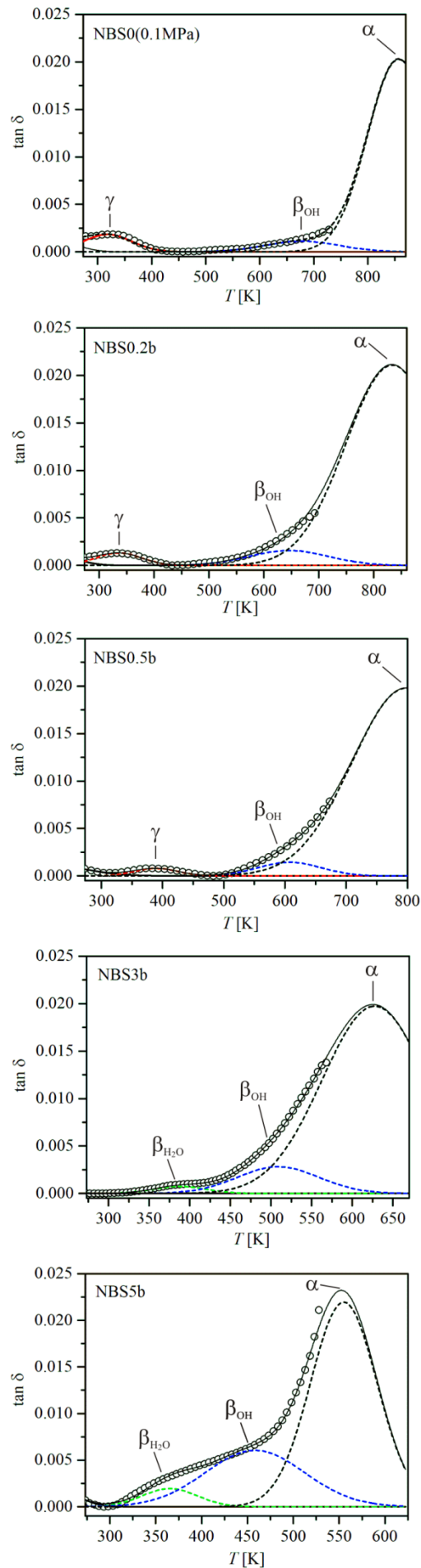
Fig. 8. Deconvoluted mechanical loss spectra of anhydrous and hydrous NBS glasses. Note the disappearance of the γ-peak at 0.5 wt.% H_2O and the subsequent appearance of a second β-relaxation mode in NBS3b (see text for details).

The peak at highest temperature is assigned to the α- relaxation [20,29,137] , i.e. the structural relaxation at the glass transition temperature. The α- relaxation peak is only poorly constrained by experimental data points. As mentioned above this mode cannot be measured by DMTA due to the progressive viscous sample bending under the applied static load. Because of the frequency dependence of α-relaxation, T_α, cannot be simply approximated by the T_g values listed in Tab.1. The shear modulus (G_∞) would be required for an estimation of T_α (see [13]) which was unfortunately not determined for the NBS glasses. For all NBS glasses we fitted the α peaks with similar heights (Fig. 4). We are aware that this procedure can cause a certain inaccuracy in the determination of the temperature and peak height, especially for the β-mode, which appears as a shoulder of the α-relaxation. In order to estimate the influence of the evaluation method we compared two different approaches with different peak heights and temperatures of the α-relaxation mode for a high-bearing water (NBS5b) and a low water-bearing (NBS0.5b) sample. α peak heights of 0.05 and 0.02 and peak temperatures of 590 and 553 K respectively has been chosen for NBS5b. For NBS0.5b α peak heights of 0.03 and 0.02 and peak temperatures of 843 and 798 K respectively were considered. For both water contents neither the height of α peak heights nor of its peak temperatures was found to have noticeable effect on the sub- T_g modes. The derived peak heights as well as the peak temperature positions of the relaxation modes are plotted as a function of the total water content in Fig. 9a,b. The chosen α peak positions are found to be lower in the case of intermediate water contents (Fig. 9a). With increasing water content the temperature of β_{OH} decreases significantly up to 1 wt.% H_2O and decreases further to a less extend. Up to 0.5 wt.% H_2O the peak height remains constant but increases clearly in the range between 0.5 and 5 wt.% H_2O. This trend correlates well with the increase of OH groups. The most pronounced increase is observed from 3 to 5 wt.% H_2O (Fig. 9b). In this range of water contents the β_{H2O} mode appears, shifts slightly towards lower temperature and

rises in height. In contrast, the *y*-relaxation peak shifts strongly to higher temperature and decreases in height until it diminishes at 0.5 wt.% H_2O.
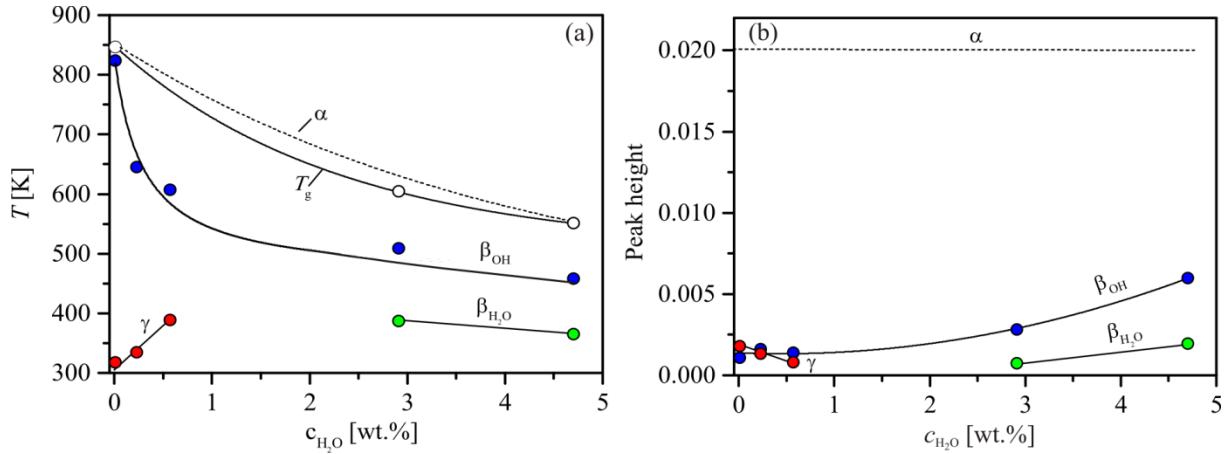
Fig. 9. Temperature (a) and peak height (b) vs. water content of DMA relaxation peaks (*a*, β_{OH}, β_{H2O}, and *γ*) for *f*=7.125 Hz. The dashed line illustrates the estimated peak temperatures and heights for the only partially measurable *a*-relaxation mode (see text for details). Lines are indented as visual guides. For comparison T_g values determined with DTA are presented in (a) for NBS glasses with similar water contents (NBS3 and NBS5, see Tab.1).

The derived data supports the assignment of the relaxation modes in the study of Reinsch et al. [13] and is consistent with the evolution of water species distribution in the NBS glasses [chapter 2A]. OH groups are the dominating water species up to 7 wt.% H_2O. The content of hydroxyl groups is expected to level off with further increasing water content. Significant amounts of molecular water are first present at 3 wt.% H_2O and increase strongly between 3 and 5 wt.% H_2O.

5. Conclusion

It is well known that water strongly affects the α-relaxation and decrease the polymerization of the glass network. The very good agreement of T_g and T_{12} data for the investigated NBS glasses is in line with α- relaxation studies on silicate, aluminosilicate and borate glasses.

Comparison to T_g data from literature reveal that initially polymerized aluminosilicate glasses as e.g. albite are stronger affected by the incorporation of water compared to more depolymerized glasses e.g. phonolite. On the other hand, the depolymerized float glass with only silicon as network former show a similar evolution of T_g vs. H_2O as initially polymerized glasses with Al + Si as networker formers. It is reasonable that a higher rigidity and the strength of the connections in the float glass network are responsible for the pronounced decrease of T_g with increasing water content.

As revealed by the model of the reduced glass transition temperature [88,45] the base glass composition is an important parameter influencing the efficiency of hydroxyl groups and molecular water respectively on T_g. The parameters weighting the influence of OH groups and molecular water strongly differ for rhyolite and float glass as well as for borate and borosilicate glasses. These findings show that the assumption of an uniform behavior of T_g^* with water content is possibly not an adequate solution for different glass compositions as verified by the presented data. However, the model is suitable to describe the general trend of T_g^* and the respective influence of different water species.

Internal friction measurements showed that the relaxation processes in the NBS glasses are very complex. The superimposition of α- β- and γ- relaxation modes suggest a cooperative process including possibly alkalis as well as molecular water and OH groups in combination with network relaxation. These findings reveal important information in terms of water-related relaxation mechanisms occurring at crack tips where water is preferentially accumulated.

Summary and Conclusion

The influence of structurally bonded water on the network of borosilicate- and borate glasses as well as on relaxation processes was investigated in the present study.

Total water contents as well as contents and hydrogen bond strength of hydrous species and connections of hydroxyl groups to network forming species were analyzed by Karl-Fischer Titration, mid-infrared and near-infrared spectroscopy. Mid-infrared analysis of hydrous borate glasses revealed absorption modes at 3440 cm^{-1}, 3500 cm^{-1} and around 3230 cm^{-1} which are assigned to weakly and moderately H-bonded hydrous species. In hydrous borosilicate glasses a triplet at 2900, 2350 and 1750 cm^{-1} is observed in addition to the pronounced OH stretching vibration band of weakly H-bonded species at 3580 cm^{-1} and is attributed to OH groups and water molecules which are strongly H-bonded, to non-bridging oxygen.

In hydrous borate glasses, observed features at 5200, 4750 and 4600 cm^{-1} in the near- infrared are attributed to molecular water species (5200 cm^{-1}) and to vibrations of BO_4-OH (4750 and 4600 cm^{-1}). One additional feature at 4900 cm^{-1} is assigned to BO_3-OH. Consistent with simple silicate and aluminosilicate glasses [40,43,44,66] the linear molar absorption coefficient ε_{4600} for NCB glasses decreases with increasing alkali content from 1.47 ± 0.08 l·mol^{-1}·cm^{-1} for NCB5 to 0.99 ± 0.13 l·mol^{-1}·cm^{-1} for NCB15 and to 0.92 ± 0.08 l·mol^{-1}·cm^{-1} for NCB25. In contrast, ε_{5200} does not vary between different borate glasses 0.52 ± 0.12 L·mol^{-1}·cm^{-1} for NCB5 to 1.53 ± 0.10 l·mol^{-1}·cm^{-1} for NCB15 and to 0.63 ± 0.11 l·mol^{-1}·cm^{-1} for NCB25. The derived water species contents reveal that dissociated water is by far the dominating water species in the range of investigated water contents (up to 7.5 wt.% H_2O).

In addition to the molecular water peak at 5200 cm^{-1} in hydrous borosilicate glasses, absorption modes at 4500 and 4700 cm^{-1} are due to SiO_4-OH and BO_4-OH vibrations respectively. Based on the two band evaluation method for the modes at 4500 and 4700 cm^{-1},

an absorption coefficient of $\varepsilon_{4500+4700} = 1.52$ (± 0.04) l·mol^{-1}·cm^{-1} for the OH-related bands and of $\varepsilon_{5200} = 1.08$ (± 0.05) l·mol^{-1}·cm^{-1} for molecular water was determined. In contrast to the borate glasses, molecular water becomes the predominant water species at water contents above 7 wt.% H_2O in the borosilicate glasses. An individual quantification of the proportions of Si-OH and B-OH was not possible, since no independent information of the relative abundance of both OH species is available and the ratio of respective peak intensities does not vary strong enough with water content. However, based on absorption coefficients for silicate glasses known from literature and the absorption coefficients of B-OH determined from borate glasses, the B-OH/Si-OH ratio is estimated to be ≈ 0.8 in the borosilicate glasses.

The break-up of oxygen bridges by formation of OH groups lead to large structural modifications in hydrous borosilicate glasses at water contents ≤ 3 wt.% H_2O as indicated by the density data, Raman and NMR spectroscopy. The incorporation of water contents ≤ 3 wt.% H_2O initially causes a density increase, which is correlated with the formation of tetrahedral coordinated boron. N_4 increases from 88.2 (± 1)% in the dry compressed sample to 98.2 (± 1)% upon addition of 3 wt.% H_2O. With further increase in water content, N_4 remains virtually unchanged and the density decreases significantly.

Raman measurements suggest that BO_4 groups are preferentially bonded to Q^3 species, which seem to be stabilized by linkage to BO_4 tetrahedra. While in silicate glasses Q^4 as well as Q^3 species are affected by water incoporation, the depolymerization mechanism in NBS glasses is primarily based on the direct conversion from Q^4 to Q^2.

In the case of initially fully polymerized borate glasses a significantly smaller influence of water on boron speciation was found. For instance, in NCB25 glass N_4 increases from 53.4% in the dry compressed glass to 57.5% with the addition of 6 wt.% H_2O. This increase of N_4 is much smaller compared to the pronounced effect of alkalis on boron coordination in borate glasses and therefore point to different roles of Na_2O and H_2O on boron coordination. This conclusion is further supported by the observed changes in boron coordination in hydrous

borosilicate glasses. The higher coordination state of boron upon the addition of water is probably a result of chemical changes (e.g. network depolymerization) accompanied by changes in T_f. Therefore a quantitative comparison with the well-known changes caused by Na_2O addition is difficult. However, it is clear that increasing Na_2O/B_2O_3 much above that of the NBS0 composition would decrease, not increase N_4 [152] in the anhydrous NBS glass: indeed the N_4 values observed for the H_2O-rich glasses (>99%) are well above the maximum seen in any ambient-pressure anhydrous sodium borosilicate (about 89%).

The findings obtained from hydrous and anhydrous borate- and borosilicate glasses [5,80,90,124], clearly point to the importance of modifier cations to support the formation of tetrahedrally coordinated boron in hydrous glasses. If the coordination polyhedra of the modifier cations can be satisfied by NBOs or OH groups the formation of BO_4 upon water incorporation is promoted.

Breaking of oxygen bridges as a consequence of water incorporation results in a reduction of viscosity and T_g in the hydrous borate-and borosilicate glasses. For both glasses the decrease of T_g and T_{12} upon water addition was found to be in very good agreement. In borosilicate glasses the strongest decrease of T_g has been found at low water contents, while the decrease of T_g in borate glasses was less pronounced and more continuously. This observation can be attributed to the different bond strength of network forming species and the rigidity of the network. Comparison to T_g data of hydrous silicate [139,140] and aluminosilicate glasses [141] revealed that initially polymerized glasses are more sensitive in terms of depolymerization upon water incorporation then glasses already containing some NBOs.

The base glass composition is an crucial parameter influencing the efficiency of hydroxyl groups and molecular water on T_g, as revealed by the model of the reduced glass transition temperature [45,88]. The individual influence of water species on T_g was found to differ strongly for a float glass and a rhyolite glass as well as for the borate and borosilicate glasses.

Consistent with the internal friction study on hydrous silicate glasses, a water-related β-relaxation mode was indentified in the hydrous borosilicate glasses. Discrimination between individual water species is possible at water contents above 3 wt.%. However, the mechanical loss spectra are characterized by superimposed relaxation modes, suggesting a complex cooperative process possibly including alkalis as well as molecular water and OH groups in combination with network relaxation. Such water-related relaxation mechanisms play an important role in water-rich regions, which occur e.g., at crack tips. These hydrous regions would be characterized by a much lower glass transition temperature and hence a strongly extended ability to accumulate stress.

References

[1]   W. Vogel, Struktur und Kristallisation der Gläser, 2nd ed., 1971.

[2]   Y.D. Yiannopoulos, G.D. Chryssikos, E.I. Kamitsos, Structure and Properties of Alkaline Earth Borate Glasses, Phys. Chem. Glas. 42 (2001) 164–172.

[3]   T. Yano, N. Kunimine, S. Shibata, M. Yamane, Structural Investigation of Sodium Borate Glasses and Melts by Raman Spectroscopy. II. Conversion between BO_4 and BO_2O^- units at High Temperature, J. Non. Cryst. Solids. 321 (2003) 147–156.

[4]   S. Sen, Z. Xu, J.F. Stebbins, Temperature Dependent Structural Changes in Borate, Borosilicate and Boroaluminate Liquids: High-Resolution ^{11}B, ^{29}Si and ^{27}Al NMR Studies, J. Non. Cryst. Solids. 226 (1998) 29–40.

[5]   B.C. Schmidt, N. Zotov, R. Dupree, Structural Implications of Water and Boron Dissolution in Albite Glass, J. Non. Cryst. Solids. 337 (2004) 207–219.

[6]   S. Lee, K. Mibe, Y. Fei, G. Cody, B. Mysen, Structure of B_2O_3 Glass at High Pressure: A ^{11}B Solid-State NMR Study, Phys. Rev. Lett. 94 (2005) 165507-1–4.

[7]   L. Wondraczek, S. Sen, H. Behrens, R. Youngman, Structure-Energy Map of Alkali Borosilicate Glasses: Effects of Pressure and Temperature, Phys. Rev. B. 76 (2007) 14202-1–8.

[8]   J.C. Mauro, P.K. Gupta, R.J. Loucks, Composition Dependence of Glass Transition Temperature and Fragility. II. A Topological Model of Alkali Borate Liquids., J. Chem. Phys. 130 (2009) 234503-1–8.

[9]   P.K. Gupta, M.L. Lui, P.J. Bray, Boron Coordination in Rapidly Cooled an in Annealed Aluminium Borosilicate Glass Fibers, J.Am.Ceram. Soc. 68 (1985) C-82.

[10]   M.M. Smedskjaer, R.E. Youngman, S. Striepe, M. Potuzak, U. Bauer, J. Deubener, et al., Irreversibility of Pressure Induced Boron Speciation Change in Glass, Sci. Rep. 4 (2014) 1–5.

[11]   H.R. Shaw, Obsidian-H_2O viscosities at 1000 and 2000 bars in the temperature range 700 to 900°C, J Geophy Res. 68 (1963) 6337–6343.

[12]   D.B. Dingwell, C. Romano, K.-U. Hess, The Effect of Water on the Viscosity of a Haplogranitic Melt under P-T-X Conditions Relevant to Silicic Volcanism, Contrib. to Mineral. Petrol. 124 (1996) 19–28.

[13]   S. Reinsch, R. Müller, J. Deubener, H. Behrens, Internal Friction of Hydrated Soda-Lime-Silicate Glasses, J. Chem. Phys. 139 (2013) 174506-1–6.

[14]   R.F. Bartholomew, B.L. Butler, H.L. Hoover, C.K. Wu, Infrared Spectra of a Water-Containing Glass, 63 (1980) 481–485.

[15]   H. Scholze, Der Einbau des Wassers in Gläsern (I), Glas. Berichte. 3 (1959) 81–88.

[16]   H. Scholze, Der Einbau des Wassers in Gläsem (II), Glas. Berichte. 4 (1959) 142–152.

[17]   E. Stolper, The Speciation of Water in Silicate Melts, Geochim. Cosmochim. Acta. 46 (1982) 2609–2620.

[18]   R.J. Ryder, G.E. Rindone, Internal Friction of Simple Alkali Silicate Glasses Containing Alkaline-Earth Oxides: I, Experimental Results, J. Am. Ceram. Soc. 43 (1960) 662–669.

[19]   R.J. Ryder, G.E. Rindone, Internal Friction of Simple Alkali Silicate Glasses Containing Alkaline-Earth Oxides: II, Interpretation and Discussion, J. Am. Ceram. Soc. 44 (1961) 532–540.

[20]   W.A. Zdaniewski, G.E. Rindone, The Internal Friction of Glasses, J. Mater. Sci. 14 (1979) 763–775.

[21]   M. Coenen, Mechanische Relaxation von Silikatgläsern eutektischer Zusammensetzung, Zeitschrift Für Elektrochem. 65 (1961) 903–908.

[22]   B. Roling, M. Ingram, Analysis of Mechanical Losses due to Ion-Transport Processes in Silicate Glasses, Phys. Rev. B. 57 (1998) 14192–14199.

[23]   J.W. Fleming, D.E. Day, Relation of Alkali Mobility and Mechanical Relaxation in Mixed-Alkali Silicate Glasses, J. Am. Ceram. Soc. 55 (1972) 186–192.

[24]   J.E. Shelby, D.E. Day, Mechanical Relaxation in Mixed-Alkali Silicate Glasses : I , Results, J. Am. Ceram. Soc. 52 (1969) 169–174.

[25]   J.E. Shelby, D.E. Day, Mechanical Relaxations in Mixed Alkali Silicate Glasses : II, Discussion, J. Am. Ceram. Soc. 74 (1969) 182–187.

[26]   K.E. Forry, Two Peaks in the Internal Friction as a Function of Temperature in Soda Silicate Glasses, J. Am. Ceram. Soc. 40 (1957) 90–94.

[27]   R.E. Strakna, H.T. Savage, Ultrasonic Relaxation loss in SiO_2, GeO_2, B_2O_3, and As_2O_3 Glass, J. Appl. Phys. 35 (1964) 1445–1450.

[28]   H. de Waal, Influence of Proton Exchange on Internal Friction in Alkali Silicate Glasses, J. Am. Ceram. Soc. 52 (1969) 165–166.

[29]   D.E. Day, Internal Friction of Glasses with Low Water Contents, J. Am. Ceram. Soc. 57 (1974) 530–533.

[30]   A. Ismail, A. Abdel-Latif, D.E. Day, Internal Friction of Proton-Exchanged Li_2O-Al_2O_3-$2SiO_2$ glass, J. Am. Ceram. Soc. 55 (1972) 254–256.

[31]   D.E. Day, J.M. Stevels, Internal Friction of $NaPO_3$ Glasses Containing Water, J. Non. Cryst. Solids. 11 (1973) 459–470.

[32]   M.S. Maklad, N.J. Kreidl, Some Effects of OH Groups on Sodium Silicate Glasses, Sci. Tech. Comm. 9th Intl. Congr. Glas. 1 (1971) 75–100.

[33]   S. Indris, P. Heitjans, H. Behrens, R. Zorn, B. Frick, Fast Dynamics of H_2O in Hydrous Aluminosilicate Glasses Studied with Quasielastic Neutron Scattering, Phys. Rev. B. 71 (2005) 64205-1–9.

[34]   B.C. Schmidt, H. Behrens, T. Riemer, R. Kappes, R. Dupree, Quantitative Determination of Water Speciation in AluminosilicateGlasses: A Comparative NMR and IR Spectroscopic Study, Chem. Geol. 174 (2001) 195–208.

[35]   S. V. Nemilov, The Review of Possible Interrelations between Ionic Conductivity, Internal Friction and the Viscosity of Glasses and Glass Forming Melts within the Framework of Maxwell Equations, J. Non. Cryst. Solids. 357 (2011) 1243–1263.

[36]   J. V. Fitzgerald, Anelasticity of Glasses: II, Internal Fiction and Sodium Ion Diffusion in Tank Plate Glass, A Typical Soda-Lime Silica Glass, J. Am. 34 (1951) 339–342.

[37]   A.C. Wright, S.A. Feller, A.C. Hannon, Borate Glasses, Crystals & Melts, 1997.

[38]   V.K. Michaelis, P.M. Aguiar, S. Kroeker, Probing Alkali Coordination Environments in Alkali Borate Glasses by Multinuclear Magnetic Resonance, J. Non. Cryst. Solids. 353 (2007) 2582–2590.

[39]   M. Schuch, C. Trott, P. Maass, Network Forming Units in Alkali Borate and Borophosphate Glasses and the Mixed Glass Former Effect, RSC Adv. 1 (2011) 1370–1382.

[40]   E. Stolper, Water in Silicate Glasses: An Infrared Spectroscopic Study, Contrib. to Mineral. Petrol. 81 (1982) 1–17.

[41]   Y. Zhang, Kinetics of the Reaction $H_2O+0 = 2OH$ in Rhyolitic Glasses Upon Cooling : Geospeedometry and Comparison with Glass Transition, Geochim. Cosmochim. Acta. 61 (1997) 2167–2173.

[42]   H. Behrens, M. Nowak, Quantification of H_2O Speciation in Silicate Glasses and Melts by IR Spectroscopy - in situ versus Quench Techniques, Phase Transitions. 76 (2003) 45–61.

[43]   H. Behrens, C. Romano, M. Nowak, F. Holtz, Near-Infrared Spectroscopic Determination of Water Species in Glasses of the system $MAlSi_3O_8$ (M= Li,Na,K): An Interlaboratory Study, Chem. Geol. 128 (1996) 41–63.

[44]   L. a. Silver, P.D. Ihinger, E. Stolper, The Influence of Bulk Composition on the Speciation of Water in Silicate Glasses, Contrib. to Mineral. Petrol. 104 (1990) 142–162.

[45]   J. Deubener, R. Müller, H. Behrens, G. Heide, Water and the Glass Transition Temperature of Silicate Melts, J. Non. Cryst. Solids. 330 (2003) 268–273.

[46]   A. Stuke, H. Behrens, B. Schmidt, R. Dupree, H_2O Speciation in Float Glass and Soda Lime Silica Glass, Chem. Geol. 229 (2006) 64–77.

[47]   H. Behrens, A. Stuke, Quantification of H_2O Contents in Silicate Glasses using IR Spectroscopy- a Calibration Based on Hydrous Glasses Analyzed by Karl-Fischer Titration, Glas. Sci. Technol. 76 (2003) 176–189.

[48]   J. Acocella, M. Tomozawa, E.B. Watson, The Nature of Dissolved Water in Sodium Silicate Glasses and its Effect on Various Properties, J. Non. Cryst. Solids. 65 (1984) 355–372.

[49]   F. Pouchou, J.L., Pichoir, Quantitative Analysis of Homogeneous or Stratified Microvolumes Applying the Model "PAP," Plenum Press, New York, 1991.

[50]   J. Berndt, A Combined Rapid-Quench and H_2 -Membrane Setup for Internally Heated Pressure Vessels: Description and Application for Water Solubility in Basaltic Melts, Am. Mineral. 87 (2002) 1717–1726.

[51]   H. Behrens, Determination of Water Solubilities in High-Viscosity Melts: An Experimental Study on $NaAlSi_3O_8$ and $KAlSi_3O_8$ Melts, Eur. J. Miner. 7 (1995) 905–920.

[52]   H. Behrens, G. Müller, An Infrared Spectroscopic Study of Hydrogen Feldspar ($HAlSi_3O_8$), Mineral. Mag. 59 (1995) 15–24.

[53]   H. Behrens, M. Meyer, F. Holtz, D. Benne, M. Nowak, The Effect of Alkali Ionic Radius , Temperature, and Pressure on the Solubility of Water in $MAlSi_3O_8$ melts (M=Li,Na,K,Rb), Chem. Geol. 174 (2001) 275–289.

[54]   O. V Mazurin, Y.V. Gankin, Glass Transition Temperature : Problems of Measurements and Analysis of the Existing Data, Glas. Technol. Eur. J. Glas. Sci. Technol. Part A. 49 (2008) 229–233.

[55]   O. V. Mazurin, Problems of Compatibility of the Values of Glass Transition Temperatures Published in the World Literature, Glas. Phys. Chem. 33 (2007) 22–36.

[56]   D. Massiot, F. Fayon, M. Capron, I. King, S. Le Calvé, B. Alonso, et al., Modelling One- and Two-Dimensional Solid-State NMR Spectra, Magn. Reson. Chem. 40 (2002) 70–76.

[57]   M.M. Smedskjaer, J.C. Mauro, S. Sen, Y. Yue, Quantitative Design of Glassy Materials Using Temperature-Dependent Constraint Theory, Chem. Mater. 22 (2010) 5358–5365.

[58]   E.I. Kamitsos, G.D. Chryssikos, Borate Glass Structure by Raman and Infrared Spectroscopies, J. Mol. Struct. 247 (1991) 1–16.

[59]   B.C. Schmidt, Effect of Boron on the Water Speciation in (Alumino)Silicate Melts and Glasses, Geochim. Cosmochim. Acta. 68 (2004) 5013–5025.

[60]   C. Romano, D.B. Dingwell, K.U. Hess, The Effect of Boron on the Speciation of Water in Haplogranitic Melts, Per. Miner. 64 (1995) 413–431.

[61]   D.P. Zarubin, Infrared Spectra of Hydrogen Bonded Hydroxyl Groups in Silicate Glasses. A re-Interpretation, Phys. Chem. Glas. 40 (1999) 184–192.

[62]   S. Yamashita, H. Behrens, B.C. Schmidt, R. Dupree, Water speciation in Sodium Silicate Glasses Based on NIR and NMR Spectroscopy, Chem. Geol. 256 (2008) 231–241.

[63]   A.C. Withers, H. Behrens, Temperature-Induced Changes in the NIR Spectra of Hydrous Albitic and Rhyolitic Glasses between 300 and 100 K, Phys. Chem. Miner. 27 (1999) 119–132.

[64]   S. Newman, E.M. Stolper, S. Epstein, Measurement of Water in Rhyolitic Glasses: Calibration of an Infrared Spectroscopic Technique, Am. Mineral. 71 (1986) 1527–1541.

[65]   F. Geotti-Bianchini, H. Geißler, F. Krämer, H. Smith, Ian, Recommended Procedure for the IR Spectroscopic Determination of Water in Soda-Lime-Silica Glass, Glas. Ber. Glas. Sci. Technol. 72 (1999) 103–111.

[66]   S. Ohlhorst, H. Behrens, F. Holtz, Compositional Dependence of Molar Absorptivities of Near-Infrared OH-and H_2O Bands in Rhyolitic to Basaltic Glasses, Chem. Geol. 174 (2001) 5–20.

[67]   B.C. Schmidt, R. Dupree, Effect of Water on the Structure of Melts and Glasses along the Join $NaAlSi_3O8–NaBS_{i3}O_8$, EOS. Trans. AGU, 83(47) Fall Meet. Suppl., Abstr. V72B-1318. (2002).

[68]   H. Behrens, C. Romano, M. Nowak, F. Holtz, D.B. Dingwell, Near-Infrared Spectroscopic Determination of Water Species in Glasses of the System $MAlSi_3O_8$ (M= Li, Na, K): An Intralobratory Study, Chem. Geol. 128 (1996) 41–63.

[69]   H. Behrens, S. Yamashita, Water Speciation in Hydrous Sodium Tetrasilicate and Hexasilicate Melts: Constraint from High Temperature NIR Spectroscopy, Chem. Geol. 256 (2008) 306–315.

[70]   P.D. Ihinger, Y. Zhang, E.M. Stolper, The Speciation of Dissolved Water in Rhyolitic Melt, Geoch. 63 (1999) 3567–3578.

[71]   J.R. Sowerby, H. Keppler, Water Speciation in Rhyolitic Melt Determined by in-situ Infrared Spectroscopy, Am. Mineral. 84 (1999) 1843–1849.

[72]   M. Nowak, H. Behrens, Water in Rhyolitic Magmas: Getting a Grip on a Slippery Problem, Earth Planet. Sci. Lett. 184 (2001) 515–522.

[73]   Y. Liu, Y. Zhang, H. Behrens, H_2O Diffusion in Dacitic Melts, Chem. Geol. 209 (2004) 327–340.

[74]   S. Ohlhorst, H. Behrens, F. Holtz, Water Speciation in Aluminosilicate Glasses and Melts, Appl. Mineral. Res. Econ. Technol. Cult. Pro 6th Int. Conf. Appl. Miner. 1 Balkema (2000) 193–196.

[75]   R. Botcharnikov, H. Behrens, F. Holtz, Solubility and Speciation of C–O–H Fluids in Andesitic Melt at T=1100–1300°C and P=200 and 500 MPa, Chem. Geol. 229 (2006) 125–143.

[76]   D. Massiot, C. Bessada, J.P. Coutures, F. Taulelle, A Quantitative Study of ^{27}Al MAS NMR in Crystalline YAG, J. Magn. Reson. 90 (1990) 231–242.

[77]   L.B. Alemany, D. Massiot, B.L. Sherriff, M.E. Smith, F. Taulelle, Observation and Accurate Quantification of ^{27}Al MAS NMR Spectra of Some Al2SiO5 Polymorphs Containing Sites with Large Quadrupole Interactions, Chem. Phys. 177 (1991) 301–306.

[78]   H. Scholze, Glas: Natur, Struktur und Eigenschaften, 3rd ed., Springer Verlag Berlin Heidelberg New YorkLondon Paris Tokyo, 1988.

[79]   P.K. Gupta, Proceedings of the International Congress on Glass, Unbublished. New Dehli (1986).

[80]   J.F. Stebbins, S.E. Ellsworth, Temperature Effects on Strucutre and Dynamics in Borate and Borosilicate Liquids: High-Resolution and High-Temperature NMR results, J.Am.Ceram. Soc. 79 (1996) 2247–56.

[81]   T.J.M. Visser, J.M. Stevels, Rheological Porperties of Boric Oxide and Alkali Borate Glasses, J. Non. Cryst. Solids. 7 (1972) 376–394.

[82]   M. Grimsditch, A. Polian, A.C. Wright, Irreversible Structural Changes in Vitreous B_2O_3 under Pressure, Pysical Rev. B. 54 (1996) 152–155.

[83]   J. Wu, J. Deubener, J.F. Stebbins, L. Grygarova, H. Behrens, L. Wondraczek, et al., Structural Response of a Highly Viscous Aluminoborosilicate Melt to Isotropic and Anisotropic Compressions, J. Chem. Phys. 131 (2009) 104504-1–10.

[84]   P.J. Bray, E.J. Holupka, The Potential of NMR Techniques For Studies of the Effects of Thermal History on Glass Structure, J. Non. Cryst. Solids. 71 (1985) 411–428.

[85]   L. Wondraczek, S. Krolikowski, H. Behrens, Kinetics of Pressure Relaxation in a Compressed Alkali Borosilicate Glass, J. Non. Cryst. Solids. 356 (2010) 1859–1862.

[86]   H.R. Shaw, Obsidian-H_2O Viscosities at 1000 and 2000 Bars in the Ttemperature Range 700° to 900°C, J. Geophys. Res. 68 (1963) 6337–6343.

[87]   J.E. Shelby, G.L. McVay, Influence of Water on the Viscosity and Thermal Expansion of Sodium Trisilicate Glasses, J. Non. Cryst. Solids. 20 (1976) 439–449.

[88]   M. Tomozawa, M. Takata, J. Acocella, E.B. Watson, T. Takamori, Thermal Properties of Na_2O $3SiO_2$ Glasses with High Water Content, J. Non. Cryst. Solids. 56 (1983) 343–348.

[89]   P. Del Gaudio, H. Behrens, J. Deubener, Viscosity and Glass Transition Temperature of Hydrous Float Glass, J. Non. Cryst. Solids. 353 (2007) 223–236.

[90]   U. Bauer, H. Behrens, M. Fechtelkord, S. Reinsch, J. Deubener, Water- and Boron Speciation in Hydrous Soda-Lime-Borate Glasses, J. Non. Cryst. Solids. 423–424 (2015) 58–67.

[91]   Y.Z. Yue, Characteristic Temperatures of Enthalpy Relaxation in Glass, J. Non. Cryst. Solids. 354 (2008) 1112–1118.

[92]   G. Meerlender, Viskositäts-Temperatur Verhalten des Standardglases I der DGG, Glas. Berichte. 47 (1974) 1–3.

[93]   R. Brückner, G. Demharter, Systematische Untersuchung über die Anwendbarkeit von Penetrationsviskosimetern, Glas. Ber. 48 (1974) 12–18.

[94]   N. Böse, G. Klingenberg, G. Meerlender, Viscosity Measurements of Glass Melts-Certification of Reference Material, Glas. Ber. Glas. Sci. Technol. 74 (2001) 115–126.

[95]   R. Brückner, Y. Yue, J. Deubener, Progress in the Rheology of Glass and Melts, Glas. Ber. Glas. Sci. Technol. 70 (1997) 261–271.

[96]   R.J. Stevenson, D.B. Dingwell, S.L. Webb, N.S. Bagdassarov, The Equivalence of Enthalpy and Shear Stress Relaxation in Rhyolitic Obsidians and Quantification of the Liquid-Glass Transition in Volcanic Processes, J. Volcanol. Geotherm. Res. 68 (1995) 297–306.

[97]   L. Wondraczek, H. Behrens, Y. Yue, J. Deubener, G.W. Scherer, Relaxation and Glass Transition in an Isostatically Compressed Diopside Glass, J. Am. Ceram. Soc. 90 (2007) 1556–1561.

[98]   M.A. Ramos, J.A. Moreno, S. Vieira, C. Prieto, J.F. Fernández, Correlation of Elastic, Acoustic and Thermodynamic Poperties in B_2O_3 Glasses, J. Solid State Chem. 221 (1997) 170–180.

[99]   K.L. Goetschius, The Effect of Composition on the Viscosity, Crystallization and Dissolution of Simple Borate Glasses and Compositional Design of Borate Based Bioactive Glasses, Missouri Univ. Sci. Technol. (2014).

[100]   J. Deubener, H. Behrens, R. Müller, S. Zietka, S. Reinsch, Kinetic Fragility of Hydrous Soda-Lime-Silica Glasses, J. Non. Cryst. Solids. 354 (2008) 4713–4718.

[101]   S. Sakka, K. Matusita, T. Watanabe, K. Kamiya, Effects of Small Amounts of Water on the Viscosity, Glass Transition Temperature and Vickers Hardness of Silicate Glasses, Yogyo Kyokai-Shi. 89 (1981) 577–584.

[102]   G. Hetherington, K.H. Jack, J.C. Kennedy, The Viscosity of Vitreous Silica, Phys. Chem. Glas. 5 (1964) 130–136.

[103]   S. Zietka, J. Deubener, H. Behrens, R. Müller, Glass Transition and Viscosity of Hydrated Silica Glasses, Phys. Chem. Glas. Eur. J. Glas. Sci. Technol. B. 48 (2007) 380–387.

[104]   P.J. Lezzi, M. Tomozawa, An Overview of the Strengthening of Glass Fibers by Surface Stress Relaxation, Int. J. Appl. Glas. Sci. 6 (2015) 34–44.

[105]   T. Bakos, S.N. Rashkeev, S.T. Pantelides, H_2O and O_2 Molecules in Amorphous SiO_2: Defect Formation and Annihilation Mechanisms, Phys. Rev. B - Condens. Matter Mater. Phys. 69 (2004) 195206-1–9.

[106]   G.K. Lockwood, S.H. Garofalini, Bridging Oxygen as a Site for Proton Adsorption on the Vitreous Silica Surface, J. Chem. Phys. 131 (2009).

[107]   Y. Xiao, A.C. Lasaga, Ab Initio Quantum Mechanical Studies of the Kinetics and Mechanisms of Silicate Dissolution: H^+ (H_3O^+) Catalysis, Geochim. Cosmochim. Acta. 58 (1994) 5379–5400.

[108]   K.L. Geisinger, G. V. Gibbs, A. Navrotsky, A Molecular Orbital Study of Bond Length and Angle Variations in Framework Structures, Phys. Chem. Miner. 11 (1985) 266–283.

[109]   K. Ito, C.T. Moynihan, C.A. Angell, Thermodynamic Determination of Fragility in Liquids and a Fragile-to-Strong Liquid Transition in Water, Nature. 398 (1999) 492–495.

[110]   C. a Angell, Liquid Fragility and the Glass Transition in Water and Aqueous Solutions, Chem. Rev. 102 (2002) 2627–2650.

[111]   M.B. Østergaard, R.E. Youngman, M.N. Svenson, S.J. Rzoska, M. Bockowski, L.R. Jensen, et al., Temperature-Dependent Densification of Sodium Borosilicate Glass, RSC Adv. 5 (2015) 78845–78851.

[112]   J. Wu, J.F. Stebbins, Quench Rate and Temperature Effects on Boron Coordination in Aluminoborosilicate Melts, J. Non. Cryst. Solids. 356 (2010) 2097–2108.

[113]   S. Striepe, M.M. Smedskjaer, J. Deubener, U. Bauer, H. Behrens, M. Potuzak, et al., Elastic and Micromechanical Properties of Isostatically Compressed Soda–Lime–Borate Glasses, J. Non. Cryst. Solids. 364 (2013) 44–52.

[114]   M.M. Smedskjaer, J.C. Mauro, R.E. Youngman, C.L. Hogue, M. Potuzak, Y. Yue, Topological Principles of Borosilicate Glass Chemistry., J. Phys. Chem. B. 115 (2011) 12930–46.

[115]   S. Sen, Temperature Induced Structural Changes and Transport Mechanisms in Borate, Borosilicate and Boroaluminate Liquids: High-Resolution and High-Temperature NMR Results, J. Non. Cryst. Solids. 253 (1999) 84–94.

[116]   D.R. Neuville, D. de Ligny, G.S. Henderson, Advances in Raman Spectroscopy Applied to Earth and Material Sciences, Rev. Mineral. Geochemistry. 78 (2014) 509–541.

[117]   N. Zotov, H. Keppler, The Influence of Water on the Structure of Hydrous Sodium Tetrasilicate Glasses, Am. Mineral. 83 (1998) 823–834.

[118]   H. Scholze, Zur Frage der Unterscheidung zwischen H_2O- Molekülen und OH-Gruppen in Gläsern und Mineralen, Naturwissenschaften. 47 (1960) 226.

[119]   C.-K. Wu, Nature of Incorporated Water in Hydrated Silicate Glasses, J. Am. Ceram. Soc. 63 (1980) 453–457.

[120]   C.W. Mandeville, J.D. Webster, J. Rutherford, Malcome, E. Taylor, Bruce, A. Timbal, K. Faure, Determination of Molar Absorptivites for Infrared Absorption Bands of H2O in Andesitic Glasses, Am. Mineral. 87 (2002) 813–821.

[121]   L. Du, J.F. Stebbins, Nature of Silicon-Boron Mixing in Sodium Borosilicate Glasses: A High-Resolution ^{11}B and ^{17}O NMR Study, J. Phys. Chem. B. 107 (2003) 10063–10076.

[122]   L.-S. Du, J.F. Stebbins, Site Preference and Si/B Mixing in Mixed-Alkali Borosilicate Glasses: A High-Resolution ^{11}B and ^{17}O NMR study, J. Chem. Mater. 15 (2003) 3913–3921.

[123]   F. Angeli, O. Villain, S. Schuller, T. Charpentier, D. de Ligny, L. Bressel, et al., Effect of Temperature and Thermal History on Borosilicate Glass Structure, Phys. Rev. B. 85 (2012) 54110.

[124]   J.F. Stebbins, Dynamics and Structure of Silicate and Oxide Melts: Nuclear Magnetic Resonance Studies, in: Rev. Mineral., 1995: pp. 191–246.

[125]   C. Huang, A.N. Cormack, Structural Differences and Phase Separation in Alkali Silicate Glasses, J. Chem. Phys. 95 (1991) 3634.

[126]   C. Huang, A.N. Cormack, The Structure of Sodium Silicate Glass, J. Chem. Phys. 93 (1990) 8180–8186.

[127]   J. Wu, J.F. Stebbins, Effects of Cation Field Strength on the Structure of Aluminoborosilicate Glasses: High-Resolution ^{11}B, ^{27}Al and ^{23}Na MAS NMR, J. Non. Cryst. Solids. 355 (2009) 556–562.

[128]   D. Manara, A. Grandjean, D.R. Neuville, Structure of Borosilicate Glasses and Melts: A Revision of the Yun, Bray and Dell Model, J. Non. Cryst. Solids. 355 (2009) 2528–2531.

[129]   E.I. Kamitsos, G.D. Chryssikos, M.A. Karakassides, Vibrational spectra of Magnesium-Sodium-Borate Glasses. 2. Raman and Mid-Infrared Investigation of the Network Structure, J. Phys. Chem. 91 (1987) 1067–1073.

[130]   M. Lenoir, A. Grandjean, Y. Linard, B. Cochain, D.R. Neuville, The Influence of Si , B Substitution and of the Nature of Network-Modifying Cations on the Properties and Structure of Borosilicate Glasses and Melts, Chem. Geol. 256 (2008) 315–324.

[131]   P.F. McMillan, G.H. Wolf, Vibrational Spectroscopy of Silicate Liquids, Rev. Mineral. 32 (1995) 247–315.

[132]   D. a. McKeown, A.C. Buechele, C. Viragh, I.L. Pegg, Raman and X-ray Absorption Spectroscopic Studies of Hydrothermally Altered Alkali-Borosilicate Nuclear Waste Glass, J. Nucl. Mater. 399 (2010) 13–25.

[133]   D.E. Day, G.E. Rindone, Internal Friction of Progressively Crystallized Glasses, J. Am. Ceram. Soc. 44 (1961) 161–167.

[134]   M. Tomozawa, R.W. Hepburn, Surface Structural Relaxation of Silica Glass: A possible Mechanism of Mechanical Fatigue, J. Non. Cryst. Solids. 345–346 (2004) 449–460.

[135]   S. V Nemilov, Physical Ageing of Silicate Glasses at Room Temperature : General Regularities as a Basis for the Theory and the Possibility of a priori Calculation of the Ageing Rate, Glas. Phys. Chem. 26 (2000) 511–530.

[136]   S.M. Wiederhorn, Influence of Water Vapor on Crack Propagation in Soda-Lime Glass, J. Am. Ceram. Soc. 50 (1967) 407–414.

[137]   R. Brückner, Charakteristische physikalische Eigenschaften der oxydischen Hauptglasbildner und ihre Beziehung zur Struktur der Gläser, Glas. Berichte. 37 (1964) 536–548.

[138]   R.W. Douglas, W.L. Armstrong, J.P. Edward, D. Hall, A Penetration Viscometer, Glas. Technol. 6 (1965) 52–55.

[139]   Y. Zhang, Z. Xu, Y. Liu, Viscosity of Hydrous Rhyolitic Melts Inferred from Kinetic Experiments, and a new Viscosity Model, Am. Mineral. 88 (2003) 1741–1752.

[140]   D. Giordano, A.R.L. Nichols, D.B. Dingwell, Glass Transition Temperatures of Natural Hydrous melts: A Relationship with Shear Viscosity and Implications for the Welding Process, J. Volcanol. Geotherm. Res. 142 (2005) 105–118.

[141]   M.A. Bouhifd, A. Whittington, J. Roux, P. Richet, Effect of Water on the Heat Capacity of Polymerized Aluminosilicate Glasses and Melts, Geochim. Cosmochim. Acta. 70 (2006) 711–722.

[142]   J.F. Stebbins, S. Kroeker, S.K. Lee, T.J. Kiczenski, Quantifcation of Five- and Six-Coordinated Aluminum Ions in Aluminosilicate and Fluoride-Containing Glasses by High-Field, High-Resolution ^{27}AlNMR, J. Non. Cryst. Solids. 275 (2000) 1–6.

[143]   Q. Zeng, H. Nekvasil, C.P. Grey, In Support of a Depolymerization Model for Water in Sodium Aluminosilicate Glasses:, Geochim. Cosmochim. Acta. 64 (2000) 883–896.

[144]   S.C. Kohn, R. Dupree, M.E. Smith, A Multinuclear Magnetic Resonance Study of the Structure of Hydrous Albite Glasses, Geochim. Cosmochim. Acta. 53 (1989) 2925–2935.

[145]   W.J. Malfait, R. Verel, P. Ardia, C. Sanchez-Valle, Aluminum Coordination in Rhyolite and Andesite Glasses and Melts: Effect of Temperature, Pressure, Composition and Water Content, Geochim. Cosmochim. Acta. 77 (2012) 11–26.

[146]   X. Xue, M. Kanzaki, Al coordination and water speciation in hydrous aluminosilicate glasses: Direct evidence from high-resolution heteronuclear ^{1}H-^{27}Al correlation NMR, Solid State Nucl. Magn. Reson. 31 (2007) 10–27.

[147]   X. Xue, Water Speciation in Hydrous Silicate and Aluminosilicate Glasses: Direct Evidence from ^{29}Si-^{1}H and ^{27}Al-^{1}H Double-Resonance NMR, Am. Mineral. 94 (2009) 395–398.

[148]   A. Whittington, P. Richet, F. Holtz, Water and the Viscosity of Depolymerized Aluminosilicate Melts, Geochim. Cosmochim. Acta. 64 (2000) 3725–3736.

[149]   J.M. Jewell, c. M. Shaw, J.E. Sehlby, Effects of Water Content on Aluminosilicate Glasses and the Relation to Strong/Fragile Liquid Theory, J. Non. Cryst. Solids. 152 (1993) 32–41.

[150]   S. Reinsch, C. Roessler, U. Bauer, R. Müller, J. Deubener, H. Behrens, Water, the other Network Modifier in Borate Glasses, J. Non. Cryst. Solids. 432 (2015) 208–217.

[151]   H. Rötger, Elastische Nachwirkung durch Wärmediffusion (thermische Reibung) und Materialdiffusion (eigentlich innere Reibung) bei periodischen und aperiodischen Vorgang, Glas. Berichte. 19 (1941) 192–200.

[152]   W.J. Dell, P.J. Bray, S.Z. Xiao, 11B NMR Strudies and Structural Modeling of Na$_2$O-B$_2$O$_3$-SiO$_2$ Glasses of High Soda Content, J. Non. Cryst. Solids. 58 (1983) 1–16.

Appendix

CURRICULUM VITAE

Persönliche Daten

Name:	Ute Dietrich, geb. Bauer
Geburtsdatum und Ort:	20.10.1985 in Hannover

Beruflicher Werdegang

01/2015 - 12/2015   Mutterschutz/Elternzeit

Seit 08/2012   Wissenschaftliche Mitarbeiterin am Institut für Mineralogie der Leibniz Universität Hannover
Projekt: "Topological Engineering of Ultra Strong Glasses (SPP1594)"

02 - 07/2012   Wissenschaftliche Hilfskraft am Institut für Mineralogie der Leibniz Universität Hannover

01/2008 - 04/2012   Studentische Hilfskraft am Institut für Mineralogie der Leibniz Universität Hannover

Studium

02/2012	Erlangen des Hochschulgrades Master of Science (M.Sc.). Schwerpunkt Mineralogie/Geochemie
	Titel der Masterarbeit: "Lithium Diffusion in silikatischen Gläsern". Note: 1,1
01/2010	Erlangen des Hochschulgrades Bachelor of Science (B.Sc.)
	Titel der Bachelorarbeit: " Löslichkeit von H_2O und CO_2 in pegmatitischen Schmelzen". Note: 1,3
08/2008	Praktikum bei der GEO-data, Gesellschaft für Logging-Service mbH, Hannover
10/2006	Immatrikulation im Studiengang „Geowissenschaften" an der Leibniz Universität Hannover

Sprachen

Deutsch	Muttersprache
Englisch	Verhandlungssicher
Spanisch	Grundkenntnisse

Liste der Publikationen

Journals

2016

Reinsch, S., Roessler, C., **Bauer, U**., Müller, R., Deubener, J., Behrens, H. (2016): Water, the other network modifier in borate glasses, Journal of Non-Crystalline Solids 432 pp. 208-217.

2015

Bauer, U., Behrens, H., Fechtelkord, M., Reinsch, S., Deubener, J. (2015): Water- and boron speciation in hydrous soda–lime–borate glasses, Journal of Non-Crystalline Solids 423–424 pp. 58–67.

2014

Smedskjaer, M. M., Youngman, R. E., Striepe, S., Potuzak, M., **Bauer, U.**, Deubener, J., Behrens, H., Mauro, J., C. & Yue, Y. (2014): Irreversibility of Pressure Induced Boron Speciation Change in Glass, Scientific Reports 4, 3770.

2013

Bauer, U., Welsch, A.-M., Behrens, H., Rahn, J., Schmidt, H., Horn, I. (2013): Li Diffusion and the Effect of Local Structure on Li Mobility in Li_2O–SiO_2 Glasses, J. Phys. Chem. B, 2013, 117, 15184-15195.

Striepe, S., Smedskjaer, M.M., Deubener, J., **Bauer, U.**, Behrens, H., Potuzak, M., Youngman, R.E., Mauro, J.C., Yue, Y. (2013): Elastic and micromechanical properties of isostatically compressed soda-lime-borate glasses, Journal of Non-Crystalline Solids 364 (1), pp. 44-52.

Abstracts

2014

Bauer, U., Behrens, H., Fechtelkord, M. (2014): Structural investigation of soda-lime borate glasses: The influence of water and boron speciation, Annual Meeting of German Society of Glass Technology and International Conference on Advances in Fusion and Processing of Glass, Aachen, Germany

Bauer, U., Behrens, H., Fechtelkord, M. (2014): Boron and water speciation in hydrated soda-lime borate glasses, Flow and Fracture of Advanced Glasses, Weimar, Germany.

2013

Bauer, U., Welsch, A.-M., Behrens, H., Horn, I., Rahn, J. (2013): Lithium self-diffusion and electrical conductivity in lithium silicate glasses, International Congress on Glass, Prague, Czech Republic

2012

Bauer, U., Behrens H., Welsch, A-M., Horn, I., Ross, S., Rahn, J. (2012): Lithium diffusion in lithium trisilicate glasses, Material Science and Engineering congress 2012 Darmstadt, Germany

2011

Bauer, U., Behrens H., Welsch, A-M., Horn, I., Ross, S. (2011): Lithium diffusion and electrical conductivity in Li-silicate glasses, 9th Silicate Melt Workshop, La Petite Pierre, Alsace, France

Welsch, A.M., **Bauer, U.**, Behrens, H., Horn, I. (2011): Lithium dynamics in $Li_2Si_3O_7$ and $LiAlSi_2O_6$ glasses, Deutsche Mineralogische Gesellschaft section meeting petrology, Bochum, Germany